Structural and Functional Evaluation of Steroidogenic Cytochrome P450 Enzymes

By

Elyse M. Petrunak

Submitted to the graduate degree program in Medicinal Chemistry and the Graduate Faculty of the University of Kansas in partial fulfillment of the requirements for the degree of Doctor of Philosophy.

_____

Chairperson Emily E. Scott

_____

Jeffrey Aubé

_____

Blake Peterson

_____

Audrey Lamb

_____

Jed Lampe

Date Defended: July 24, 2015

The Dissertation Committee for Elyse M. Petrunak

certifies that this is the approved version of the following dissertation:

Structural and Functional Evaluation of Steroidogenic Cytochrome P450 Enzymes

_____

Chairperson Emily E. Scott

Date approved: July 24, 2015

ABSTRACT

Cytochromes P450 (CYP450) are heme-containing monooxygenase enzymes that perform a variety of functions in humans, including xenobiotic metabolism and the production of endogenous signaling molecules. Six isoforms of cytochrome P450 including cytochrome P450 17A1 (CYP17A1) and cytochrome P450 21A2 (CYP21A2), are responsible for the generation of steroid hormones, making these enzymes crucial for development and homeostasis. However in certain pathological conditions, inhibition of steroidogenic cytochrome P450 enzymes can be therapeutically useful. For prostate cancers dependent on androgens such as dihydrotestosterone for tumor growth and proliferation, inhibition of CYP17A1, a required enzyme in androgen biosynthesis, is a promising treatment strategy. Although inhibition of CYP17A1 has been successful clinically, its additional roles in the biosynthesis of other steroid hormones and its similarity to other steroidogenic P450 enzymes can bring about off-target effects. An understanding of the structure and function of CYP17A1, as well as other steroidogenic countertarget enzymes such as CYP21A2, could therefore be fundamental to developing improved inhibitors of this enzyme for the treatment of prostate cancer.

CYP17A1 performs two different reactions in the same active site to generate androgens, a hydroxylation reaction followed by a carbon-carbon bond cleavage (or lyase) reaction. While the second, carbon-carbon bond cleavage reaction commits a steroid to the androgen pathway, the initial hydroxylation reaction is also necessary for the production of glucocorticoids. Human CYP17A1 performs the hydroxylation reaction on two structurally similar substrates, Δ4-progesterone and Δ5-pregnenolone, which only exhibit differences on the A ring on the opposite end of the steroid from the carbon which is hydroxylated by CYP17A1. Following hydroxylation, Δ5-17α-hydroxypregnenolone will undergo the second lyase reaction, but the Δ4-

17α-hydroxyprogesterone does not. To elucidate a structural basis for preferential lyase turnover of Δ5 steroids by human CYP17A1, the crystal structure of the enzyme containing a background mutation was determined in the presence of both hydroxylase substrates and both lyase substrates. These structures reveal some similarities in binding among all four substrates but also differences in positions relative to the heme iron between hydroxylase substrates, the poor lyase substrate 17α-hydroxyprogesterone, and the efficient lyase substrate 17α-hydroxypregnenolone. Observed differences in distances between 17α-hydroxyprogesterone or 17α-hydroxypregnenolone and the heme iron may reflect differential stabilization of the proposed intermediate for the 17,20-lyase reaction. In addition to substrates, steroidal inhibitors of CYP17A1 can have different configurations of the A ring. X-ray crystal structures of a series of inhibitors with such modifications were also determined with CYP17A1 to compare active site interactions among A-ring modified steroidal inhibitors. Modifications to the A ring of steroidal inhibitor abiraterone did not alter direct contacts with CYP17A1, but did change indirect contacts with the enzyme through active site water networks. The structure of CYP17A1 with one A-ring modified inhibitor was resolved to 2.0 Å, making it the highest resolution crystal structure of CYP17A1 to date, and revealed an additional steroid binding site in the periphery of enzyme that had not been fully appreciated in previous CYP17A1 structures.

CYP17A1 and redox partner proteins were recombinantly expressed in *E. coli* and purified, providing a well-defined and well-controlled system for evaluation of CYP17A1 function and inhibition. This strategy was employed to compare hydroxylase and lyase deficiencies among clinically-reported mutants of the enzyme, as well as steroidal and non-steroidal clinical inhibitors for selective inhibition of the lyase reaction compared to the hydroxylase reaction. Most clinical inhibitors of CYP17A1 demonstrated 1- to 3- fold selectivity

for 17,20-lyase inhibition over 17α-hydroxylase inhibition. Only one of the four inhibitors to reach clinical trials, *S*-orteronel, demonstrated 3- to 5- fold selectivity for 17,20-lyase inhibition compared to inhibition of progesterone and pregnenolone 17α-hydroxylase reactions. However, its enantiomer, *R*-orteronel demonstrated 8- to 11-fold selectivity. X-ray crystal structures of CYP17A1 with non-steroidal inhibitors reported to selectively inhibit the lyase reaction were also determined to investigate the structural basis for lyase selectivity.

Finally, some CYP17A1 inhibitors have also been shown to interact with another P450 responsible for steroid biosynthesis, CYP21A2. The physiological consequences of off-target CYP21A2 inhibition by compounds developed to target CYP17A1 are complex. The crystal structure of human CYP21A2 was determined to provide a structural comparison to CYP17A1 and potentially aid in the design of inhibitors more selective for CYP17A1 over CYP21A2. Some structural features of the CYP17A1 active site, including a hydrophobic pocket over the I helix, are not conserved in CYP21A2. Exploitation of this pocket is a potential strategy for the development of inhibitors with reduced affinity for CYP21A2.

In aggregate, the studies described herein use structural information coupled with functional analysis to better understand steroidogenic cytochromes P450. These enzymes act as targets and countertargets in the treatment of hormone dependent diseases including prostate cancer. More detailed knowledge of how these enzymes interact with both substrates and inhibitors could inform the development of better prostate cancer therapeutics.

ACKNOWLEDGEMENTS

I am extremely grateful to those who have supported me throughout my graduate education. This work includes specific scientific contributions from Dr. Natasha DeVore, Dr. Steven Rogers, Patrick Porubsky, Dr. Charlie Fehl, Dr. Victoria Jasion, and Dr. Fernando Estrada, which are noted in their respective chapters. I owe much gratitude to Scott Lab members past and present: Dr. Natasha DeVore, Dr. Linda Blake, Dr. Agnes Walsh, Dr. Fernando Estrada, Aaron Bart, Dr. Victoria Jasion, Dr. Andrea Skinner, Eva Stephens, Dr. Youbin Tu, and Dr. Malika Godamudunage for providing a supportive environment that has helped me grow as a scientist and a person.

I am also grateful to those serving on my committee: Dr. Jeffrey Aubé, Dr. Audrey Lamb, Dr. Blake Peterson, and Dr. Jed Lampe. Additional thanks are due to Dr. Jeff Aubé for workspace and instrumentation and Patrick Porubsky for GC/MS guidance and maintenance. Most importantly, I owe enormous thanks to my advisor Dr. Emily Scott for her outstanding mentorship and constant support. I feel very fortunate to have been part of your lab.

My graduate education wouldn't have been possible without financial support from multiple sources. This work was funded by the University of Kansas Cancer Center, National Institutes of Health grant GM102505, and the University of Kansas School of Graduate Studies Dissertation Year Fellowship. All crystallographic data was collected at the Stanford Synchrotron Radiation Lightsource at Stanford University, which is supported by the US Department of Energy.

Finally, I would like to thank my family and friends for their encouragement during my graduate career and throughout my education. I would never have made it this far without all of your love and support.

Table of Contents Page

List of Figures Page

List of Tables Page

Chapter 1.

Introduction

Introduction to Cytochromes P450

Cytochromes P450 are a superfamily of heme-containing monooxygenase enzymes expressed by a wide variety of life forms spanning from bacteria to humans. Under reducing conditions, these enzymes activate molecular oxygen to catalyze the insertion of a single oxygen atom onto a substrate carbon. While members of the superfamily share a general structural motif and mechanism for activation of molecular oxygen, the reactions catalyzed by cytochromes P450 can serve an array of functions. The human genome encodes for 57 different cytochromes P450 (Table 1.1). Of the 38 isoforms that have a known substrate, nearly 40% primarily act on xenobiotics and appear to play a role in the clearance of exogenous compounds[1]. The remaining cytochromes P450 turn over endogenous substrates, including steroid hormones, fatty acids, eicosanoids, and vitamins. The work described in this dissertation focuses primarily on human cytochrome P450 enzymes responsible for the biosynthesis of steroid hormones.

Table 1.1: Human cytochrome P450 enzymes sorted by major substrate class

Steroids	Xenobiotics	Fatty Acids	Eicosanoids	Vitamins	Unknown
1B1	1A1	2J2	4F2	2R1	2A7
7A1	1A2	4A11	4F3	24A1	2S1
7B1	2A6	4B1	4F8	26A1	2U1
8B1	2A13	4F12	5A1	26B1	2W1
11A1	2B6		8A1	26C1	3A43
11B1	2C8			27B1	4A22
11B2	2C9				4F11
17A1	2C18				4F22
19A1	2C19				4V1
21A2	2D6				4X1
27A1	2E1				4Z1
39A1	2F1				20A1
46A1	3A4				27C1
51A1	3A5				
	3A7				

Cytochrome P450 Spectroscopic Features and Catalytic Cycle

The reactions carried out by cytochromes P450 are mediated by a heme prosthetic group, which gives these enzymes their distinct spectroscopic profile. The UV-visible absorbance maximum of the heme (known as the Soret peak) reflects both the redox state and the environment of the iron. This iron is coordinated on the proximal face of the heme by the thiolate group of a cysteine (Figure 1.1). In the absence of ligand, the ferric iron (Fe^{3+}) is typically coordinated to a water molecule on the distal face of the heme, which results in a Soret peak at ~417 nm (Figure 1.1)[2]. Binding of ligands in the active site on the distal side of the heme typically displaces the water, leaving the ferric iron coordinated only to the pyrrolic nitrogens of the porphyrin and the thiolate. This results in a blue-shifting of the Soret peak to ~393 nm referred to as a "Type I shift"[2]. In circumstances where the heteroatom of a ligand directly coordinates the heme iron upon displacement of the water molecule, the Soret peak is redshifted to ~424 nm, referred to as a "Type II shift"[2]. The type of shift (I or II) can sometimes inform the

orientation of ligands in the cytochrome P450 active site. Perhaps more importantly, the amount of absorbance change upon titration with a known concentration of ligand is used to determine dissociation constants (K_d) for enzyme-ligand complexes[3].

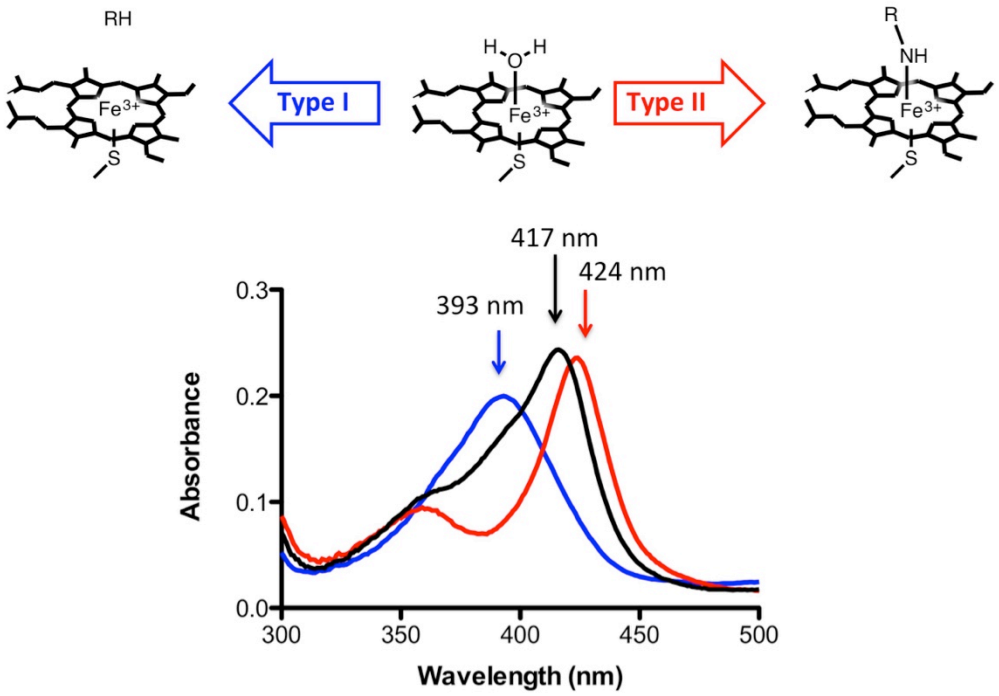

Figure 1.1: The absorbance maximum of the Soret band is dependent on the coordination state of the heme iron. The oxidized state, in which the heme iron binds to an active site water (black trace) absorbs at 417 nm. The presence of a ligand can result in a type I spectrum in which the Soret band absorbs at ~393 nm (blue trace), or (if a heteroatom coordinates to the heme) a type II spectrum with Soret band absorbance at 424 nm (red trace).

The Soret band absorbance can be used to determine the concentration of heme proteins, but for cytochromes P450 the protein concentration is often determined in the enzyme's reduced state, with the heme bound to carbon monoxide. Reduction of the heme iron from the ferric state (Fe^{3+}) to the ferrous state (Fe^{2+}) is accompanied by a less dramatic change in Soret band absorbance compared to those brought about by changes in the iron coordination state. However, subsequent addition of carbon monoxide results in a strong shift in Soret band absorbance to 450 nm upon coordination to ferrous cytochrome P450. Usually viewed as a

reduced carbon monoxide difference spectrum (Figure 1.2), this spectral characteristic is distinctive for heme proteins with thiolate coordination to the iron. Under the same conditions, a shift of the Soret band to 420 nm is sometimes observed, resulting in "P420". Although the underlying change in heme coordination state responsible for P420 remains debated[4,5], species that demonstrate this spectral shift are considered catalytically inactive[5].

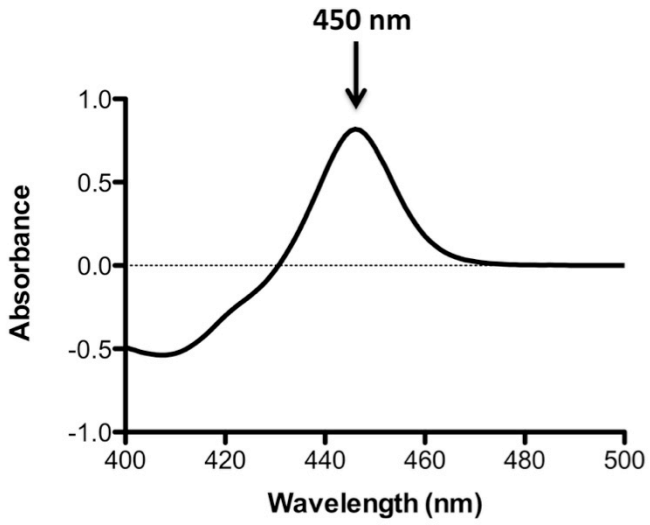

Figure 1.2: Treatment of reduced cytochrome P450 with carbon monoxide results in a characteristic shift of the Soret peak to 450 nm.

The phenomena underlying some of the aforementioned change in spectral characteristics (binding of substrate and reduction of the heme iron) comprise the first two steps of the cytochrome P450 catalytic cycle (Figure 1.3)[6]. Displacement of the active site water upon substrate binding **(a** to **b)** increases the iron redox potential and facilitates reduction of the heme iron from the ferric state to the ferrous state **(b** to **c)** by the redox partner protein NADPH-cytochrome P450 reductase. Ferrous heme binds molecular oxygen to form the dioxygen complex **(d),** and the dioxygen complex undergoes an additional one electron reduction by a redox partner protein (either NADPH-cytochrome P450 reductase or cytochrome b_5) to generate a ferric peroxyanion intermediate **(e)**. A proton is delivered to the peroxyanion species to form

the ferric hydroperoxo complex **(f)**. Substrate hydroxylation requires a second protonation of the hydroperoxo species, which then undergoes homolytic cleavage to expel water. The resulting ferryl oxo species **(g)** called "compound I" is postulated to be the key intermediate in P450 hydroxylation. Compound I abstracts a hydrogen from a substrate carbon to form a free radical, which then interacts with the oxygen of the ferryl species to yield a hydroxyl group on the substrate carbon (Figure 1.4). This mechanism for substrate hydroxylation is known as the Groves' rebound mechanism[7,8].

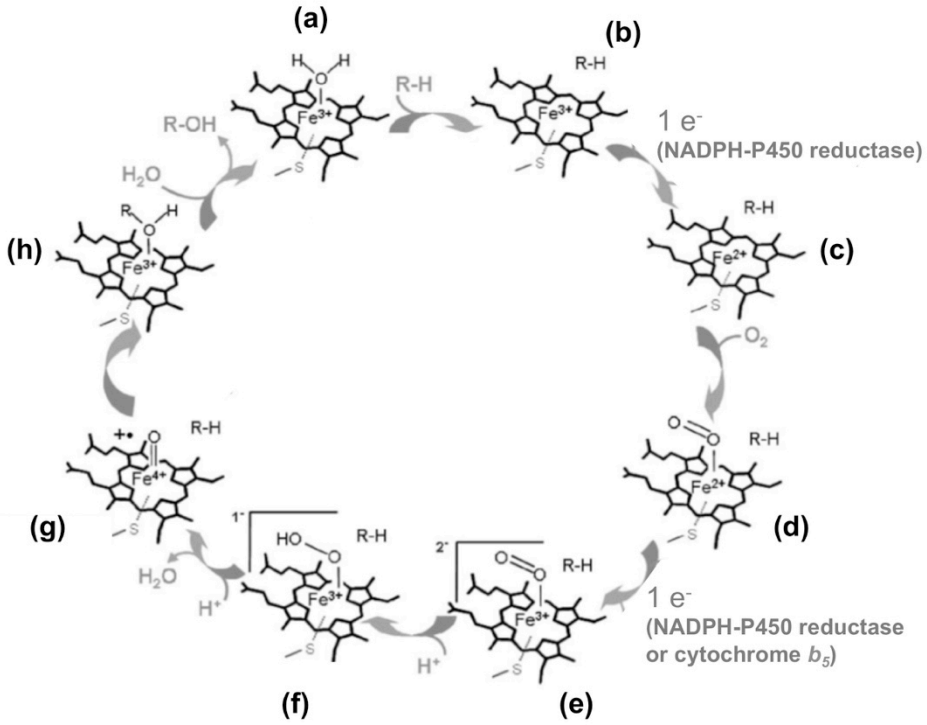

Figure 1.3: Catalytic cycle of cytochrome P450 enzymes. Figure is adapted from Munro *et al*.[9]

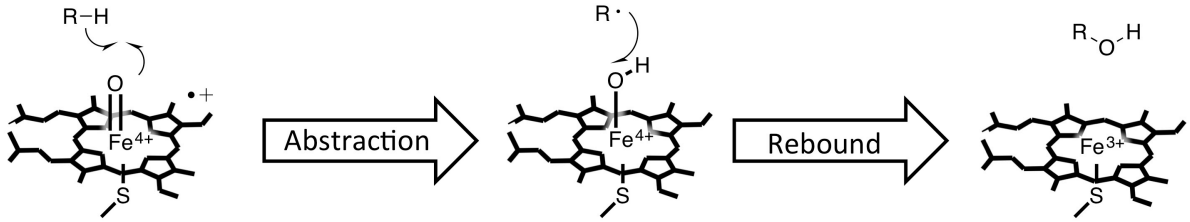

Figure 1.4: Groves' mechanism for cytochrome P450 hydroxylation reactions by hydrogen abstraction and rebound via the ferryl oxo intermediate.

Although the Groves' mechanism involving compound I as a key catalytic intermediate reflects our best understanding of how cytochromes P450 perform more common hydroxylation reactions, some P450 enzymes catalyze more unusual reactions including carbon-carbon bond cleavage, or lyase, reactions that are proposed to involve a different key catalytic intermediate. Catalysis of the lyase reaction has only been observed for a limited number of cytochrome P450 enzymes. Multiple mechanisms for the CYP17A1-mediated 17,20-lyase reaction have been reported in the literature[10,11]. In a mechanism proposed by Akhtar and coworkers, the key catalytic intermediate for the carbon-carbon bond cleavage reaction is the dioxygen peroxo species **(e)** or **(f)** in contrast to the ferryl oxo complex **(g)** (Figure 1.3)[10]. The distal oxygen of the peroxo intermediate is thought to act as a nucleophile on an acyl carbon, and subsequent homolytic cleavage of the O-O bond results in a deacetylation to form a free carbon radical (Figure 1.5). Hydrogen abstraction by the Fe(III)-O complex affords a double bond yielding a ketone. The most compelling studies to support this mechanism for carbon-carbon bond cleavage examined incorporation of isotopically-labeled oxygen into the deformylation products of CYP19A1[10], an enzyme that generates estrogens by aromatization of androgens. However, more recent reexamination of these studies using more advanced instrumentation produced conflicting results suggesting that deformylation of testosterone proceeds through the ferryl oxo

catalytic intermediate[11]. Consequently, the reactive oxygen species responsible for carbon-carbon bond cleavage reactions in cytochrome P450 enzymes is still subject to debate.

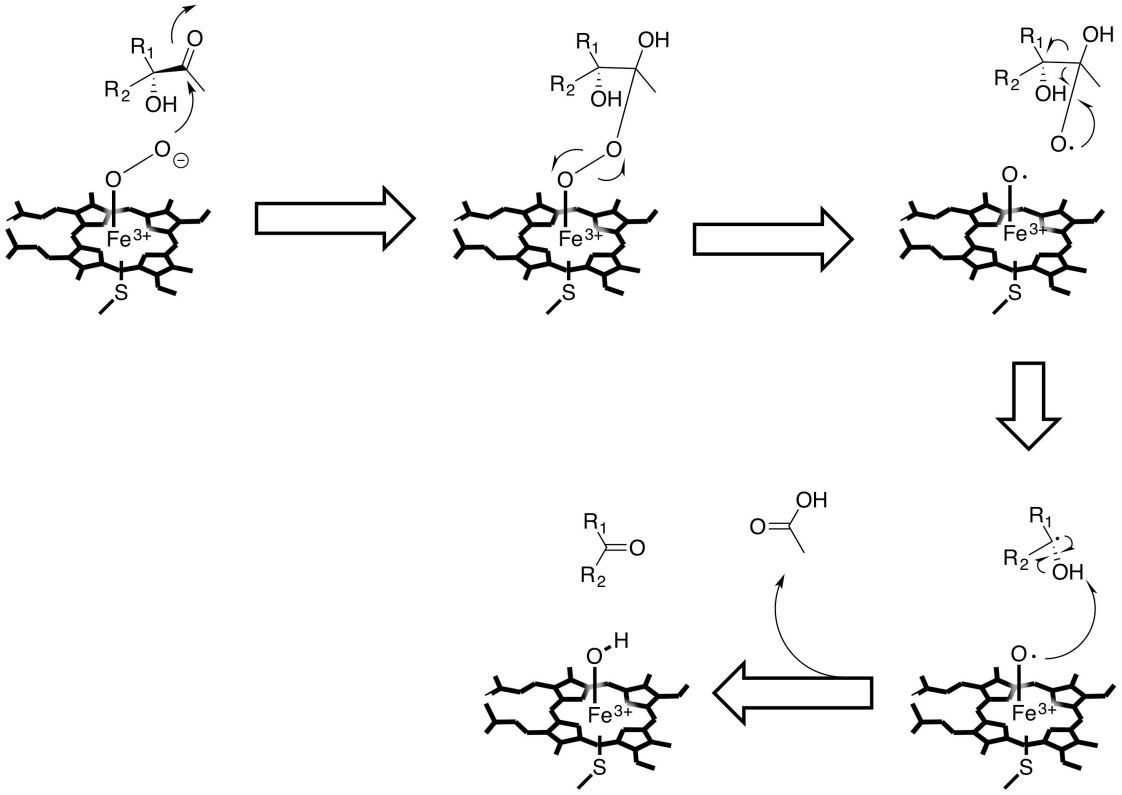

Figure 1.5: Proposed mechanism for cytochrome P450 carbon-carbon bond cleavage reaction via dioxygen catalytic intermediate[10].

General Structure of Cytochrome P450 Enzymes

The first high-resolution crystal structure of a cytochrome P450 (a soluble, bacterial isoform known as $P450_{cam}$) was reported in 1985[12]. Since this time, over 600 X-ray crystal structures of cytochromes P450 have been deposited into the Protein Data Bank. Although some members of the P450 superfamily share little more than 40% sequence identity, the overall fold of cytochromes P450 (Figure 1.6) is conserved among different organisms and subcellular localizations, from the first structure of $P450_{cam}$ to the membrane-associated mammalian isoforms investigated more recently. All P450 enzymes are largely α-helical and are comprised

of 12 major helices (labeled A-L), with a number of minor helices that may or may not be present in a given P450 structure (one of the most common examples being the B′ helix). The heme prosthetic group and adjacent active site is buried within the protein and isolated from the surface of the enzyme in most structures of cytochromes P450. In addition to the structural elements described, the N-terminus of most mammalian cytochromes P450 forms a helix (20-30 residues in length) that is embedded in the membrane of the endoplasmic reticulum. Due to its positioning in the membrane, this N-terminal portion of the enzyme is unlikely to directly participate in catalysis. This portion of the protein is usually truncated from the main catalytic domain for structural studies, and often for enzymology studies as well since cytochromes P450 are functional in its absence[13-15].

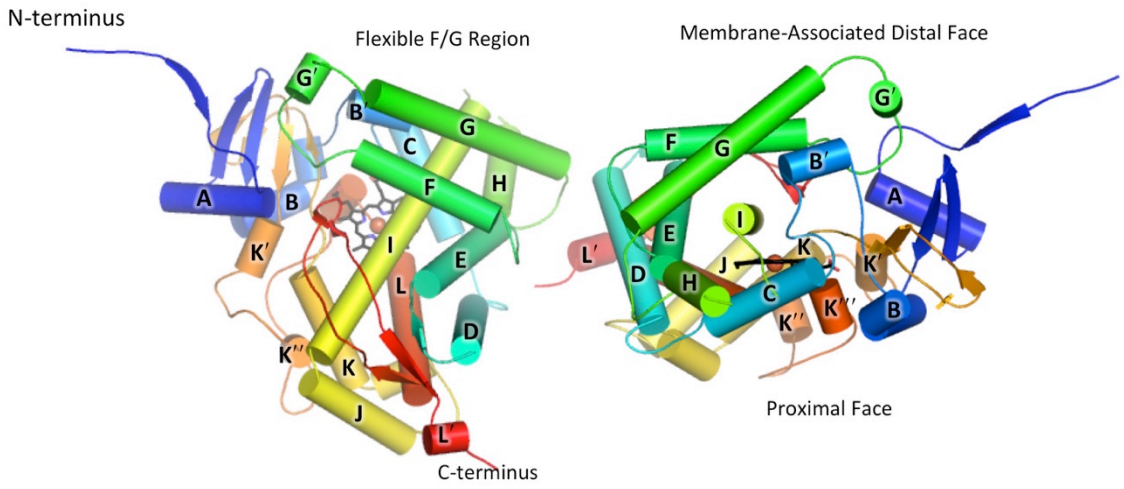

Figure 1.6: Conserved fold of cytochrome P450 catalytic domain. The protein is colored from N- to C-terminus in blue to red (Jones' rainbow), and shown from the distal, membrane binding face of the enzyme (left) and perpendicular to the central I helix (right). Heme cofactor is displayed in black sticks with orange iron sphere.

The most conserved elements of cytochromes P450 are the portions of the protein that interact directly with the heme cofactor and are necessary for general catalytic function. This includes the catalytically-essential cysteine proximal to the heme iron and located on a loop region preceding the L helix, as well as the structural elements surrounding it including helices I

and L[16]. The regions of cytochrome P450 structures showing the greatest degree of variation include the B′ helix and the region between the F and G helices. These elements converge to form a "roof" for the active site opposite to the heme "floor". Studies on prokaryotic cytochrome P450s first implicated the F and G structural elements in ligand entry and exit[16-19]. In membrane-associated mammalian cytochrome P450s, the F/G loop is longer, forms a highly hydrophobic surface of the enzyme's catalytic domain, and is most likely buried into the membrane[16,20]. In most mammalian cytochrome P450 structures this region is also likely to undergo significant conformational changes to permit ligand penetration and egress from the otherwise buried active site. The rabbit membrane P450 CYP2B4 has been crystallized in both an "open" conformation, in which the B′ to C region and the F/G loop are dissociated to form a cleft into the active site, thereby enabling ligand entry and exit[21], as well as a "closed" form[18], suggesting transition between these states. Similar smaller scale conformational changes have now been observed for other membrane cytochrome P450 enzymes and often involve these same structural elements[22,23].

In addition to binding small molecule ligands, cytochrome P450 catalysis requires binding with partner proteins. All cytochromes P450 rely on a redox partner for electron transfer. NADPH-cytochrome P450 oxidoreductase (CPR or reductase) is the primary electron source for most membrane-associated mammalian P450 enzymes, although adrenodoxin can act as the redox partner for mitochondrial cytochromes P450. CPR is a membrane-bound ~78 kDa multidomain protein that conducts electron transfer from NADPH to the heme iron of the cytochrome P450 through two separate flavin cofactors. Binding of POR to cytochrome P450 is mediated by electrostatic interactions between a negatively charged surface on POR and positively charged residues on the proximal face of the P450, which is the same face of the P450

that bears the heme-coordinated proximal cysteine. Residues of mammalian cytochrome P450 enzymes involved in this interaction have been identified by mutagenesis and are largely located on helices B, C, J, K, H, and L surrounding the proximal cysteine (Figure 1.6)[24]. Cytochromes P450 are also known to interact with a smaller heme-containing protein also anchored in the membrane, cytochrome b_5. The site of cytochrome b_5 binding on the CYP450 has been shown to partially overlap with that of CPR via mutagenesis studies[25], consistent with mutually exclusive reductase and cytochrome b5 binding demonstrated using NMR[26]. The presence of cytochrome b_5 can variably augment, inhibit, or have no effect on catalytic turnover by cytochrome P450, depending on the individual cytochrome P450 isoform and often the substrate of the reaction[24]. Although cytochrome b_5 is potentially capable of electron transfer to P450, the apo form of the enzyme in which the heme cofactor has been extracted also has been shown to augment the catalytic activity of some P450 enzymes[27,28]. This suggests that cytochrome b_5 may also alter P450 catalysis through allosteric effects by inducing a conformational change in the P450. The nature of such a conformational change remains largely unexplored, although initial studies suggest that cytochrome b_5 binding on the proximal face of CYP17A1 changes the backbone conformation of residues on the distal face involved in substrate entry and product exit[26].

Cytochrome P450 Enzymes in Steroid Biosynthesis

Human cytochromes P450 play a major role in a variety of physiological processes including the biosynthesis and metabolism of steroid hormones. The steroidal scaffold is ubiquitous in human biology, with small changes to its structure resulting in very different physiological effects. The processes controlled or influenced by steroid hormones depend on the hormone class (Table 1.2) and include development of secondary sex characteristics

(masculinization or feminization), fertility, stress response/inflammation, and salt/fluid balance. These hormones function by activating their cognate nuclear receptors, which in turn promote transcription of specific target genes.

Table 1.2: Members of steroid classes and associated bioactivity.

Class	Bioactivity	Steroids
Androgen	Masculinizing	Testosterone
		Dihydrotestosterone
Estrogen	Feminizing	Estradiol
		Estriol
Progestagen	Maintain pregnancy	Progesterone
		Pregnenolone
Mineralocorticoid	Sodium balance	Aldosterone
		11-Deoxycorticosterone
Glucocortioid	Stress response	Cortisol
		Corticosterone

To date, there are six human isoforms of cytochrome P450 enzymes known to contribute to the production of steroid hormones (Figure 1.7). $CYP450_{scc}$ (CYP11A1) is required for conversion of cholesterol (a 27-carbon steroid) to pregnenolone, a 21-carbon progestagen from which all other steroid hormones are derived. Pregnenolone and its derivatives are referred to as "Δ5" steroids because of a double bond between carbons 5 and 6. This configuration of the steroid A ring can be altered to a configuration known as "Δ4" by shifting the placement of the double bond between carbons 4 and 5, and oxidizing carbon 3 to a ketone by 3β-hydroxysteroid dehydrogenase (3βHSD), as occurs to form progesterone and its derivatives. Both Δ4 and Δ5 progestagens (progesterone and pregnenolone, respectively) act as substrates for CYP17A1 which converts 21-carbon progestagens to 19-carbon androgens. CYP17A1 accomplishes this task via two discrete reactions that were once believed to be performed by two completely

different enzymes[29]. CYP17A1 first hydroxylates the progestagen substrate at carbon 17, called the17α-hydroxylase reaction, followed by cleavage of the bond between carbons 17 and 20, called the 17,20-lyase reaction. The product of the first reaction is capable of dissociating from the enzyme and undergoing catalysis by different steroidogenic enzymes. The Δ4 progestagens, including progesterone and the intermediate CYP17A1 product 17α-hydroxyprogesterone can be converted to weak corticosteroids deoxycorticosterone and 11-deoxycortisol, respectively, by CYP21A2. These products can under go further hydroxylations by CYP11B1 and CYP11B2, which are responsible for generating more potent corticosteroids with glucocorticoid bioactivity (specifically cortisol) or mineralocorticoid bioactivity (specifically aldosterone). Generally, the downstream products of 17-hydroxylation by CYP17A1 tend to act as glucocorticoids, while corticosteroids without hydroxylation at C17 act as mineralocorticoids, making CYP17A1 a crucial enzyme in mediating the levels of both classes of corticosteroids.

When the 17α-hydroxylase metabolite undergoes the second CYP17A1-mediated 17,20-lyase reaction, it is converted to a 19-carbon androgen. These 17,20-lyase products can subsequently be converted into testosterone and the most potent androgen, dihydrotestosterone, via 17α-hydroxysteroid dehydrogenase and 5α-reductase, respectively. Androgens with Δ4 configuration (androstenedione and testosterone) can be converted to 18-carbon estrogens via aromatization and carbon-carbon bond cleavage by CYP19A1.

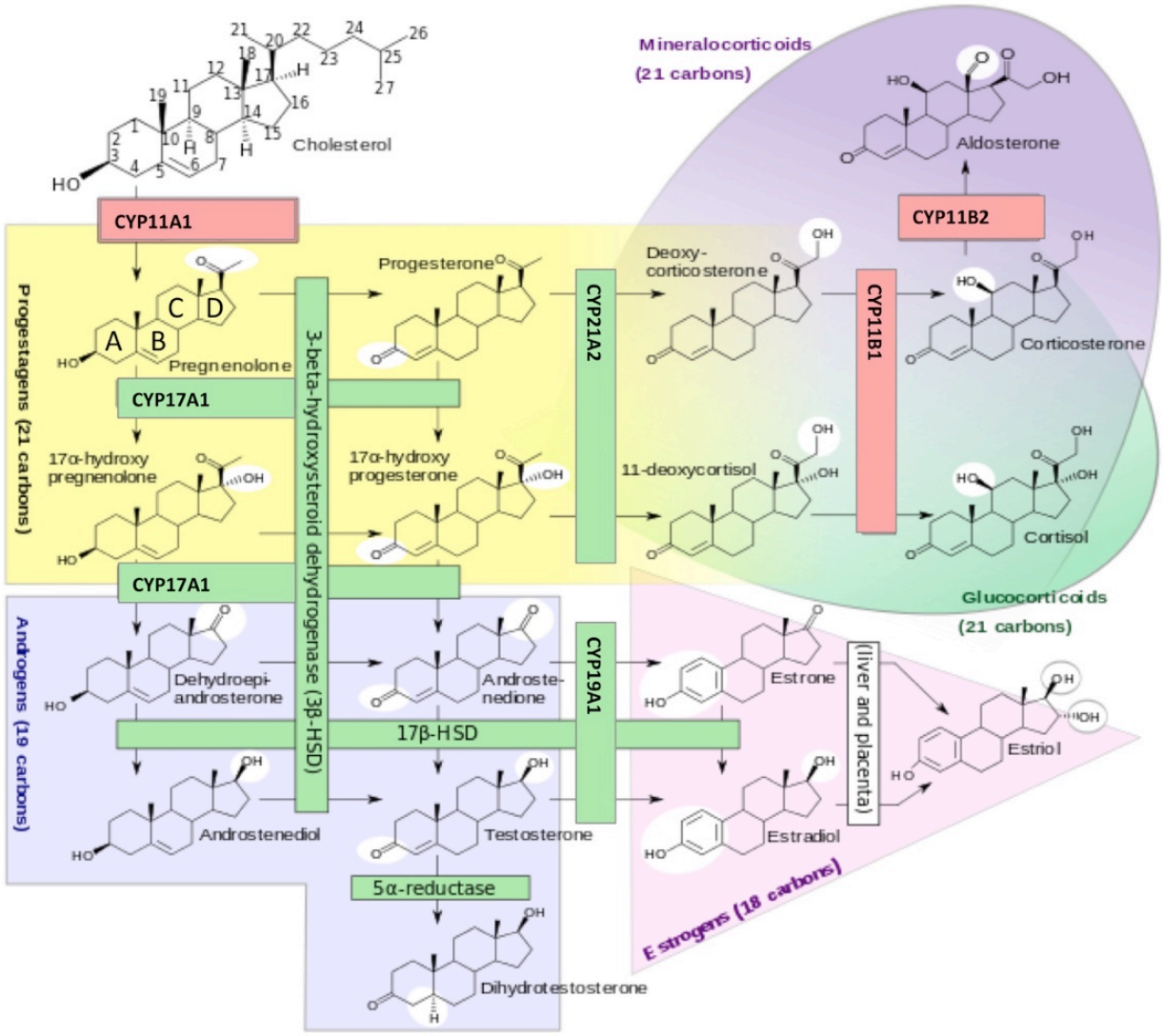

Figure 1.7: Biosynthesis of steroids. Figure adapted with permission from Mikael Haggestrom[30].

Although CYP17A1-mediated androgen production typically proceeds via Δ4 or Δ5 steroids, androgens can also be generated through an alternate "backdoor" pathway as a consequence of pathological states[31,32]. This alternate route for androgen production relies of conversion of 17α-hydroxyprogesterone to the reduced 17α-hydroxyallopregnanolone (Figure 1.8). 17α-hydroxyallopregnanolone is an efficient substrate for the CYP17A1-mediated 17,20-lyase reaction[33]. The 17,20-lyase product, androsterone, is then converted to dihydrotestosterone by hydroxysteroid dehydrogenase enzymes.

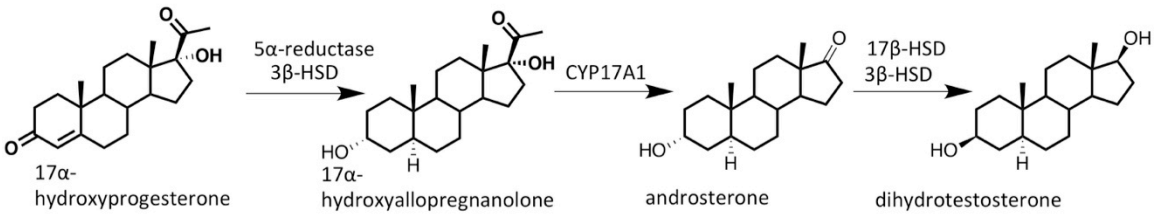

Figure 1.8: Dihydrotestosterone can be generated from 5α-reduced 17α-hydroxyallopregnanolone via the backdoor pathway. Participating enzymes include 5α-reductase, 3β-hydroxysteroid dehydrogenase (3β-HSD), and 17β-hydroxysteroid dehydrogenase (17β-HSD).

The role of P450 enzymes in steroid biosynthesis makes them crucial players in human health and disease. Some illnesses are the result of cytochrome 450 deficiencies or mutation of key residues in some steroidogenic cytochrome P450 enzymes. For example, congenital adrenal hyperplasia, a disorder characterized by ineffective glucocorticoid production and the androgen overproduction, is almost always the result of mutations on CYP21A2 or CYP11B1[34]. Inhibition of steroidogenic cytochrome P450 enzymes is desirable in some disease states, including sex hormone dependent cancers. Inhibition of CYP19A1 via small molecule inhibitors has been successfully utilized to treat estrogen-dependent breast cancer[35]. Inhibition of CYP17A1 is becoming a more common strategy for the treatment of androgen-dependent prostate cancer, but its ancillary role in corticosteroid biosynthesis and its similarity to other steroidogenic cytochrome P450 enzymes such as CYP21A2 complicate efforts to selectively target androgen biosynthesis by this enzyme.

CYP17A1 as a Target for the Treatment of Prostate Cancer

Prostate cancer is the most common cancer among American men and the second-leading cause of cancer-related deaths within the aforementioned demographic[36]. More than 80% of

prostate cancers rely on androgens, normally produced in the testes and adrenal gland, for tumor growth and proliferation[37]. Androgen deprivation therapy reduces the amount of circulating tumor-promoting androgens and has become the first line of treatment for more advanced stages of the disease. This can be achieved through either surgical orchiectomy or by preventing the secretion of gonadotropins that initiate androgen production in the testes (the primary site of androgen production) through the use of gonadotropin-releasing hormone (GnRH) agonists or antagonists. Although traditional androgen deprivation therapy significantly reduces the amount of circulating androgens, it does not prevent androgen biosynthesis in the adrenal gland. In addition to androgens produced through the normal function of the adrenal gland, tumor cells in advanced prostate cancer frequently develop the capacity for androgen production[38]. Androgen receptor antagonists are often administered in conjunction with GnRH agonists or antagonists to prevent receptor activation by such extragonadal androgens. Unfortunately long-term antagonism of the androgen receptor promotes the acquisition of various mutations that increase its affinity for the androgens responsible for its activation, or render it constitutively active[39].

Androgen deprivation therapy will often achieve an initial response in patients as indicated by a drop in the cancer biomarker prostate specific antigen (PSA). Unfortunately, over 80% of patients receiving this therapy relapse within 24 months of its outset and are diagnosed with "castration-resistant" prostate cancer[40]. A different treatment strategy is therefore necessary to manage advanced prostate cancer.

The most promising alternative to traditional ADT is the inhibition of androgen biosynthesis by inhibition of CYP17A1, which is required for production of androgens in all tissues via both normal and "backdoor" biosynthetic pathways. Preventing CYP17A1 catalysis

should therefore eliminate all circulating androgens capable of activating the androgen receptor and fueling tumor progression.

The first identified inhibitor of CYP17A1 was the antifungal agent ketoconazole, which was used off-label to treat castration-resistant prostate cancer. Although ketoconazole was shown to temporarily decrease PSA levels in patients, its promiscuous inhibition of xenobiotic-metabolizing cytochrome P450 enzymes made it a strong risk factor for drug-drug interactions and hepatotoxicity[41].

Knowledge of the role played by CYP17A1 in androgen biosynthesis allowed the development of more rationally-designed inhibitors. Analogs of pregnenolone, a steroidal substrate of the enzyme, were designed with iron-coordinating heteroaromatic rings built onto carbon 17, which is known to be hydroxylated by CYP17A1[42]. One such inhibitor, abiraterone, progressed rapidly through clinical trials. The prodrug form, abiraterone acetate, received FDA approval in 2012 for administration in combination with glucocorticoid predinsone. The X-ray crystal structure of CYP17A1 with abiraterone[43] shows that the pyridine ring on C17 does indeed coordinate the heme iron (Figure 1.9). The 3-hydroxyl group on the A-ring of the steroid participates in the only other direct interaction with CYP17A1, forming a hydrogen bond to asparagine 202 in the F helix.

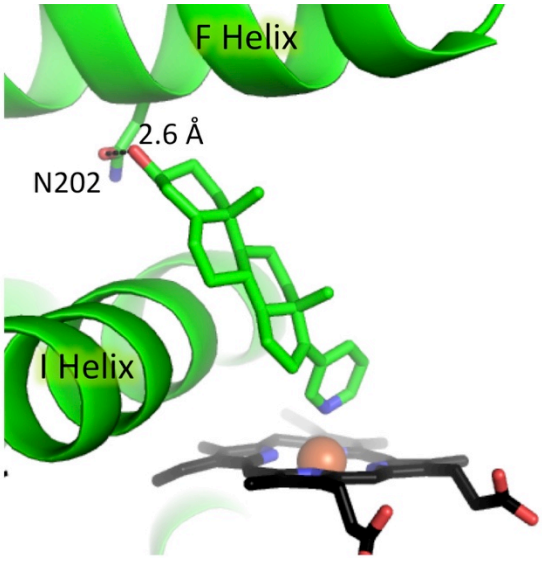

Figure 1.9: X-ray crystal structure of CYP17A1 with abiraterone[43] (shown in green sticks) demonstrates coordination of the inhibitor to the heme cofactor (shown in black sticks) and hydrogen bonding to residue N202.

In clinical trials, abiraterone in combination with prednisone was shown to reduce levels of circulating testosterone (and other androgens),[44,45] lower serum PSA levels,[45,46] and improve overall survival[47]. However, many patients also reported serious side effects from this course of treatment including hypertension, hypokalemia, and peripheral edema—all of which suggested an uncontrolled excess of mineralocorticoids[47].

As discussed previously in this chapter, CYP17A1 is not only responsible for androgen biosynthesis. It is also crucial to the production of glucocorticoids. The first of two reactions performed by CYP17A1 is a 17α-hydroxylase reaction, which generates intermediate products that can be converted into glucocorticoids (via CYP21A2 and CYP11B1) or androgens (via the 17,20-lyase reaction performed by CYP17A1). Inhibition of the first reaction (17α-hydroxylase) therefore results not only in lower circulating levels of androgens, but also decreases in the levels of circulating glucocorticoids. Glucocorticoid deficiency promotes the secretion of adrenocorticotropin hormone (ACTH), which then stimulates production of the

mineralocorticoids 11-deoxycorticosterone and corticosterone. This eventually leads to the secondary mineralocorticoid excess and the observed side effects in patients receiving abiraterone, even when prednisone is administered alongside abiraterone to mitigate such side effects. This secondary mineralocorticoid excess affects not only individuals undergoing CYP17A1 inhibition as prostate cancer treatment, but is also seen in individuals with CYP17A1 mutations that prevent normal 17α-hydroxyation by the enzyme[34], supporting the importance of CYP17A1 17α-hydroxylase function in maintaining corticosteroid balance.

The second reaction performed by CYP17A1 commits the 17α-hydroxylated steroids to the androgen pathway, and its inhibition is therefore crucial to achieve the desired response in patients with prostate cancer. Recently, there has been an initiative to develop compounds that selectively inhibit the 17,20-lyase reaction necessary for androgen biosynthesis, while allowing the 17α-hydroxylation crucial to corticosteroid balance to proceed normally.

It is not clear whether it would even be possible to selectively inhibit a single reaction in contrast to another reaction performed within a single shared active site. To do so requires extensive functional knowledge of the enzyme responsible. The studies conducted as part of this dissertation seek not only to expand functional knowledge of CYP17A1, but to also place it within a structural context by examining how CYP17A1 interacts with various substrates and inhibitors through X-ray crystallography.

Although the 17α-hydroxylase and 17,20 lyase reactions performed by CYP17A1 share an active site, there are some marked differences between the two that include the type of substrate turned over, requirement of partner proteins, and likely even the reactive oxygen species responsible for catalysis. As described earlier, both Δ4 steroids (such as progesterone) and Δ5 steroids (such as pregnenolone) are substrates for CYP17A1. The 17α-hydroxylase

reaction is known to proceed efficiently for both Δ4 progesterone and Δ5 pregnenolone, with some differences in the regioselectivity of the hydroxylation between the two. For example, 10-30% of the progesterone hydroxylation product is a secondary 16α-hydroxylated metabolite, while the corresponding metabolite is not observed for pregnenolone[48,49]. In contrast, the 17,20-lyase reaction proceeds with 11-fold higher efficiency for the Δ5 steroid, 17α-hydroxypregnenolone compared to its Δ4 counterpart, 17α-hydroxyprogesterone[28,50]. The structural basis for substrate preference based on the configuration of the steroid A ring in 17,20-lyase turnover and hydroxylase regioselectivity is explored in further detail as part of Chapter 3. The effects of A ring configuration on steroidal inhibitor interactions with CYP17A1 were also investigated and will be discussed in Chapter 4.

Another distinct difference in the 17-hydroxylase and 17,20 lyase reactions performed by CYP17A1 is the dependence of reaction rate on the partner protein cytochrome b_5. As mentioned previously, cytochrome b_5 can enhance, inhibit, or have no effect on cytochrome P450 turnover. While cytochrome b_5 is reported to have little effect on the rate of the CYP17A1 hydroxylase reaction, it significantly enhances turnover of 17,20-lyase reaction, and is virtually required for this reaction to proceed[28,51].

Finally, the two reactions performed by CYP17A1 are suggested to proceed via two different reactive oxygen species within the P450 catalytic cycle. Hydroxylation by cytochrome P450 enzymes is fairly well understood, and the 17α-hydroxylation is therefore most likely to proceed through the Groves' rebound mechanism, mediated by the ferryl oxo species called compound I(Figure 1.4, **g**). The 17,20-lyase reaction is a carbon-carbon bond cleavage reaction, which is more unusual for a cytochrome P450. The lyase reaction is not well understood as

alluded to previously, though studies with isotopically-labeled molecular oxygen have suggested that a ferric dioxygen species is responsible for catalysis of this reaction (Figure 1.5).

The possibility of selective inhibition of the 17,20-lyase reaction compared to hydroxylation is supported by some evidence based on clinically-observed mutations of CYP17A1. There are dozens of reported mutations in CYP17A1, most of which compromise both hydroxylation and 17,20-lyase function[43]. Examples include F114V and D116V, mutations of active site residues identified in patients with diagnosed 17α-hydroxylase/17,20-lyase deficiencies[52]. However, there have also been some reports of single-site mutations that appear to selectively prevent the 17,20-lyase reaction while allowing 17α-hydroxylation. Some of these residues (R347 and R358) are located on the proximal face of the enzyme and are known to contribute to binding of cytochrome b_5, which is necessary for 17,20-lyase turnover[53]. Mutation of residue E305 on the I helix to a glycine has been observed in a human male evaluated for gynecomastia resulting from very low androgen levels, but showed no abnormalities in corticosteroid balance. Further evaluation of this active site mutation similarly has confirmed that the mutation permits hydroxylation of both progesterone and pregnenolone, but prevents turnover of 17α-hydroxypregnenolone to DHEA[54]. This suggests that some features of the CYP17A1 active site may have different roles in the 17,20 lyase and hydroxylase reactions. Chapter 5 will examine the functional characterization of clinically-observed mutations in CYP17A1.

In addition to lyase-selective mutations, small molecule inhibitors of CYP17A1 have been identified that are reported to show selectivity for inhibition of the 17,20-lyase reaction over inhibition of 17α-hydroxylation, among them orteronel and VT-464. These inhibitors are not based on the steroidal scaffold, but instead share a naphthalene ring core and a

heteroaromatic substituent. Orteronel, an inhibitor developed by Takeda Pharmaceuticals, was reported to show 5-fold selectivity for inhibition of the 17,20-lyase reaction compared to the 17α-hydroxylase reaction *in vitro*[55]. Throughout clinical trials, orteronel was still administered in combination with prednisone, so it is not known if 5-fold selectivity for the 17,20-lyase reaction would substantially alleviate the mineralocorticoid-associated side effects, although some adverse effects (peripheral edema and hypokalemia) were reported less by patients receiving orteronel and prednisone in Phase III clinical trials than by patients receiving abiraterone and prednisone in the corresponding clinical trial for abiraterone[47,56]. Despite improvement in radiographic progression-free survival, orteronel failed to improve overall survival in Phase III clinical trials and its development was terminated in 2014.

The other non-steroidal inhibitor, VT-464, was also identified as a "lyase-selective" inhibitor of CYP17A1[57] and is currently in Phase II clinical trials[58]. VT-464 was reported to demonstrate 10-fold selectivity for 17,20-lyase inhibition compared to hydroxylase inhibition[57], but information regarding its *in vivo* efficacy and side effect profile have yet to be released.

Evaluation of the clinically-relevant CYP17A1 inhibitors, including abiraterone, orteronel, VT-464, and galeterone (an additional steroidal inhibitor currently in Phase III clinical trials) is subject to much variation in experimental conditions. These inhibitors are evaluated based on IC_{50} values determined under varied conditions, including different systems (whole cell vs. microsomal vs. purified proteins), varying substrates for the hydroxylase reaction (Δ4-progesterone vs. Δ5-pregnenolone), and different substrate concentrations. All of these factors can influence the apparent IC_{50} value, and there have been no reports of side-by-side evaluations for rank order potency of CYP17A1 inhibition and selective inhibition of the 17,20-lyase reaction of all four inhibitors that have been assessed in clinical trials. Chapter 6 focuses on

evaluation of these inhibitors side-by-side in a purified system to establish their relative potencies and determine whether or not the reported selectivity for 17,20-lyase inhibition by some inhibitors is actually mediated by CYP17A1.

The use of a steroidal scaffold for CYP17A1 inhibitors such as abiraterone make them susceptible to interaction with other receptors and steroid-metabolizing enzymes. One such enzyme is CYP21A2, which is responsible for corticosteroid biosynthesis. Abiraterone has been shown to bind and inhibit CYP21A2 (Victoria Jasion and Charlie Fehl, unpublished data). The effect of this interaction on the long-term efficacy of CYP17A1 inhibitors and corticosteroid levels has yet to be established. Off-target inhibition of CYP21A2 significantly complicates the steroid balance *in vivo*. CYP21A2 inhibition likely alters mineralocorticoid and glucocorticoid levels involved in the observed corticosteroid-related side effects, and might also increase levels of CYP17A1 substrate capable of overwhelming inhibition. Evaluation of the effects of CYP21A2 inhibition would be facilitated by the development of CYP17A1 inhibitors that are selective against CYP21A2 inhibition. However, such inhibitors have not been available and the structure of CYP21A2 was not known until recently to guide the design of such compounds. To inform the design of inhibitors with higher selectivity for CYP17A1 over CYP21A2, human CYP21A2 was crystallized in the presence of abiraterone and its structure was solved at a resolution of 2.74 Å. Despite an inability to model in ligand due to poor ligand density, the structure is consistent with the newly published structure of CYP21A2 with progesterone[59], as will be discussed further in Chapter 7.

Conclusion

Cytochrome P450 enzymes serve a variety of physiological functions, including the biosynthesis of steroid hormones. These steroid hormones are important for the development of secondary sex characteristics and regulating homeostasis, but they can also fuel tumor growth in hormone-dependent cancers. Due to the role of CYP17A1 in the biosynthesis of androgens, on which the majority of prostate cancers are dependent, its inhibition is a promising strategy for the treatment of prostate cancer. One of the challenges in using CYP17A1 inhibition to treat prostate cancer is effectively preventing androgen biosynthesis (via the 17,20-lyase reaction) without compromising its role in the generation of other physiologically-relevant classes of steroid hormones (via the 17α-hydroxylase reaction) or inhibiting other steroidogenic enzymes such as CYP21A2. The research described herein employs structural studies, enzymology, and inhibitor evaluation to better understand CYP17A1 function and inform the design of more potent and selective inhibitors of this enzyme as treatment for prostate cancer.

REFERENCES

(1) Guengerich, F. P.; Cheng, Q. *Pharmacol. Rev.* **2011**, *63*, 684.
(2) Jefcoate, C. R. *Methods Enzymol.* **1978**, *52*, 258.
(3) Schenkman, J. B.; Jansson, I. *Methods Mol. Biol.* **2006**, *320*, 11.
(4) Perera, R.; Sono, M.; Sigman, J. A.; Pfister, T. D.; Lu, Y.; Dawson, J. H. *Proc. Natl. Acad. Sci. U. S. A.* **2003**, *100*, 3641.
(5) Sun, Y.; Zeng, W.; Benabbas, A.; Ye, X.; Denisov, I.; Sligar, S. G.; Du, J.; Dawson, J. H.; Champion, P. M. *Biochemistry* **2013**, *52*, 5941.
(6) Denisov, I. G.; Sligar, S. G. In *Cytochrome P450: Structure, Mechanism and Biochemistry*; 4th ed.; Ortiz de Montellano, P., Ed.; Springer: New York, 2015, p 111.
(7) Groves, J. T.; McClusky, G. A. *Biochem. Biophys. Res. Commun.* **1978**, *81*, 154.
(8) Guengerich, F. P. *J. Biochem. Mol. Toxicol.* **2007**, *21*, 163.
(9) Munro, A. W.; Girvan, H. M.; McLean, K. J. *Nat. Prod. Rep.* **2007**, *24*, 585.
(10) Akhtar, M.; Wright, J. N.; Lee-Robichaud, P. *J. Steroid Biochem. Mol. Biol.* **2011**, *125*, 2.
(11) Yoshimoto, F. K.; Guengerich, F. P. *J. Am. Chem. Soc.* **2014**, *136*, 15016.
(12) Poulos, T. L.; Finzel, B. C.; Gunsalus, I. C.; Wagner, G. C.; Kraut, J. *J. Biol. Chem.* **1985**, *260*, 16122.

(13) von Wachenfeldt, C.; Richardson, T. H.; Cosme, J.; Johnson, E. F. *Arch. Biochem. Biophys.* **1997**, *339*, 107.
(14) Cosme, J.; Johnson, E. F. *J. Biol. Chem.* **2000**, *275*, 2545.
(15) Johnson, E. F.; Stout, C. D. *J. Biol. Chem.* **2013**, *288*, 17082.
(16) Poulos, T. L.; Johnson, E. F. In *Cytochrome P450: Structure, Mechanism, and Biochemistry*; 4th ed.; Ortiz de Montellano, P., Ed.; Springer: New York, 2015; Vol. I, p 3.
(17) Poulos, T. L.; Finzel, B. C.; Howard, A. J. *Biochemistry* **1986**, *25*, 5314.
(18) Scott, E. E.; White, M. A.; He, Y. A.; Johnson, E. F.; Stout, C. D.; Halpert, J. R. *J. Biol. Chem.* **2004**, *279*, 27294.
(19) Zhao, Y.; White, M. A.; Muralidhara, B. K.; Sun, L.; Halpert, J. R.; Stout, C. D. *J. Biol. Chem.* **2006**, *281*, 5973.
(20) De Lemos-Chiarandini, C.; Frey, A. B.; Sabatini, D. D.; Kreibich, G. *J. Cell Biol.* **1987**, *104*, 209.
(21) Scott, E. E.; He, Y. A.; Wester, M. R.; White, M. A.; Chin, C. C.; Halpert, J. R.; Johnson, E. F.; Stout, C. D. *Proc. Natl. Acad. Sci. U. S. A.* **2003**, *100*, 13196.
(22) Ekroos, M.; Sjogren, T. *Proc. Natl. Acad. Sci. U. S. A.* **2006**, *103*, 13682.
(23) Wester, M. R.; Johnson, E. F.; Marques-Soares, C.; Dijols, S.; Dansette, P. M.; Mansuy, D.; Stout, C. D. *Biochemistry* **2003**, *42*, 9335.
(24) Waskell, L.; Kim, J. P. In *Cytochrome P450: Structure, Mechanism, and Biochemistry*; 4th ed.; Ortiz de Montellano, P., Ed.; Springer: New York, 2015; Vol. I, p 33.
(25) Ahuja, S.; Jahr, N.; Im, S. C.; Vivekanandan, S.; Popovych, N.; Le Clair, S. V.; Huang, R.; Soong, R.; Xu, J.; Yamamoto, K.; Nanga, R. P.; Bridges, A.; Waskell, L.; Ramamoorthy, A. *J. Biol. Chem.* **2013**, *288*, 22080.
(26) Estrada, D. F.; Skinner, A. L.; Laurence, J. S.; Scott, E. E. *J. Biol. Chem.* **2014**, *289*, 14310.
(27) Yamazaki, H.; Nakamura, M.; Komatsu, T.; Ohyama, K.; Hatanaka, N.; Asahi, S.; Shimada, N.; Guengerich, F. P.; Shimada, T.; Nakajima, M.; Yokoi, T. *Protein Expr. Purif.* **2002**, *24*, 329.
(28) Auchus, R. J.; Lee, T. C.; Miller, W. L. *J. Biol. Chem.* **1998**, *273*, 3158.
(29) Nakajin, S.; Hall, P. F. *J. Biol. Chem.* **1981**, *256*, 3871.
(30) Haggstrom, M.; Richfield, D. In *Wikiversity Journal of Medicine* 2014.
(31) Kamrath, C.; Hochberg, Z.; Hartmann, M. F.; Remer, T.; Wudy, S. A. *J. Clin. Endocrinol. Metab.* **2012**, *97*, E367.
(32) Auchus, R. J. *Trends Endocrinol. Metab.* **2004**, *15*, 432.
(33) Gupta, M. K.; Guryev, O. L.; Auchus, R. J. *Arch. Biochem. Biophys.* **2003**, *418*, 151.
(34) Auchus, R. J.; Miller, W. L. In *Cytochrome P450: Structure, Mechanism, and Biochemistry*; 4th ed.; Ortiz de Montellano, P., Ed.; Springer: New York, 2015; Vol. II, p 851.
(35) Dowsett, M. *J. Steroid Biochem. Mol. Biol.* **1991**, *39*, 805.
(36) Edwards, B. K.; Noone, A. M.; Mariotto, A. B.; Simard, E. P.; Boscoe, F. P.; Henley, S. J.; Jemal, A.; Cho, H.; Anderson, R. N.; Kohler, B. A.; Eheman, C. R.; Ward, E. M. *Cancer* **2013**.
(37) Yin, L.; Hu, Q. *Nat. Rev. Urol.* **2014**, *11*, 32.
(38) Montgomery, R. B.; Mostaghel, E. A.; Vessella, R.; Hess, D. L.; Kalhorn, T. F.; Higano, C. S.; True, L. D.; Nelson, P. S. *Cancer Res.* **2008**, *68*, 4447.

(39) Grist, E.; de Bono, J. S.; Attard, G. *J. Steroid Biochem. Mol. Biol.* **2015**, *145*, 157.
(40) Gomez, L.; Kovac, J. R.; Lamb, D. J. *Steroids* **2015**, *95*, 80.
(41) Small, E. J.; Baron, A. D.; Fippin, L.; Apodaca, D. *J. Urol.* **1997**, *157*, 1204.
(42) Potter, G. A.; Barrie, S. E.; Jarman, M.; Rowlands, M. G. *J. Med. Chem.* **1995**, *38*, 2463.
(43) DeVore, N. M.; Scott, E. E. *Nature* **2012**, *482*, 116.
(44) O'Donnell, A.; Judson, I.; Dowsett, M.; Raynaud, F.; Dearnaley, D.; Mason, M.; Harland, S.; Robbins, A.; Halbert, G.; Nutley, B.; Jarman, M. *Br. J. Cancer.* **2004**, *90*, 2317.
(45) Ryan, C. J.; Smith, M. R.; Fong, L.; Rosenberg, J. E.; Kantoff, P.; Raynaud, F.; Martins, V.; Lee, G.; Kheoh, T.; Kim, J.; Molina, A.; Small, E. J. *J. Clin. Oncol.* **2010**, *28*, 1481.
(46) Danila, D. C.; Morris, M. J.; de Bono, J. S.; Ryan, C. J.; Denmeade, S. R.; Smith, M. R.; Taplin, M. E.; Bubley, G. J.; Kheoh, T.; Haqq, C.; Molina, A.; Anand, A.; Koscuiszka, M.; Larson, S. M.; Schwartz, L. H.; Fleisher, M.; Scher, H. I. *J. Clin. Oncol.* **2010**, *28*, 1496.
(47) Fizazi, K.; Scher, H. I.; Molina, A.; Logothetis, C. J.; Chi, K. N.; Jones, R. J.; Staffurth, J. N.; North, S.; Vogelzang, N. J.; Saad, F.; Mainwaring, P.; Harland, S.; Goodman, O. B., Jr.; Sternberg, C. N.; Li, J. H.; Kheoh, T.; Haqq, C. M.; de Bono, J. S.; Investigators, C.-A.-. *Lancet Onco.l* **2012**, *13*, 983.
(48) Swart, P.; Swart, A. C.; Waterman, M. R.; Estabrook, R. W.; Mason, J. I. *J. Clin. Endocrinol. Metab.* **1993**, *77*, 98.
(49) Yoshimoto, F. K.; Zhou, Y.; Peng, H. M.; Stidd, D.; Yoshimoto, J. A.; Sharma, K. K.; Matthew, S.; Auchus, R. J. *Biochemistry* **2012**, *51*, 7064.
(50) Fluck, C. E.; Miller, W. L.; Auchus, R. J. *J. Clin. Endocrinol. Metab.* **2003**, *88*, 3762.
(51) Katagiri, M.; Kagawa, N.; Waterman, M. R. *Arch. Biochem. Biophys.* **1995**, *317*, 343.
(52) Van Den Akker, E. L.; Koper, J. W.; Boehmer, A. L.; Themmen, A. P.; Verhoef-Post, M.; Timmerman, M. A.; Otten, B. J.; Drop, S. L.; De Jong, F. H. *J. Clin. Endocrinol. Metab.* **2002**, *87*, 5714.
(53) Lee-Robichaud, P.; Akhtar, M. E.; Wright, J. N.; Sheikh, Q. I.; Akhtar, M. *J. Steroid Biochem. Mol. Biol.* **2004**, *92*, 119.
(54) Sherbet, D. P.; Tiosano, D.; Kwist, K. M.; Hochberg, Z.; Auchus, R. J. *J. Biol. Chem.* **2003**, *278*, 48563.
(55) Yamaoka, M.; Hara, T.; Hitaka, T.; Kaku, T.; Takeuchi, T.; Takahashi, J.; Asahi, S.; Miki, H.; Tasaka, A.; Kusaka, M. *J. Steroid Biochem. Mol. Biol.* **2012**, *129*, 115.
(56) Saad, F.; Fizazi, K.; Jinga, V.; Efstathiou, E.; Fong, P. C.; Hart, L. L.; Jones, R.; McDermott, R.; Wirth, M.; Suzuki, K.; MacLean, D. B.; Wang, L.; Akaza, H.; Nelson, J.; Scher, H. I.; Dreicer, R.; Webb, I. J.; de Wit, R.; investigators, E.-P. *Lancet Oncol.* **2015**, *16*, 338.
(57) Rafferty, S. W.; Eisner, J. R.; Moore, W. R.; Schotzinger, R. J.; Hoekstra, W. J. *Bioorg. Med. Chem. Lett.* **2014**, *24*, 2444.
(58) *Clinicaltrials.gov* 2015.
(59) Pallan, P. S.; Wang, C.; Lei, L.; Yoshimoto, F. K.; Auchus, R. J.; Waterman, M. R.; Guengerich, F. P.; Egli, M. *J. Biol. Chem.* **2015**, *290*, 13128.

Chapter 2.

Methods

INTRODUCTION

Since the following chapters all focus on steroidogenic cytochrome P450 enzymes, many of the methods used for expression, purification, and analysis of these enzymes are used repeatedly as part of this work. The following chapter will describe methods common for CYP17A1, mutants of CYP17A1, and human P450 oxidoreductase as these methods are referred to in several different chapters. Expression and purification of rat cytochrome b_5 was performed by Natasha DeVore, a former lab member, as reported[1] and will not be discussed.

Purification of CYP21A2 is only relevant to chapter 7 and will be discussed there in more detail. Crystallization of cytochrome P450/ligand complexes vary throughout and will therefore be discussed individually in each relevant chapter.

METHODS

CYP17A1 Mutagenesis

The gene encoding CYP17A1 bearing an N-terminal truncation of the transmembrane helix (residues 2-19), a leading sequence "AKKT" from residues 20-23, and a four histidine tag at the C-terminus had previously been inserted into the pCWori$^+$ vector[2] containing the β-lactamase gene to generate the pCW/17A1Δ19H construct used throughout. Site-directed mutagenesis to generate CYP17A1 mutants A105L, F114V, D116V, R347H, and R358Q was carried out using Quikchange Lightning Site-Directed Mutagenesis Kit (Agilent).

Expression of Cytochrome P450 17A1[2,3]

E. coli cells (100 µL, JM109 strain) were combined with 1 µL of the pCW17A1Δ19H plasmid and incubated at 4 °C for thirty minutes. Cells were heated to 42 °C for 30 seconds and cooled to 4 °C for two minutes. Newly transformed cells were spread onto lysogeny broth agarose plates containing 50 µg/mL ampicillin or 100 µg/mL carbenicillin for plasmid selection. Plates were incubated overnight at 37 °C.

All media described in the following section contains 50 µg/mL ampicillin or 100 µg/mL carbenicillin to select for the pCWori+ vector. Starter cultures of lysogeny broth (5 mL) were inoculated with a single colony from an aforementioned plate and incubated at 37 °C with 220 rpm shaking for 6-8 hours. To scale up the culture volume, overnight cultures of lysogeny broth (250 mL) were inoculated with 50 µL of the starter culture and incubated overnight at 37 °C with 220 rpm shaking. Finally, terrific broth (1 L/ 2.8 L Ferbach flask) was inoculated with 10 mL of the latter overnight culture and incubated at 37 °C with 220 rpm shaking until reaching an optical density at 600 nm of 0.6-0.8. Expression of CYP17A1 was induced by addition of β-D-1-thiogalactopyranoside to a concentration of 0.5 mM. At the same time, expression media was also supplemented with 0.61 mM δ-aminolevulinic acid to augment heme biosynthesis. Cultures were incubated at 28 °C with 140 rpm shaking for an additional 48-72 hours. Cells were pelleted by repeated centrifugation at ~6000 x *g* and resuspended in 50 mM Tris HCl, pH 7.4, 20% glycerol, and 300 mM NaCl and stored at -80 °C until purification.

Purification of Cytochrome P450 17A1[2,3]

All stages of the purification were performed at 4 °C. CYP17A1 A105L mutant used for crystallization with substrates was purified using buffers supplemented with 50 μM of the intended substrate.

Cell pellets were thawed and lysed by sonication on ice (6 x 30 seconds with one minute intervals). Lysate was centrifuged at 9900 x *g* for 15 minutes to remove cellular debris. Membrane proteins were extracted by stirring the supernatant in the presence of 2% Emulgen-913 (Desert Biologicals) for 60 to 90 minutes followed by ultracentrifugation (100,000 x *g*) for one hour.

Supernatant was loaded onto a column (~30 mL) of Ni-NTA resin (GE Healthcare) pre-equilibrated with Ni buffer (50 mM Tris-HCl, pH 7.4, 20% glycerol, 300 mM NaCl, and 0.2% Emulgen 913). The column was subsequently washed with 2 column volumes (CV) of Ni buffer followed by 6 CV of Ni buffer supplemented with 100 mM glycine to remove contaminants forming non-specific interactions with the resin. Protein was eluted using 4 CV of Ni buffer supplemented with 100 mM glycine and 80 mM histidine. Elution fractions were pooled based on absorbance at a wavelength corresponding to the heme Soret peak (417 nm).

Pooled fractions were diluted 3 to 5-fold in CM buffer (50 mM Tris-HCl, pH 7.4, 20% glycerol, and 100 mM glycine) supplemented with 0.2% of the detergent Emulgen-913 and then loaded onto a 5 mL carboxymethyl sepharose fast-flow column (GE Healthcare) pre-equilibrated with CM buffer. The column was washed with 10 CV of CM buffer without detergent prior to elution with 5 CV CM buffer without detergent but supplemented with 500 mM NaCl. Fractions were pooled based on absorbance at 417 nm.

Pooled fractions were concentrated to ~1 mL and loaded onto a 120 mL Superdex 200 gel filtration column (GE Healthcare) pre-equilibrated with SEC buffer containing 50 mM Tris-HCl, pH 7.4, 20% glycerol, 100 mM glycine, and 500 mM NaCl. Chromatography was performed using an isocratic flow of the aforementioned SEC buffer. Fractions corresponding to the major peak absorbing at 417 nm were collected and pooled.

The concentration of cytochrome P450 used for binding assays and crystallography was determined based on heme absorbance in the absolute spectrum of the collected fractions[4]. Baseline absorbance from 700-250 nm was recorded for SEC buffer (800 µL, in both reference and sample cuvettes). A sample of the collected fractions (100 µL) was added to the sample cuvette and absorbance was recorded from 700-250 nm. Concentration of cytochrome P450 was determined based on Beer's Law, $c = \frac{A}{\varepsilon l}$, where A is the absorbance corresponding to the heme Soret peak (417 nm for unbound cytochrome P450, 393 or 424 nm for cytochrome P450 bound to type I or type II ligands, respectively), ε is the extinction coefficient of the heme Soret peak (a value of 0.100 $\mu M^{-1} cm^{-1}$ was used in all of the studies described herein) and *l* is the pathlength of the cuvette (1 cm).

Cytochrome P450 used for assays measuring enzymatic turnover or inhibition was quantified by shift in heme absorbance observed in the reduced carbon monoxide difference spectrum[4]. A sample of the collected fractions (100 µL) was diluted 9-fold in SEC buffer and treated with a few grains of sodium dithionite to reduce the enzyme. Baseline absorbance was recorded from 500-400 nm. The sample was treated with carbon monoxide (~50 bubbles) and absorbance measured from 500-400 nm. Spectra were recorded every minute until no further increase in absorbance at 450 nm was observed. Concentration of cytochrome P450 was determined using Beer's Law, $c = \frac{A}{\varepsilon l}$, where A is the absorbance at 450 nm, ε is the extinction

coefficient of reduced, carbon monoxide-bound heme ($0.091 \mu M^{-1}cm^{-1}$) and *l* is the pathlength of the cuvette (1 cm).

Mutagenesis, Expression, and Purification of Human P450 Oxidoreductase[3,5]

The gene for human NADPH-cytochrome P450 reductase bearing an N-terminal truncation of residues 2-27 and a C-terminal tag of three glycine residues followed by four histidine residues (G_3H_6) inserted into a pET22 vector was provided by the lab of Dr. Walter Miller[5]. Mutagenesis of residue 59 from lysine to glutamine to prevent proteolysis frequently observed at this site was conducted using Quikchange Lightning site-directed mutagenesis kit (Agilent).

The resulting pET22 vector with truncated hPORG_3H_6 K59Q insert (1 µL) was added to 50 µL of C41(DE3) competent cells and incubated on ice for 30 minutes. Cells were heat-shocked at 42 °C for 30 seconds, and returned to ice for 2 minutes. Transformed cells were spread on lysogeny broth agarose plates supplemented with 50 µM ampicillin and incubated overnight at 37 °C.

All expression media in the following was supplemented with 50 µM ampicillin or 100 µM carbenicillin to select for the pET vector. A starter culture consisting of lysogeny broth (5 mL) was inoculated with a single colony from the aforementioned plate and incubated at 37 °C for 6-8 hours with 220 rpm shaking. An overnight culture (250 mL lysogeny broth) was inoculated with 50 µL of the starter culture and incubated at 37 °C for ~18 hours.

Terrific broth (1 L/2.8 L Fernbach Flask) was inoculated with 35 mL overnight culture and incubated at 28 °C with 220 rpm shaking to an optical density of 0.4 at 600 nm. Expression was induced by addition of β-D-1-thiogalactopyranoside to a concentration of 0.5 mM.

Expression media was also supplemented with riboflavin to a concentration of 100 μM to facilitate flavin synthesis. Cells were incubated at 28 °C with 190 rpm shaking for 48 hours and harvested by repeated centrifugation at 6000 x *g* for 10 minute intervals. Cells were resuspended in buffer containing 20 mM Tris HCl, pH = 8.0, 300 mM NaCl, and 20% glycerol and frozen at -80 °C until purification.

All stages of $hPORG_3H_6$ K59Q purification were conducted at 4 °C. Cells were thawed and treated with a protease cocktail that included phenylmethylsulfonylfluoride (1 mM), aprotinin (10 μg/mL), leupeptin (10 μM), and pepstatin A (10 μM). Cells were lysed via sonication (5 x 1 minute with 1 minute intervals on ice) and centrifuged at 9900 x *g* for 15 minutes to remove cellular debris. Membrane proteins were extracted from the resulting supernatant by stirring in the presence of the detergent Triton X-100 (0.1% v/v) for 2.5-3.5 hours, followed by ultracentrifugation at 100,000 x *g* for 1 hour.

The reductase-containing supernatant was loaded onto a 40 mL column of Ni-NTA resin (GE Healthcare) that had been pre-equilibrated with reductase purification buffer (20 mM Tris HCl, pH 7.4, 300 mM NaCl, 20% glycerol, and 0.1% Triton X-100). The bound protein was washed with 2 CV of reductase purification buffer followed by 6 CV of reductase purification buffer supplemented with 100 mM glycine. The desired reductase protein was eluted by treating the column with 4 CV of reductase purification buffer supplemented with 100 mM glycine and 80 mM histidine. Fractions were pooled based on absorbance at 453 nm and 375 nm which correspond to the absorbance maxima of the enzyme's flavin cofactors.

The pooled fractions (30-50 mL) were dialyzed three times against 1 L of buffer containing 20 mM KPi, pH 7.4, and 20% glycerol. Each round of dialysis had a minimum duration of 8 hours.

The concentration of hPORG$_3$H$_6$ K59Q was determined via cytochrome *c* reduction assay. One unit of functional reductase is defined as the amount necessary to reduce 1 µmol of cytochrome *c* per minute. A sample of the dialyzed protein was diluted 50-fold in phosphate buffer (300 mM KPi, pH 7.7) and 2 µL of diluted sample added to a cuvette containing 988 µL of phosphate buffer with 0.05 mM cytochrome *c*. Reduced nicotinamide adenine dinucleotide phosphate (NADPH) was added to the cuvette to a concentration of 0.1 mg/mL and the reduction of cytochrome c was monitored over 300 seconds as an increase in absorbance at 550 nm.

The concentration of hPORG$_3$H$_6$ K59Q was calculated based on rate of cytochrome c reduction using the following equation[6]:

$$\frac{\Delta\text{Absorbance/min}}{21 \times 0.002\ \text{mL sample}} \times \text{dilution factor} = \frac{\text{x units/mL}}{4\ \text{units/nmol}} = \frac{\text{nmol}}{\text{L}}\ \text{hPORG}_3\text{H}_6\ \text{K59Q}$$

Spectral Ligand Binding Assay[7]

As described in Chapter 1, most cytochrome P450 enzymes are isolated in the resting state with a water coordinated to the heme iron. Addition of ligand that displaces the active site water results in a "type I" spectral shift of the heme Soret peak from 417 nm to ~393 nm. Addition of ligand that not only displaces the active site water, but also coordinates the heme iron itself, results in a "type II" spectral shift of the heme Soret peak from 417 nm to ~424 nm. Based on these spectral shifts, the fraction of ligand-bound cytochrome P450 can be monitored during titration with a ligand, and can be used to determine a dissociation constant (K_d) for the enzyme-ligand complex.

Cytochrome P450 17A1 was prepared at a concentration of 0.1 µM in buffer containing 50 mM Tris-HCl, pH 7.4, 20% glycerol, 100 mM glycine, and 500 mM NaCl. Five milliliters of the protein solution were added to both sample and reference cuvettes with 5 cm pathlength. The

absorbance was baselined from 500 to 300 nm and a spectrum was recorded from 500 to 300 nm to ensure the baseline was flat. The sample cuvette was titrated with ligand, while the reference cuvette was titrated with equivalent volumes of solvent. Following each addition, the solution containing CYP17A1 was incubated with ligand for 8 minutes at room temperature prior to collecting spectra from 500 – 300 nm. Iterative ligand titrations were performed and subsequent spectra collected until no change in absorbance was observed following several additions. Concentration of solvent did not exceed 2% over the course of titration.

Dissociation constants (K_d) were determined using Graphpad Prism 5 (Graphpad Software). Ligand concentration was plotted against change in absorbance (A_{max}-A_{min}) using the nonlinear least-squares regression to the following equation:

$$[ML] = \frac{-b \pm \sqrt{b^2 - 4ac}}{2a}$$

$$a = -1, b = K_d + L_{total} + A_{max}, c = -1 \times L_{total} \times A_{max}$$

where *[ML]* is total binding, K_d is the dissociation constant, L_{total} is the total concentration of ligand in solution, and A_{max} is the maximum absorbance[8].

Progesterone Hydroxylation Assay[2,3]

Hydroxylation of progesterone by CYP17A1 and CYP17A1 mutants was monitored by HPLC coupled with UV/Vis detection (Shimadzu Scientific Instruments). The reconstituted protein system (50 pmol CYP17A1 with 200 pmol hPORG_3H_6 K59Q) was added to buffer (50 mM Tris HCl, pH 7.4, 5 mM magnesium chloride) containing progesterone (0-200 μM) to yield a total volume of 480 μL. Samples were incubated at 37 °C for 3 minutes prior to initiation of reactions. Reduced nicotinamide adenine diphosphate (NADPH) was added to samples to a concentration of 1 mM to initiate P450 catalysis. After 10 minutes reactions were quenched by

addition of 20% trichloroacetic acid (300 µL) to precipitate all proteins. Precipitated proteins were removed by centrifugation at 4500 x g for 8 minutes. Standards contained varying quantities of 17α-hydroxyprogesterone, 16α-hydroxyprogesterone, or 21-hydroxyprogesterone in buffer (50 mM Tris HCl, pH=7.4, 5 mM magnesium chloride) with 1 mM NADPH and 300 µL of 20% trichloroacetic acid.

Thirty-five microliters of standards and samples were injected onto a Luna C18, 5 micron, 50 x 4.60 mm column (Phenomenex, Torrance, CA) and separated using a mobile phase consisting of 40% acetonitrile, 59.99% deionized water and 0.012% acetic acid and a flow rate of 1 mL/minute. Metabolites were detected at 248 nm with retention times of ~5.5 minutes, ~4.1 minutes, and ~2.2 minutes for 17α-hydroxyprogesterone, 21-hydroxyprogesterone, and 16α-hydroxyprogesterone, respectively.

To determine steady-state kinetic parameters, enzymatic activity (in pmol product/min/pmol P450) was determined using the slope of linear regression generated based on standards. Kinetic parameters were determined by Graphpad Prism 5 (Graphpad Software, San Diego, CA) based on the least-squares nonlinear fit of the data to the following equation:

$$Y = \frac{V_{max} \times [S]}{K_m + [S]}$$

where V_{max} is maximal velocity of the reaction, K_m is the Michaelis-Menten constant, and *[S]* is the concentration of substrate.[9]

Pregnenolone Hydroxylation /17α-Hydroxypregnenolone 17,20-Lyase Assay[3,10]

Hydroxylation of pregnenolone and the 17,20-lyase reaction of 17α-hydroxypregnenolone by CYP17A1 and CYP17A1 mutants were monitored by gas chromatography/mass spectrometry using an Agilent 5975 Series GC/MS (Agilent Technologies). The reconstituted protein system

(50 pmol CYP17A1 with 200 pmol hPORG_3H_6 K59Q for pregnenolone hydroxylation, with 200 pmol of rat cytochrome b_5 added for the 17,20-lyase reaction) was added to buffer (50 mM Tris HCl, pH 7.4, 5 mM magnesium chloride) containing pregnenolone (0-7 μM) or 17α-hydroxypregnenolone (0-20 μM) to yield a total volume of 480 μL. All samples were incubated at 37 °C for 3 minutes prior to initiation of reactions. Reduced nicotinamide adenine diphosphate (NADPH) was added to samples to a concentration of 1 mM to initiate P450 catalysis. After 10 minutes, reactions were quenched by protein precipitation with the addition of 20% trichloroacetic acid (300 μL) supplemented with the internal standard estriol (8.66 μg/mL). Standards contained varying quantities of the 17α-hydroxypregnenolone or dehydroepiandrosterone (DHEA) metabolites in buffer (50 mM Tris HCl, pH 7.4, 5 mM magnesium chloride) with 1 mM NADPH and 300 μL of 20% trichloroacetic acid and were supplemented with 8.66 μg/mL estriol as an internal standard.

Six-hundred and fifty microliters of both samples and standards were loaded onto SPE columns (HLB cartridge, 1 mL, 30 mg packing) pre-equilibrated with 2 mL methanol, followed by 2 mL H_2O. The columns were washed with 1 mL H_2O following sample loading and steroids eluted using 1 mL of methanol followed by 3 mL of 1:2 dichloromethane:methanol. Solvent was removed from the elutant, and the resulting dried material was resuspended in 100 μL derivitization reagent (a 4:2:1 mixture of N-methyl-N-(trimethylsilyl)-trifluoroacetamide/ammonium iodide/dithioerythritol) and heated to 60 °C for 40-60 minutes. Following derivatization, silylated metabolites were quantified by GC/MS. Each sample (3 μL for lyase and 5 μL for hydroxylase) was injected onto a capillary column (Agilent DB-5MS, 15 x 0.25-mm inner diameter with 0.25-micron film) using an injector temperature of 280 °C. The oven temperature (initially 215 °C) was ramped at 1 °C/min for 21.5 minutes. The electron

energy and inlet temperature were 70 eV and 280 °C, respectively. Selected ion monitoring mode was used to analyze ions corresponding to the masses of the silylated products 17α-hydroxypregnenolone (m/z=548.3, retention time ~16.5 minutes) and dehydroepiandrosterone (m/z=432.3, retention time ~7.9 minutes), which were quantified with respect to silylated estriol (m/z = 504.3, retention time ~15.7 minutes).

Steady state parameters for both pregnenolone hydroxylation and 17α-hydroxypregnenolone 17,20-lyase were determined using Graphpad Prism 5 (Graphpad Software) as described for progesterone hydroxylation.

REFERENCES

(1) Holmans, P. L.; Shet, M. S.; Martin-Wixtrom, C. A.; Fisher, C. W.; Estabrook, R. W. *Arch. Biochem. Biophys.* **1994**, *312*, 554.
(2) DeVore, N. M.; Scott, E. E. *Nature* **2012**, *482*, 116.
(3) Petrunak, E. M.; DeVore, N. M.; Porubsky, P. R.; Scott, E. E. *J. Biol. Chem.* **2014**, *289*, 32952.
(4) Schenkman, J. B.; Jansson, I. *Methods Mol. Biol.* **2006**, *320*, 11.
(5) Sandee, D.; Miller, W. L. *Endocrinology* **2011**, *152*, 2904.
(6) Shen, A. L.; Porter, T. D.; Wilson, T. E.; Kasper, C. B. *J. Biol. Chem.* **1989**, *264*, 7584.
(7) DeVore, N. M.; Smith, B. D.; Wang, J. L.; Lushington, G. H.; Scott, E. E. *Drug Metab. Dispos.* **2009**, *37*, 1319.
(8) Zhao, Y.; White, M. A.; Muralidhara, B. K.; Sun, L.; Halpert, J. R.; Stout, C. D. *J. Biol. Chem.* **2006**, *281*, 5973.
(9) Copeland, R. A. In *Evaluation of Enzyme Inhibitors in Drug Discovery: A Guide for Medicinal Chemists and Pharmacologists*; 2nd ed.; John Wiley & Sons: Hoboken, NJ, 2013.
(10) Moon, J. Y.; Kang, S. M.; Lee, J.; Cho, J. Y.; Moon, M. H.; Jang, I. J.; Chung, B. C.; Choi, M. H. *Ther. Drug Monit.* **2013**, *35*, 473.

Chapter 3.

Structures of Human Steroidogenic Cytochrome P450 17A1 (CYP17A1) with Substrates

From publication by Petrunak, E. M.; DeVore, N. M.; Porubsky, P. R.; Scott, E. E. *J. Biol. Chem.* **2014**, *289*, 32952.

INTRODUCTION

The cytochrome P450 superfamily of heme monooxygenases performs diverse physiological functions, ranging from drug and xenobiotic metabolism to hormone and vitamin biosynthesis. The human cytochrome P450 (P450)[2] enzyme 17A1 (CYP17A1) functions specifically at a critical juncture in human steroidogenesis[1]. Its initial substrates are also substrates for mineralocorticoid biosynthesis by other enzymes. CYP17A1 catalysis leads to either steroid precursors of glucocorticoids like cortisol that regulate immune response or androgens like testosterone that drive the development and maintenance of male characteristics or are converted to estrogens in females[2]. In later life, however, androgens drive the development of prostate cancer, the cancer of highest incidence and the second leading cause of cancer deaths in U.S. men, while estrogens are a long-recognized driver of hormone responsive breast cancer[3]. Thus this enzyme has garnered substantial interest as a relatively new drug target, validated by successful use of the CYP17A1 inhibitor abiraterone in men with castration-resistant prostate cancer[4-6] and its current evaluation in breast cancer patients.

Abiraterone acetate, the FDA-approved prodrug form of this CYP17A1 inhibitor, improves overall survival in men with metastatic castration-resistant prostate cancer, including patients for whom the disease has progressed following chemotherapy, with compounds such as docetaxel and the androgen receptor blocker enzalutamide[5,7]. Abiraterone binds with high

affinity to the CYP17A1 active site heme iron[8] that is essential for catalysis, which effectively and systemically prevents androgen production. However, by doing so, this inhibitor also increases the pool of precursors for mineralocorticoid production and halts CYP17A1-mediated production of glucocorticoids, which occurs in the same active site and also requires the heme iron. The resulting steroid imbalances in patients treated with abiraterone can frequently lead to hypertension, hypokalemia, and adrenocortical insufficiency, which must then be monitored and treated with additional drugs[9]. Furthermore, there is some evidence that the increase in mineralocorticoids associated with complete inhibition of CYP17A1 may facilitate the flow of androgen precursors through a "backdoor" androgen biosynthesis pathway[10], proposed to provide a possible escape route that could permit cancer progression. Selective inhibition of the CYP17A1-mediated androgen biosynthesis proven to increase overall survival, while sparing CYP17A1-mediated glucocorticoid biosynthesis to prevent corticosteroid imbalances would ameliorate both of these clinically relevant issues for prostate cancer patients. CYP17A1 impairment has also been associated with Cushing's syndrome[11], some forms of congenital adrenal hyperplasia [12], and polysystic ovary syndrome[13-15]. Substantial potential for improving prostate cancer treatment and therapies for these other diseases thus lies in an improved understanding of the mechanisms whereby CYP17A1 performs catalysis.

In general, CYP17A1 hydroxylates the mineralocorticoid precursor steroids pregnenolone and progesterone to yield 17 α-hydroxypregnenolone and 17α-hydroxyprogesterone, respectively (Figure 3.1). These resulting C17-hydroxylated steroids can serve as substrates for glucocorticoid biosynthesis or for the subsequent CYP17A1-mediated 17,20 lyase reaction to yield the androgens dehydroepiandrosterone or androstenedione (Figure

3.1). Functional variations on this general pathway for different substrates provide clues to key protein/small molecule interactions that direct catalysis.

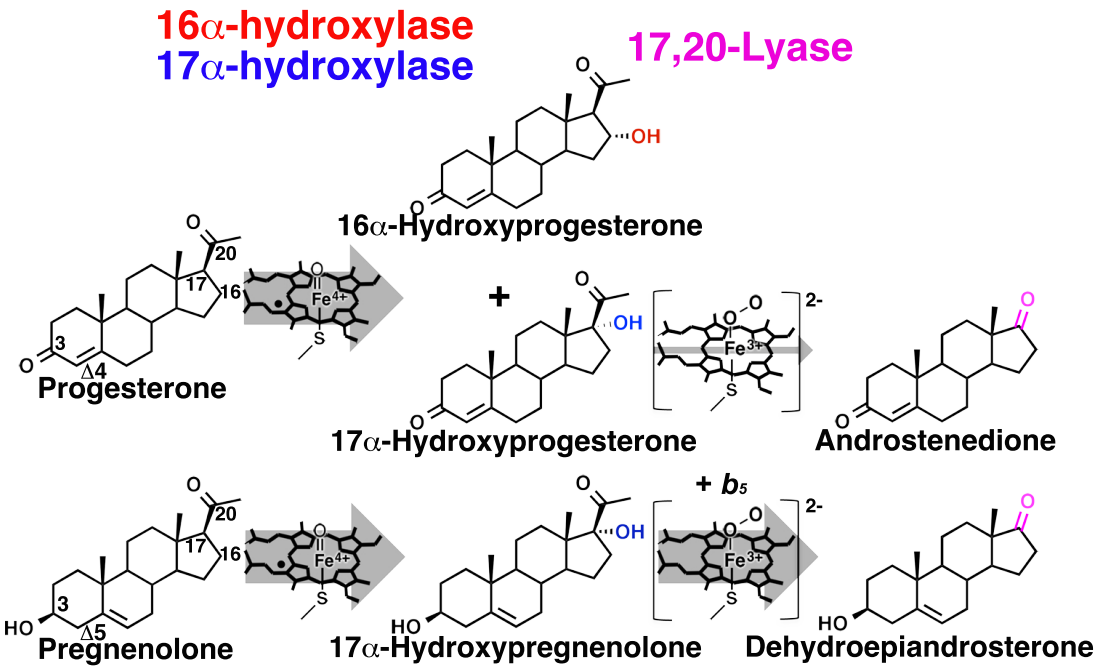

Figure 3.1: Summary of human cytochrome P450 17A1 reactions. Progesterone is hydroxylated at either C16 (minor, red) or C17 (major, blue) via Groves hydrogen abstraction and rebound mediated by the typical P450 iron (IV)-oxo intermediate [16]. The resulting 17α-hydroxyprogesterone metabolite undergoes the 17,20 lyase reaction to androstenedione (pink) with very low efficiency. Conversely, pregnenolone is hydroxylated only at C17 (blue). The resulting 17α-hydroxypregnenolone metabolite efficiently undergoes the 17,20 lyase reaction to form the 19-carbon androgen dehydroepiandrosterone (pink), proposed to occur via an iron-peroxy intermediate [17]. The latter reaction is facilitated as much as 10-fold by the presence of cytochrome b_5 [18]. CYP17A1 hydroxylase substrates progesterone and pregnenolone are also converted to mineralocorticoids and 17α-hydroxy products to glucocorticoids, largely by other cytochrome P450 enzymes.

First, while human CYP17A1 hydroxylates pregnenolone (a Δ5,3-ol steroid) only at carbon 17, progesterone (the corresponding Δ4,3-keto steroid) is hydroxylated at C17 as the major product, but also at C16 to generate an additional minor product (Figure 3.1) [19,20]. It is known that in other species CYP17A1 with Leu at position 105 generates much less 16α-hydroxyprogesterone[20] and that an A105L mutation in the human CYP17A1 enzyme decreases

progesterone 16α-hydroxylation and increases its 17α-hydroxylation[21]. Suggested to somehow alter substrate position in the CYP17A1 active site or alter protein flexibility, the structural basis for the effects of the A105L mutation wild type substrate and regio-selectivity of hydroxylation have not been elucidated experimentally.

Second, CYP17A1 also performs a carbon-carbon bond cleavage, which is unusual for cytochrome P450 enzymes[22]. For human CYP17A1 this 17,20-lyase reaction proceeds far less efficiently for the Δ4,3-keto 17α-hydroxyprogesterone substrate than for its counterpart, the Δ5,3-ol hydroxylated steroid 17α-hydroxypregnenolone (Figure 3.1). As a result, the Δ5,3-ol 17α-hydroxypregnenolone 17,20-lyase product dehydroepiandrosterone (Figure 3.1) is the physiologically-relevant intermediate in the formation of all human androgens and estrogens[23]. Although hydroxylation is well established to occur by the Groves hydrogen abstraction/oxygen rebound mechanism mediated by an Fe(IV)-oxo catalytic intermediate called Compound I[16,24] (Figure 3.1), a mechanism for cleavage of the bond between carbons 17 and 20 has been an ongoing debate in the literature. Recent data, however, favors a ferric peroxy anion intermediate (Figure 3.1)[17,25] and spectroscopic evidence has suggested that the two 17α-hydroxy steroids might interact differentially with the peroxy intermediate[26].

Third, while the presence of cytochrome b_5 has relatively little effect on the hydroxylation reactions, the presence of this small heme protein[18,27-29] substantially and selectively facilitates the 17,20-lyase reaction. Compartmentalization of b_5 and developmental changes in b_5 levels control the tissue specificity and timing of androgen production in humans. Individuals with nonfunctional b_5 are unable to perform the lyase reaction and produce sex steroids, though the hydroxylase reaction required for glucocorticoid synthesis is operational[30,31]. Facilitation of the lyase reaction by b_5 occurs without electron delivery[18]. Thus it has been

suggested that b_5 might selectively stabilize the intermediate in the lyase reaction or cause substrates to assume orientations in the CYP17A1 active site more favorable for the lyase chemistry, but the mechanism remains unresolved[32].

The structural basis for each of these effects—hydroxylase substrate regioselectivity, lyase reaction selectivity for the Δ4,3-keto vs. Δ5,3-ol 17-hydroxylated substrate, and cytochrome b_5 facilitation of the lyase vs. hydroxylase reaction—is unknown. Homology models and docking studies have suggested that substrates were likely to orient essentially parallel to the plane of the heme[33] and proposed a "bi-lobed" active site to carry out the separate hydroxylase and lyase reactions of CYP17A1[34-37]. The only known structures of CYP17A1, in the presence of the steroidal inhibitors abiraterone or TOK-001, were published recently[8]. These steroidal inhibitors both orient more nearly perpendicular to the heme, evoking the prediction of a similar binding mode for substrates[8], but the actual binding of CYP17A1 substrates is unknown.

To probe the binding orientations of the physiologically-relevant substrates and the structural basis of CYP17A1 function, a series of experimental X-ray structures were generated for CYP17A1 in complexes with both hydroxylase and both lyase substrates with the mutation A105L. Comparisons among these structures identify steric and hydrogen bonding interactions between CYP17A1 and distal portions of the substrate that play key roles in modulating spatial relationships between sites of metabolism on the opposite end of substrates and the catalytic heme iron. A steric rationale is provided for hydroxylase regioselectivity, while differences observed for hydrogen bonding and substrate positioning may form the basis for substrate selectivity of the lyase reaction. This new information informs a working hypothesis for how cytochrome b_5 might selectively facilitate the lyase reaction.

METHODS

Mutagenesis

The A105L mutant was generated via site-directed mutagenesis as described in Chapter 2.

Protein Expression and Purification

CYP17A1, CYP17A1 A105L mutant, and human NADPH-cytochrome P450 reductase were expressed and purified as described in Chapter 2. Cytochrome b_5 was produced by Natasha DeVore.

Assays

Spectral ligand binding assays were performed as described in Chapter 2. Progesterone hydroxylation, pregnenolone hydroxylation, and 17α-pregnenolone 17,20-lyase activity were all evaluated as described in Chapter 2.

Protein Crystallization, Data Collection, and Structure Determination

CYP17A1 A105L was crystallized by hanging drop vapor diffusion. Purified protein (~29 mg/mL) containing either 50 μM of one of the substrates or 10 μM abiraterone and 0.5% Emulgen-913 was mixed 1:1 to form 2 μl drops that were equilibrated against precipitant solution at 20 °C. The precipitant solution used to crystallize CYP17A1 A105L with progesterone, pregnenolone, 17α-hydroxypregnenolone, and abiraterone consisted of 100 mM Tris-HCl, pH 8.5, 25% PEG 4000 (Hampton Research), 150 mM magnesium chloride hexahydrate, and 4-6% glycerol. The precipitant solution used to crystallize CYP17A1 A105L with 17α-hydroxyprogesterone contained 175 mM Tris-HCl, pH 8.5, 30% PEG 3350 (Hampton Research), 250 mM lithium sulfate and 3% glycerol. Crystals were cryoprotected in a 7:3

mixture of mother liquor and 80% glycerol and flash cooled in liquid nitrogen. Diffraction data were collected on beamlines 14-1 and 12-2 of the Stanford Synchrotron Radiation Lightsource and processed using XDS[38]. Data collection and refinement statistics and deposition IDs in the Protein Data Bank are given in Table 3.1. Structures were solved by molecular replacement using Phaser[39] and the structure of wild type CYP17A1 (PDB 3RUK or 3SWZ[8]) as a search model using data to the respective resolution cutoff for the different structures (2.5-3.0 Å), yielding log likelihoods of 9,094-13,090. Model-building and refinement were performed iteratively with Coot[40] and PHENIX[41], respectively using data to a cutoff of $\langle I/\sigma(I) \rangle$ of 1.5 or higher in the outer shell. Hydrogens were modeled in the riding positions for protein and substrates. Reference model restraints were incorporated only for the 3.0 Å 17α-hydroxypregnenolone data set, in order to avoid overfitting. After the protein structures were essentially completed, ligands were added. The ligand-omit 2Fo-Fc maps shown were calculated in PHENIX. Ligand models were obtained from the Hetero-compound Information Center at Uppsala (HIC-Up) or constructed using the PRODRG2 server. Superpositions between CYP17A1 molecules were generated using the secondary structure matching algorithm in COOT[40]. Superposition between $P450_{cam}$ and CYP17A1 was generated by the same process, then optimized using least squares fit for the hemes, also in COOT[40]. Probe-occupied active site volumes were generated using VOIDOO[42] (probe radius = 1.4 Å; grid spacing = 0.33). Figures were prepared in PyMOL[43].

Table 3.1. Statistics for X-ray data collection and refinement of CYP17A1 A105L structures with abiraterone and substrates.

	CYP17A1 A105L abiraterone	**CYP17A1 A105L pregnenolone**	**CYP17A1 A105L progesterone**	**CYP17A1 A105L 17α-hydroxy-progesterone**	**CYP17A1 A105L 17α-hydroxy-pregnenolone**
PDB ID	4NKV	4NKW	4NKX	4NKY	4NKZ
Data Collection					
Beamline	SSRL 12-2	SSRL14-1	SSRL 12-2	SSRL 12-2	SSRL 12-2
Space group	$P2_12_12_1$	$P2_12_12_1$	$P2_12_12_1$	$P2_12_12_1$	$P2_12_12_1$
Cell dimensions					
a,b,c, (Å)	90.7, 153.3, 167.7	86.1, 152.6, 173.8	85.9, 153.0, 173.2	91.3, 151.8, 168.0	85.8, 151.1, 170.3
Molecules/a.u.	4	4	4	4	4
Resolution (Å)*	39.31–2.65 (2.79–2.65)	39.11-2.50 (2.63-2.50)	39.13-2.79 (2.94-2.79)	39.15-2.55 (2.69-2.55)	38.70-3.00 (3.17-3.00)
Total reflections*	450,626 (62,230)	557,941 (64,186)	380,303 (52,751)	511,008 (71,923)	287,854 (36,646)
Unique reflections*	68,380 (9,523)	79,365 (11,000)	56,987 (7,891)	76,008 (10,667)	44,496 (6,106)
Redundancy*	6.6 (6.5)	7.0 (5.8)	6.7 (6.7)	6.7 (6.7)	6.5 (6.0)
R_{pim}*	0.044 (0.556)	0.060 (0.717)	0.074 (0.579)	0.060 (0.666)	0.080 (0.650)
$\langle I/\sigma(I)\rangle$*	6.8 (1.5)	11.0 (2.1)	9.7 (1.5)	12.3 (1.5)	8.9 (1.5)
Completeness (%)*	99.3 (96.1)	99.3 (95.6)	99.2 (95.5)	99.1 (96.3)	98.9 (94.3)
Refinement					
Resolution (Å)	38.59-2.65	39.11-2.50	39.13-2.80	39.15-2.55	38.70-3.00
No. reflections	68,166	79,236	56,820	75,825	43,862
R/R_{free} (%)	19.1 / 24.3	18.9 / 24.5	18.4 / 25.7	17.8 / 24.4	19.1 / 26.1
Ramachandran (%)					
Favored	96.44	95.50	95.63	96.46	96.78
Allowed	3.45	4.39	4.26	3.54	3.06
Outliers	0.11	0.11	0.11	0	0.16
Wilson B factor ($Å^2$)	61.4	52.8	56.9	51.4	68.6
No. atoms/B factors ($Å^2$)					
Protein	14913 / 71.6	14852 / 71.8	14925 / 59.3	14832 / 56.8	14806 / 80.1
Ligand	104 / 36.7	92 / 61.1	92 / 46.3	96 / 52.3	96 / 65.7
Heme	172 / 50.5	172 / 50.4	172 / 41.9	172 / 44.1	172 / 63.8
Water	139 / 50.4	87 / 52.6	46 / 37.4	161 / 44.5	8 / 65.9
RMSD bond (Å)	0.011	0.008	0.008	0.007	0.010
RMSD angle (°)	1.2	1.2	1.1	1.2	1.3
Coordinate error (maximum-likelihood based) (Å)	0.41	0.34	0.41	0.33	0.39
Key bond distances and angles**					
N/O_{N202}–O3 (Å)	2.7 ± 0.1	2.8 ± 0.1	2.7 ± 0.3	2.9 ± 0.05	2.8, 2.5, 3.8, 3.0
∠C3–O3–N/O_{N202} (°) (°)	102 ± 3	121 ± 5	121 ± 7	137 ± 4	144, 132, 135, 136
C16 – Fe (Å)	5.9 ± 0.2	4.9 ± 0.2	4.8 ± 0.2	4.7 ± 0.1	5.1, 5.1, 4.6, 4.7
C17 – Fe (Å)	5.7 ± 0.1	4.8 ± 0.1	4.8 ± 0.1	5.0 ± 0.1	4.8, 4.8, 4.4, 4.6
C20 – Fe (Å)	4.6 ± 0.2	4.6 ± 0.1	4.6 ± 0.1	4.6 ± 0.2	4.6, 4.6, 4.4, 4.4

*Statistics corresponding to the highest resolution shell are in parentheses.

RESULTS

Characterization of CYP17A1 ligand binding and substrate metabolism

In order to compare the interactions of CYP17A1 with its various substrates and products, upon A105L mutation, and with structural findings, both dissociation constants and steady-state kinetic parameters were measured (Table 3.2). CYP17A1 affinities for steroid substrates and products were evaluated by monitoring the spectral shift associated with displacement of an active site water from the heme iron that occurs as ligands bind adjacent to the heme. Steady-state kinetic parameters were determined for all three substrates with appreciable product formation (progesterone and pregnenolone 17-hydroxylation reactions and the 17α-hydroxypregnenolone 17,20 lyase reaction).

Table 3.2. Substrate binding, progesterone hydroxylase activity, and steady state kinetic parameters for progesterone C17 hydroxylation by CYP17A1 wild type vs. A105L mutant.

	Wild Type	**A105L**
Steroid substrate and product K_d values (nM)		
Pregnenolone	<100[8]	<100
Progesterone	230 ± 10[8]	<100
17α-hydroxypregnenolone	210 ± 7	<100
17α-hydroxyprogesterone	330 ± 20	390 ± 90
16α-hydroxyprogesterone	8700 ± 600	8900 ± 600
Progesterone 17α-Hydroxylation kinetics		
k_{cat} (min^{-1})	1.01 ± 0.05	1.16 ± 0.01
K_m (μM)	10 ± 2	2.0 ± 0.1
Pregnenolone 17α-Hydroxylation kinetics		
k_{cat} (min^{-1})	0.39 ± 0.03	0.39 ± 0.03
K_m (μM)	0.9 ± 0.2	0.38 ± 0.09
17,20-Lyase kinetics		
k_{cat} (min^{-1})	0.24 ± 0.02	1.21 ± 0.08
K_m (μM)	1.2 ± 0.3	1.2 ± 0.3

Progesterone binds more tightly to wild type CYP17A1 than either its major (17α-) or minor (16α-) hydroxylation products, with the 16α-hydroxyl conferring a notable >80-fold decrease in affinity (Table 3.2). Similarly, pregnenolone binds wild type CYP17A1 more tightly than its 17α-hydroxylated product. Higher affinities are observed for all pregnenolone-based (Δ5,3-ol) ligands than for the corresponding progesterone (Δ4,3-keto) compounds. The effect of the A105L mutation is to increase progesterone affinity at least 2-fold, but has little effect on the already lower affinity for either progesterone hydroxylation product. Pregenenolone binds with such high affinity to both wild type and A105L that any changes in affinity due to mutation are not apparent, but the decrease in affinity that the 17α-hydroxy substituent confers on pregnenolone is offset by the A105L mutation.

Significant catalytic differences are also observed for different substrates and upon mutation (Table 3.2). The wild type CYP17A1 17-hydroxylates pregnenolone with a K_m that is 10-fold lower than for progesterone 17-hydroxylation, consistent with the rank order of the dissociation constants. Although the k_{cat} is ~3-fold lower for pregnenolone 17-hydroxylation than for progesterone 17-hydroxylation, the overall catalytic efficiency (k_{cat}/K_m) is still 4.4 higher for pregnenolone 17-hydroxylation. The A105L mutation does not alter k_{cat} for the 17-hydroxylation of either substrate, but does substantially decrease the K_m for both reactions, consistent with general increases abserved in the dissociation constants reported above.

While pregnenolone is only hydroxylated at C17, human CYP17A1 is reported to also convert progesterone to the minor 16α-hydroxylated metabolite (Figure 3.1), which can compose 10-30% of total hydroxylated metabolites depending on the system under study[21,44]. For wild type CYP17A1 in the current purified enzyme system at saturating progesterone concentrations, 16α-hydroxyprogesterone comprised 12% of the total progesterone hydroxylase activity, with

17α-hydroxyprogesterone accounting for the remainder. The A105L mutation was reported to increase 17-hydroxylation and decrease 16-hydroxylation in a cell-based system[21]. In agreement, under the same conditions used to evaluate the wild type enzyme herein, CYP17A1 A105L yielded only ~5% of the total hydroxy metabolites as the 16α-hydroxyprogesterone minor product, with 95% being the 17α-hydroxyprogesterone metabolite. Thus, these functional results agree that the A105L mutation increases the affinity of CYP17A1 for progesterone and that it does so by preferentially orienting progesterone for hydrogen abstraction at C17 over C16.

Human CYP17A1 has also been noted to produce very small amounts of 21-hydroxyprogesterone, also called 11-deoxycorticosterone, which is increased with the A105L mutation[44]. Although the current purified system yielded no detectable 21-hydroxyprogesterone at the highest substrate concentrations used for determining steady-state kinetic parameters (70 μM), at much higher progesterone concentrations (200 μM) trace amounts of 21-hydroxyprogesterone were inconsistently detected for the A105L mutant, but never for the wild type enzyme. Thus the A105L mutation appears to slightly increase the production of 21-hydroxyprogesterone.

In contrast to hydroxylation reactions, where the A105L mutation altered only the K_m, in the 17,20-lyase reaction the mutation had no effect on the K_m. Instead the mutation resulted in a 5-fold increase in k_{cat}, suggesting that the A105L mutation contributes to interactions that more readily permit the lyase reaction while having little affect on affinity.

Global overview of CYP17A1/A105L structures

Introduction of the A105L mutation increased general CYP17A1 stability during purification (and likely during expression as well), as evaluated by overall protein yield. This

consistently higher yield, perhaps in combination with an increased affinity for at least two of the steroid substrates, facilitated determination of a series of CYP17A1 A105L ligand complexes for side-by-side comparison. All crystallized in the same space group with the same packing. Comparison of the four molecules composing the asymmetric unit for one substrate complex with any of the other substrate complexes or for the inhibitor abiraterone reveals they are all very similar to each other (average root mean square deviation (RMSD) over all Cα of 0.42 ± 0.10) and to previous structures of wild type CYP17A1 bound to abiraterone and another steroidal inhibitor (average RMSD over all Cα 0.41 ± 0.10)[8]. However, for all CYP17A1 structures to date, two of the four molecules in the asymmetric unit (molecules A and B) differ slightly from the other two (molecules C and D), resulting in a higher Cα RMSD of 1.29 ± 0.06. Structural differences between these two conformations are observed at the backbone level for the N-terminus, a loop between β1 strands, and the F-G region (Figure 3.2). These regions all lie on one face of the molecule, that is proposed to be involved in membrane binding. As is true for almost all membrane P450 structures, this surface also constitutes a packing interaction with neighboring molecules in the crystalline lattice and is known to be relatively flexible. Therefore it is difficult to determine whether these differences between molecules are functionally significant. In all structures, a short loop region between helices H and I was not modeled (Figure 3.2) due to poor density, suggesting that this region is disordered. In two molecules of the structure with 17α-hydroxyprogesterone and three molecules of the structure with 17α-hydroxypregnenolone, several residues between the C and D helices were also not modeled due to ambiguous electron density.

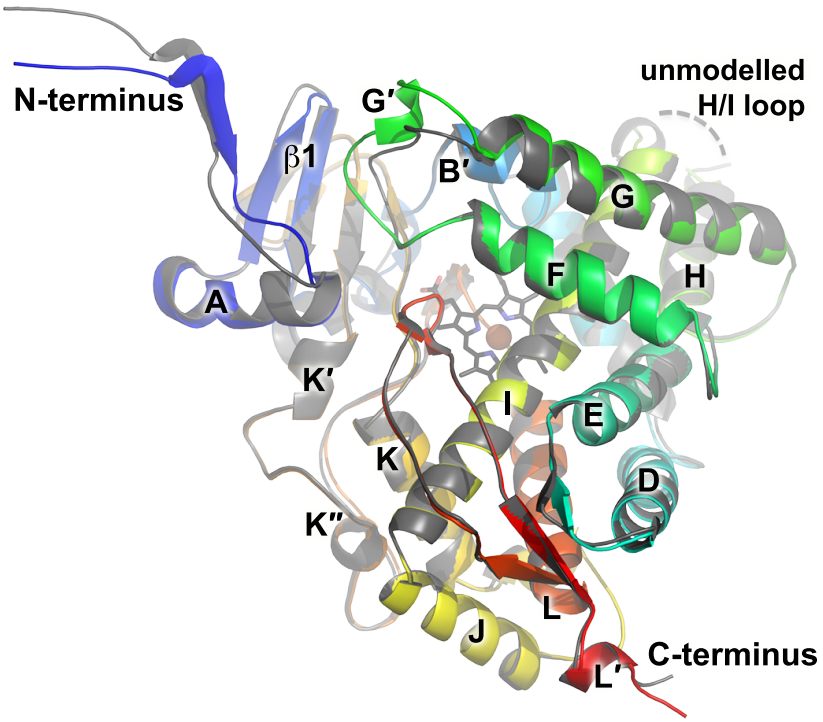

Figure 3.2: The overall structure of CYP17A1 A105L molecules A/B (shown in rainbow) and C/D (gray) have small variations in the backbone structure on one face of the enzyme, including the N-terminus, the residues between the F and G helices, and a small portion of the adjacent β1 sheet. Dashed line, HI turn residues not modeled due to weak density.

Structure of CYP17A1/A105L with Abiraterone

In order to determine the effects of the A105L mutation alone on enzyme structure, the CYP17A1/A105L structure was determined in complex with the steroidal inhibitor abiraterone and compared to that of the wild type enzyme containing this same ligand (PDB 3RUK[8]). The 2.65 Å structure of the mutant enzyme (Table 3.1) is essentially identical to the wild type enzyme at the backbone level and in all other respects, save in the local region of the single site mutation. The major difference between wild type CYP17A1 and the A105L mutant abiraterone structures is that the additional bulk due to substitution of leucine for alanine projects directly into what is part of the active site for the wild type enzyme (Figure 3.3). Reduction in overall active site volume from 677 Å for the wild type enzyme to 642 Å for the A105L mutant is due

almost entirely to this substitution. This reduction in active site volume does not alter the orientation of abiraterone or any of its interactions with the CYP17A1 active site. The steroid still lies with the unsubstituted α face against the I helix with the steroid plane forming a 60° angle from the plane of the heme. The only intermolecular hydrogen bond, between the 3β-hydroxyl group of abiraterone and Asn202, is present in both structures. Thus in this structure the impact of the A105L mutation appears to be only steric in nature

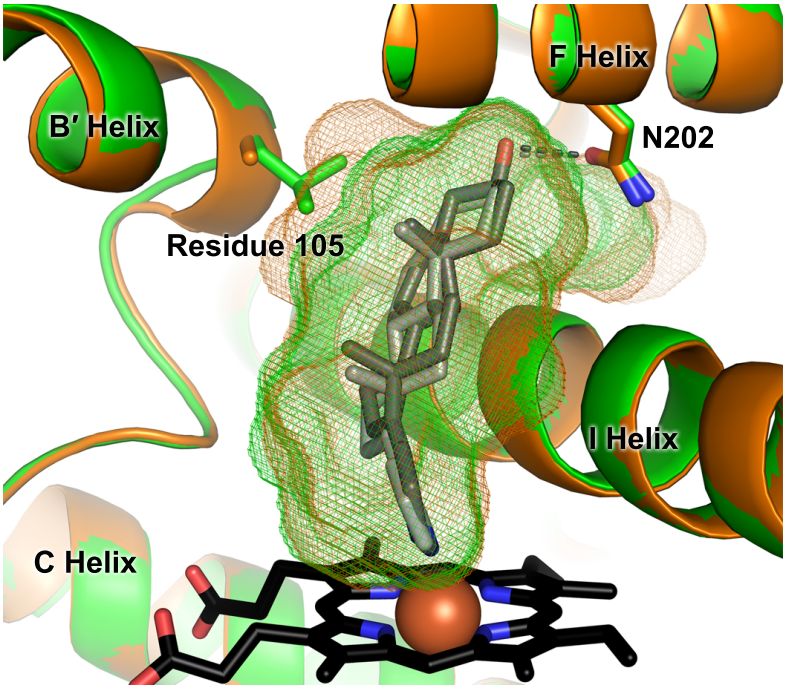

Figure 3.3: Active site of wild type CYP17A1 (orange) bound to abiraterone (PDB 3RUK)[8] overlaid with the active site of CYP17A1 A105L (green) bound to abiraterone. Mutation of residue 105 does not affect the orientation of the abiraterone inhibitor (shown in gray sticks), but reduces the active site volume specifically in the local region of the substituted side chain (wild type and A105L active site voids in orange and green mesh, respectively).

Structure of CYP17A1 A105L with Hydroxylase Substrates

Structures of the CYP17A1 A105L mutant with the 17α-hydroxylase substrates progesterone and pregnenolone were determined at resolutions of 2.80 Å and 2.50 Å, respectively (Table 3.1). In all four molecules of the asymmetric unit of both hydroxylase

substrate complexes, the ligand steroids assume the same orientation (Figure 3.4A vs. 3.4B). This general orientation is also almost identical to that previously observed for abiraterone (Figure 3.4C), with the α-face of the steroid packed against the I helix and the cyclopentanophenanthrene steroid nucleus forming a ~60° angle from the heme plane. Abiraterone forms a hydrogen bond to the side chain of Asn202 in the F helix in both the wild type structure[8] and in the A105L mutant (Figure 3.4C). Abiraterone and pregnenolone are both Δ5,3-ol steroids. Thus it is not surprising that the C3-OH of pregnenolone is also oriented to form a 2.8±0.1 Å (average) hydrogen bond to the Asn202 side chain (Figure 3.4A). The corresponding C3-keto substituent of progesterone is located to form a hydrogen bond of similar length (2.7±0.3 Å average) to Asn202 (Figure 3.4B). While progesterone must be the hydrogen bond acceptor and the amide nitrogen of Asn202 the hydrogen bond donor, the donor/acceptor relationship is less clear for pregnenolone. The pregnenolone C3 hydroxyl could be donor or acceptor, and the side chain nitrogen/oxygen could be donor/acceptor respectively depending on the side chain torsion. As a result of their similar hydrogen bonding interactions with Asn202 (distances and angles, Table 3.2) and similar packing against the I helix, the distances from C17 that is hydroxylated to the iron that would compose the catalytic iron (IV) oxo intermediate is essentially identical (4.8 ± 0.1 Å, Table 3.2) between the two hydroxylase substrates. Similarly, C16 (hydroxylated when progesterone is the substrate, but not when pregnenolone is the substrate) is also essentially same distance from the heme iron for both substrates (Table 3.2), but is located less directly over the iron than C17 (Figure 3.4A and 3.4B).

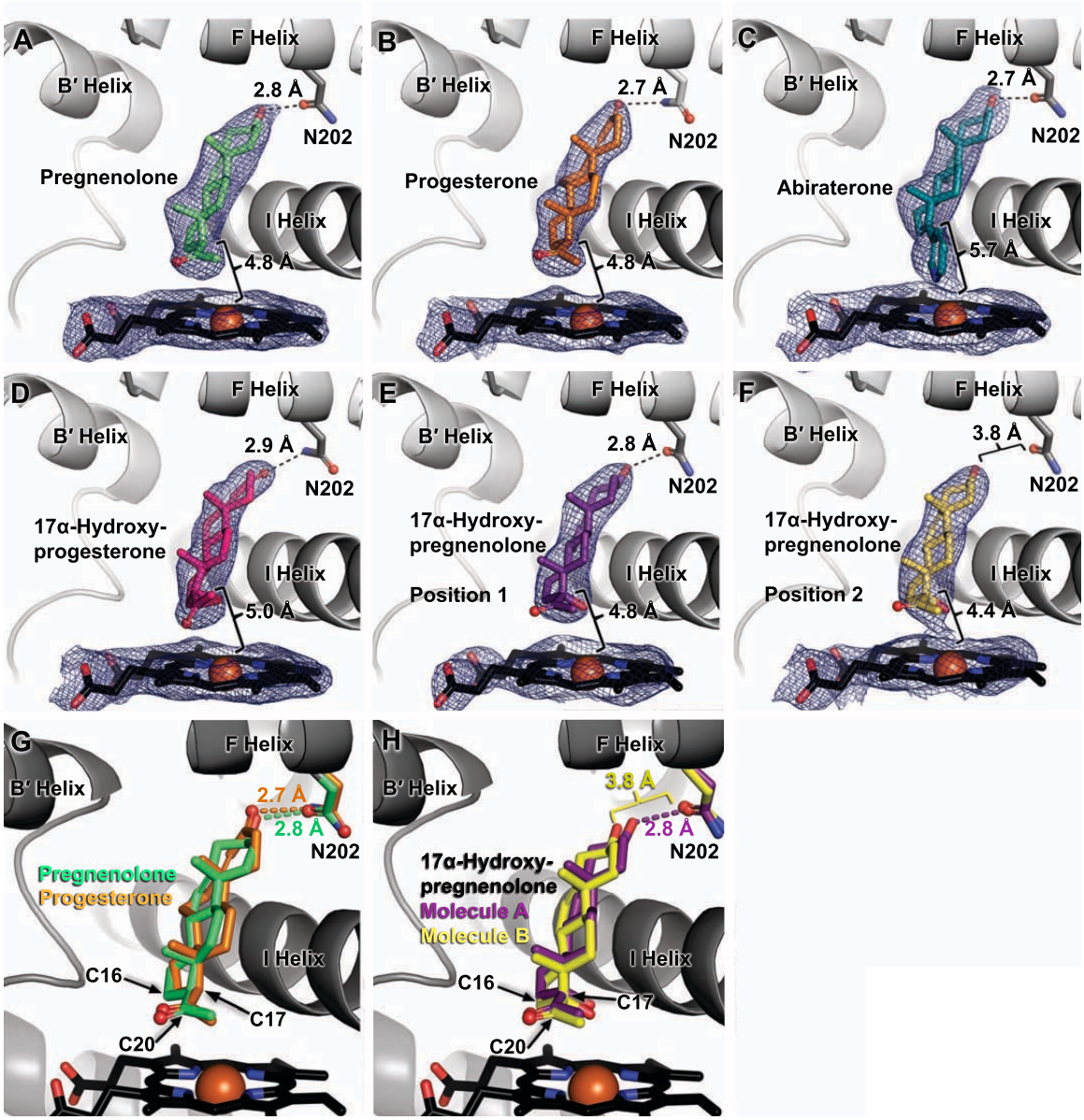

Figure 3.4: X-ray structures of CYP17A1 A105L with all four physiological substrates demonstrate overall similar orientations, with the steroid nucleus at an ~60° angle with respect to the heme plane and the steroid α-face flat against a peptide bond in the I helix. Hydroxylase substrates pregnenolone (A, green) and progesterone (B, orange) form hydrogen bonds between their respective C3 alcohol and keto substituents and the side chain amide of Asn202, an orientation termed position 1 and similar to that observed for the steroidal inhibitor abiraterone (C). The poor 17,20-lyase substrate 17α-hydroxyprogesterone (D, magenta) and is oriented similar to the hydroxylase substrates in position 1 with its C3 keto group also hydrogen bonding to Asn202. However in different molecules of the structure with the efficient lyase substrate 17α-hydroxypregnenolone, this substrate is found either in position 1 with its C3 hydroxyl hydrogen bonding to Asn202 (E, purple) or in a position closer to the heme which is too distant from Asn202 to allow hydrogen bonding (F, purple, position 2). For clarity, in panels A-F the brackets only indicate the distances between C17 and Fe. Other distances and angles are provided in Table 3.1. Electron density is shown as a 2Fo-Fc ligand omit map contoured at 1.0

sigma. In G, overlays of hydroxylase substrates pregnenolone (green) and progesterone (orange) demonstrate the similarity of their binding modes, while an overlay of 17α-hydroxypregnenolone in its two observed positions illustrates important differences in hydrogen bonding (H).

Structure of CYP17A1 A105L with 17,20-Lyase Substrates

Structures of CYP17A1/A105L co-crystallized with the efficient lyase substrate 17α-hydroxypregnenolone and the poor lyase substrate 17α-hydroxyprogesterone were determined to resolutions of 3.0 Å and 2.55 Å, respectively (Table 3.1). In the 17α-hydroxyprogesterone complex, the ligand binds very similarly in all four molecules of the crystal and very similar to the orientation observed for the hydroxylase substrates (Figure 3.4D). The hydrogen bond between the C3-keto and side chain amide of Asn202 is maintained with similar distances and angles (Table 3.1). The substrate position with respect to the I helix and heme iron (*e.g.* C17-Fe 5.0±0.1 Å, Table 3.1) is also consistent with the hydroxylase substrates, a state that will be referred to as position 1. In the 17α-hydroxypregnenolone structure, the general substrate position relative to the I helix is maintained, but the substrate is observed to occupy distinct positions that vary by their relative position between Asn202 and the heme. For two of the molecules of this structure, 17α-hydroxypregnenolone is in position 1 as observed for 17α-hydroxyprogesterone (Figure 3.4E), with its C3 alcohol forming a hydrogen bond to Asn202 (Table 3.1). However in the other two molecules of this structure, 17α-hydroxypregnenolone is found farther from Asn202 and closer to the heme iron. In its closest approach to the iron, a state referred to as position 2 (Figure 3.4F), the substrate C3 alcohol is much too far removed from Asn202 to participate in even a weak hydrogen bond (3.8 Å) and C17-Fe distance is reduced to 4.3 Å. The fourth molecule shows 17α-hydroxypregnenolone in an intermediate position. The differences in position are perhaps better illustrated by comparing the electron density associated

with ligand and heme for these various complexes. For 17α-hydroxypregnenolone in position 1 and all other CYP17A1 substrates the substrate electron density is distinct from that of the heme (Figure 3.4A, 3.4B, 3.4D, 3.4E), while for 17α-hydroxypregnenolone in position 2, closer to the heme, the substrate electron density is continuous with the heme (Figure 3.4F), more similar to that of abiraterone (Figure 3.4C). Thus overlays of the progesterone and pregnenolone complexes illustrate the high degree of similarity in their binding (Figure 3.4G) in a position and orientation also shared with 17α-hydroxyprogesterone (not shown). However an overlay of the two binding positions observed for 17α-hydroxypregnenolone illustrates differences in the hydrogen binding to N202, and a shift toward the heme.

Further variation in active site activity topography

The amino acid side chains surrounding the active site, the observable waters, and the hydrogen bonding of the I helix that the steroids pack against are not significantly different between complexes (even when 17α-hydroxypregnenolone is positioned nearer to the heme) or between molecules in each structure. Very minor differences reflect small changes in torsion angles or slightly favored rotamers to best fit the density in each structure. However in two regions these small differences result in substantial variation in active site size and topography (Figure 3.5). Rather than being correlated with a particular substrate, this appears to result primarily from the relatively small differences in the backbone for molecules A and B vs. molecules C and D. Like the wild type/abiraterone structure, the active site cavity extends beyond the C3 substituent and this varies somewhat in size, even between molecules of a particular substrate complex, due to slight differences in side chain torsions. Additionally, several molecules have extensions from the main active site extending from the region of the ligand C19 substituent, which can consist of

substantial extra volume as a result of the slight differences in the F-G' loop backbone and very slight side chain torsions. In a very few molecules one or both of these active site extensions reach the protein surface, at the intersection of the F/G' loop, $\beta_{4\text{-}1}$, and the first turn of the A helix or between the bases of the F and G helices, respectively. If expanded by breathing motions or conformational changes in the protein, these channels could play a role in ligand entry/exit. The cavity over the I helix, exiting at the base of the F and G helices would be exposed to solvent, while the cavity extension exiting in the region of the F/G' loop would be expected to be buried in the membrane.

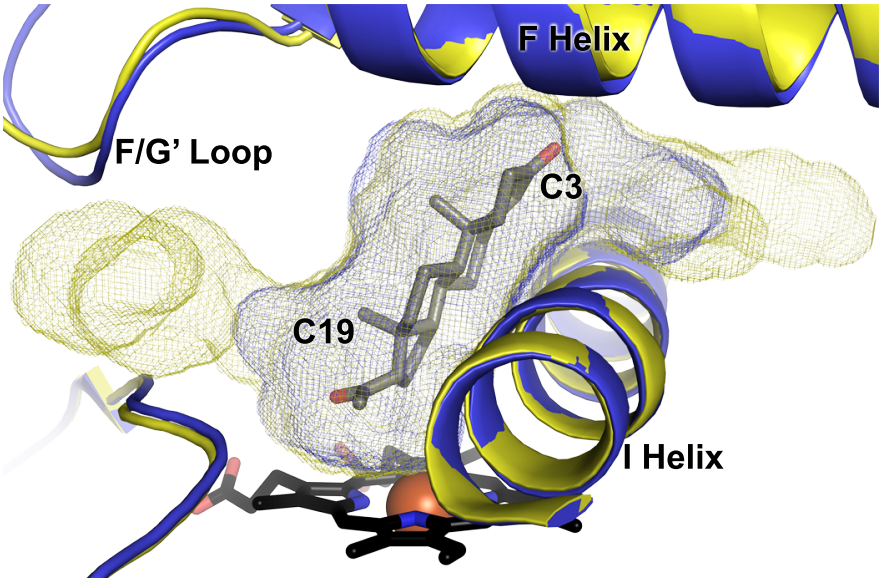

Figure 3.5: Probe-occupied cavities for the active sites of CYP17A1/A105L bound to progesterone (molecule B and D, yellow and blue, respectively) exemplify the range of volumes among the present structures. While abiraterone always exhibits a minimal active site volume similar to that shown in blue mesh, for substrates slight modifications of backbone and side chain torsions in the F-G' region and/or at the base of the F and G helices can result in a significant extension near C19 and/or enlargement of the extension off C3. In a few cases these cavities extend to the protein surface.

DISCUSSION

The reactions catalyzed by CYP17A1 have long been of substantial interest as they occur at a key juncture in human steroidogenesis, controlling the biosynthesis of mineralocorticoids,

glucocorticoids, and sex steroid androgens and estrogens. Originally thought to be performed by two different enzymes, a steroid 17α-hydroxylase and a 17,20-lyase or –desmolase, both catalytic functions were later shown to be accomplished by CYP17A1[45]. In part to explain how both reactions might occur in the single CYP17A1 active site, the concept of a "bi-lobed" active site was advanced[37], in which the different lobes would carry out the separate hydroxylase and lyase reactions. Homology models and docking studies suggested that substrates were likely to orient essentially parallel to the plane of the heme[33-35]. In contrast, the first available structures of CYP17A1, which were complexes of steroidal inhibitor analogs of pregnenolone, did not support a bi-lobed cavity and demonstrated ligand orientation more nearly perpendicular to the heme than parallel[8]. However both of these inhibitors contained nitrogen heterocycles as substituents to the steroid scaffold at C17 and coordinated to the heme iron. In the absence of further data subsequent work has been interpreted with differing models of steroid substrate orientation either parallel[44] or more perpendicular to the heme[8,26] within the CYP17A1 active site. Herein experimental structures of CYP17A1 with each of the four substrates clearly demonstrate that steroid substrates adopt a binding orientation generally consistent with that of the steroidal inhibitors in the original X-ray structures (Figure 3.4).

One possible caveat might be that all of the current structures were obtained in the presence of the A105L mutation. However the only structural difference between the wild type and A105L structures with the common ligand abiraterone was a steric difference in active site volume as the larger leucine filled active site space unoccupied by abiraterone (Figure 3.3). The mutation did not alter the orientation of the steroidal inhibitor in the CYP17A1 active site. The reduction in the excess width of the active site engendered by the alanine to leucine substitution is consistent with decreases in K_d for most substrates and decreases in hydroxylation K_m values

(Table 3.2). This evidence in accordance with functional evidence discussed below suggests that the A105L mutation does not significantly alter the primary orientation of substrate steroids important for C17 hydroxylation.

Thus, the structural results herein are first integrated with the functional hydroxylase data to propose an internally consistent hypothesis for CYP17A1 hydroxylase selectivities. The orientations observed for CYP17A1 with progesterone or pregnenolone in the current structures are consistent with production of the major 17α-hydroxy metabolites observed. In both cases C17 is oriented toward the heme iron. The C17 alpha hydrogens of both hydroxylase substrates are located such that they would be clearly most susceptible to abstraction by the iron (IV) oxo intermediate in the hydroxylase reaction. The C17 hydrogen is not located directly over the heme iron, but a few degrees off center, consistent with the moderate reported kinetic isotope effect for progesterone 17α-hydroxylation, interpreted as a bent transition state [44]. Wild type and the A105L mutant have essentially the same kinetic isotope effect for 17α-hydroxylation, 4.1 and 3.8, respectively[44], further supporting the idea that ligand orientation for 17α-hydroxylation is unperturbed by the mutation.

Combination of the current structural and functional data suggests a mechanism underlying the generation of minor progesterone metabolites. Depending on the system under study, wild type CYP17A1 also hydroxylates progesterone to yield 10-30%[21,44] of the total product as 16α-hydroxyprogesterone and has also been reported to produce trace amounts of 21-hydroxyprogesterone[44]. The C16 and C21 hydrogens flank the C17 hydrogen and the current structure positions them such that they would be the next most susceptible for hydrogen abstraction by the iron oxo intermediate (Figure 3.6A, experimental ligand position in grey sticks). In the purified system wild type CYP17A1 produced 88% of the total progesterone

metabolites with hydroxylation at C17 while the remaining 12% was the minor C16-hydroxylated product and 21-hydroxyprogesterone was not detected. Consistent with previous reports[21,44], the A105L mutation decreased the percentage of 16-hydroxylated product, increased 17-hydroxylated product, and could produce trace amounts of the 21-hydroxylated metabolite 11-deoxycorticosterone. Thus the A105L mutation, whose nearest atom is some 8-11 Å away from the site of metabolism substantially reduces 16-hydroxylation on one side of C17 and slightly increases C21 hydroxylation on the opposite side of C17, suggesting a rotation of the substrate in the active site (Figure 3.6A, proposed minor orientation in pink sticks).

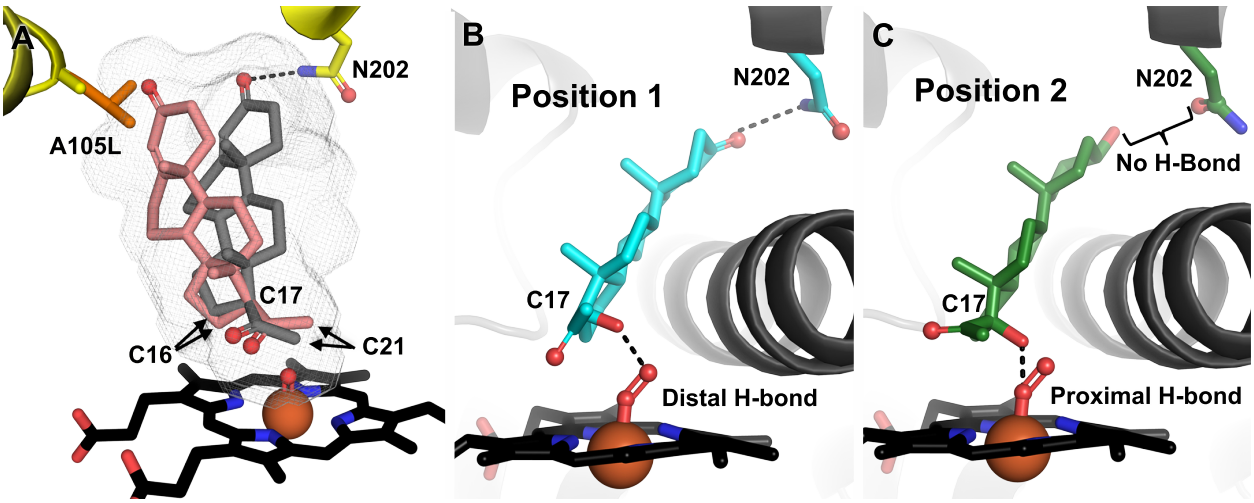

Figure 3.6: Combination of structural and functional data supports the following models for CYP17A1 catalysis. (A) Regioselectivity and substrate selectivity of hydroxylation. While the major binding modes for progesterone and pregnenolone are oriented with C17 directed toward the iron for 17α-hydroxylation (grey sticks, orientation observed in structures), the steroid core of progesterone may also adopt an alternate plane that facilitates C16 hydroxylation (salmon sticks, proposed orientation). The A105L mutation suppresses this alternate orientation, decreasing C16 hydroxylation, increasing C17 hydroxylation, and slightly increasing hydroxylation of C21 on the opposite side of the substrate. Pregnenolone may not adopt this alternate orientation favoring C16 hydroxylation because its C3 hydroxyl is restrained by a stronger hydrogen bond with Asn202. Grey mesh is CYP17A1 wild type active site cavity. B) In the current model for substrate selectivity of the lyase reaction, 17α-hydroxyprogesterone may be a poor 17,20-lyase substrate due to its positioning in the active site. This substrate is only observed hydrogen bonding to N202 such that it is farther away from the iron, and its C17 hydroxyl is predicted to hydrogen bond with the distal oxygen of the peroxy intermediate, an interaction that is not conducive to the lyase reaction. C) In contrast, 17α-hydroxypregnenolone may be a more efficient substrate for the lyase reaction because it is observed to move closer to the iron, where studies suggest the C17 hydroxy may hydrogen bond with the proximal oxygen of the catalytic peroxy intermediate. This position would facilitate nucleophilic attack of the distal oxygen on C20 to perform the lyase reaction. The well established facilitation of the lyase reaction by b_5 is consistent with an allosteric interaction favoring 17α-hydroxypregnenolone in position 2 vs. position 1.

The present structural information demonstrates that A105L occludes part of the active site volume adjacent to the B' helix (Figure 3.3). This volume is not utilized by progesterone binding in a mode consistent with 17-hydroxylation. However, the functional data suggests that the availability of active site volume near Ala105 correlates with the production of 16α-

hydroxyprogesterone. In the wild type enzyme progesterone might take advantage of the cavity space near Ala105 to adopt a variation of the observed progesterone orientation that preferentially exposes C16 for hydroxylation (Figure 3.6A, pink). Since the steroid nucleus is a relatively rigid body, reduction of volume near Ala105 would be structurally consistent with the proposition that the A105L active site topography disallows such alternative positioning of progesterone in the CYP17A1 active site, reducing production of the minor 16α-hydroxyprogesterone metabolite, increasing the catalytic efficiency of 17α-hydroxylation, and slightly increasing C21 access to the iron for hydroxylation as observed experimentally.

Thus it is proposed that in the wild type enzyme the progesterone long axis can adopt at least two orientations in the wild type active site (Figure 3.6A). The major one would pack directly against the I helix and hydrogen bond to Asn202 as observed in the crystal structure, resulting in the major 17α-hydroxy metabolite. The minor orientation would be most consistent with a shift of the long axis of the steroidal core, pivoting about C17 to move the C3 substituent into the space adjacent to Ala105 near the B' helix where it perhaps cannot hydrogen bond with Asn202. This proposed position for progesterone would move C16 towards the iron, increasing the likelihood of abstraction of one of the C16 hydrogens and subsequent hydroxylation to yield the minor product. This model is consistent with intramolecular kinetic isotope effect studies demonstrating that the A105L mutation affects the transition state for hydrogen abstraction at C16, with negligible effects on progesterone C17 hydroxylation[44]. It is therefore likely that the proposed alternative positioning is a very modest rotation of the steroid about C17 that affects the proximity of C16 to the oxygen of compound I without substantial effects on C17. Detection of the proposed progesterone minor orientation would not be likely by X-ray crystallography, especially within the context of the A105L mutation background. In summary, the contribution

of the A105L mutation to more efficient 17α-hydroxylation appears to be related to the binding of substrates and doing so in an optimal position for hydrogen abstraction at the appropriate carbon.

The current structural and functional data also suggest a potential mechanism for differential regiospecificity between hydroxylase substrates. Though the wild type active site cavity topography might suggest that pregnenolone could adopt a similar minor orientation resulting in the generation of 16α-hydroxypregnenolone, no such product is observed experimentally [19]. This could be due to a stronger hydrogen bonding interaction with Asn202 for pregnenolone compared to progesterone. Pregnenolone (and 17α-hydroxypregnenolone) have a C3 hydroxyl substituent with the ability to serve as either hydrogen bond donor or acceptor to the Asn202 side chain amide, which can also serve as donor or acceptor depending on the orientation. These substrates bind more tightly than either of the corresponding Δ4,3-keto progesterone-based substrates (Table 3.2), as reflected by at least a 2-fold decrease in the K_d and perhaps even more by the 17-hydroxylase K_m, which is a full order of magnitude lower for pregnenolone than its Δ4,3-keto counterpart progesterone. This stronger interaction with Asn202 could inhibit pregnenolone from adopting the minor orientation proposed for progesterone and prevent pregnenolone 16-hydroxylation.

A second debate in the field of steroidogenesis centers on the mechanism and substrate selectivity of the lyase reaction. Human CYP17A1 performs the 17,20-lyase reaction much more efficiently on 17α-hydroxypregnenolone to form the physiologically-relevant androgen dehydroepiandrosterone, with 50-fold lower metabolism of 17 α-hydroxyprogesterone to the corresponding 17,20-lyase product androstenedione[18,19], despite similar K_d values (Table 3.2). However the current structural results suggest a basis for this selectivity. Although both lyase

substrates can hydrogen bond to Asn202 similar to the hydroxylase substrates, the poor lyase substrate 17α-hydroxyprogesterone was only observed in this position (called position 1). In contrast, the favored lyase substrate 17α-hydroxypregnenolone is also observed closer to the heme and far enough from Asn202 that this hydrogen bond is no longer present (termed position 2). The potential significance of this substrate repositioning was investigated by modeling the proposed intermediate for the lyase reaction into both substrate complexes. The peroxy state[17,25] was modeled by incorporating the heme-bound oxygenated state observed in P450cam[46], wherein the proximal oxygen is bound to the iron and the distal oxygen is oriented toward a portion of the adjacent I helix with non-canonical hydrogen bonding. The CYP17A1 I helix shows similar non-cononical hydrogen bonding interactions at this position, though a water molecule observed in this groove for P450cam is not apparent for CYP17A1. With the iron peroxy modeled in this manner, the distance between the distal oxygen of the peroxo thought to perform nucleophilic attack on the substrate C20 position is similar for both substrate positions (~3.2 Å), but the distance between C17 and the proximal oxygen goes from 3.6 Å in position 1 to 3.0 Å in position 2. As a result, in position 1 (the only position observed for 17α-hydroxyprogesterone) the C17 hydroxyl is positioned to best interact with the *distal* oxygen of the peroxy intermediate (Figure 3.6B). In contrast, position 2 (observed only for 17α-hydroxypregnenolone) brings the C17 hydroxyl within a similar distance to the *proximal* oxygen of the peroxy intermediate (Figure 3.6C). Hydrogen bonding of the C17 hydroxyl to the distal oxygen as suggested by position 1 would tend to promote breakage of the oxygen-oxygen bond, leading to compound I and depressing the lyase reaction [26]. Hydrogen bonding of the C17 hydroxyl to the proximal oxygen, as suggested by 17α-hydroxypregnenolone in position 2, would tend to preferentially stabilize the peroxy intermediate and leave the distal oxygen

available to perform nucleophilic attack on C20 of the substrate, thereby facilitating the lyase reaction. Thus subtle positioning of the substrate over the heme-peroxy intermediate, as mediated by the distant interaction with Asn202, is proposed to modulate substrate selectivity for the lyase reaction. This hypothesis is consistent with several orthogonal lines of evidence. First, although the residue at N202 may not be the only factor, the identity of this residue appears to largely correlate with lyase specificity in various species. In human, sheep, cow, and pig, the residue at position 202 is an asparagine and these proteins preferentially perform the lyase reaction on the 17α-hydroxypregnenolone substrate to produce dehydroepiandrosterone. Conversely hamster, mouse, rat, and guinea pig have a threonine at position 202 and preferentially perform the lyase reaction on 17α-hydroxyprogesterone, yielding androstendione. Second, resonance Raman spectroscopy supports differential hydrogen bonding of the efficient and poor lyase substrates to the proximal or distal oxygens, respectively, for the ferrous dioxygen state immediately preceding the peroxy state in the P450 catalytic cycle[26]. Third, resonance Raman studies with CYP17A1 bound to CO demonstrate two distinct Fe-C-O vibrational modes exist for 17α-hydroxypregnenolone and only a single mode in the presence of hydroxylase substrates and the poor lyase substrate, 17α-hydroxyprogesterone[47]. Thus the recent functional and current structural evidence converge to strongly support two binding modes for 17α-hydroxypregnenolone, one of which is oriented appropriately to stabilize the peroxo intermediate and undergo the lyase reaction. Finally, repositioning of 17α-hydroxypregnenolone lower in the active site to promote the lyase reaction is consistent with the effects of the A105L mutation, where filling space in the distal part of the active site cavity results in a 5-fold increase in k_{cat} with no change in K_m.

A third major conundrum with respect to CYP17A1 biochemistry is how the presence of cytochrome b_5 promotes the 17,20-lyase reaction to increase androgen production in specific tissues and during human development. Cytochrome b_5 binding is not associated with electron delivery to CYP17A1, but nonetheless increases the 17,20-lyase reaction as much as 10-fold[18]. One might suggest that stabilization of the lyase iron-oxo intermediate might be accomplished if b_5 binding inhibited protonation of the iron-peroxo intermediate. The peroxo intermediate operative in the lyase reaction must first be protonated on the distal oxygen, followed by a second protonation and loss of water to yield the iron-oxo compound I intermediate required for hydroxylation. However this is incompatible with the observation that b_5 does not reduce the hydroxylation reaction. Alternatively, b_5 binding has been suggested to allosterically alter CYP17A1 conformation and/or substrate orientation to promote the lyase activity[18], but a mechanism for this has not been previously elucidated[48]. The current structural results suggest that this might occur by altering the distribution of 17α-hydroxypregnenolone in position 1 (not conducive to the lyase reaction) vs. position 2 (compatible with productive lyase chemistry). The anionic E48 and E49 residues of cytochrome b_5 are known to interact with the cationic R347, R358, and R449 CYP17A1 residues based on both mutagenesis and recent solution NMR binding studies[32,49]. This means that the b_5 binding site is on the opposite side of the heme and 11-21 Å away from the buried active site. Recently, however, solution NMR results established that b_5 binds differentially to CYP17A1 depending on whether the hydroxylase substrate pregnenolone or the lyase substrate 17α-hydroxypregnenolone is present in the buried CYP17A1 active site[49]. Cytochrome b_5 binding on the proximal side of CYP17A1 has been demonstrated to change the backbone conformations for F helix residues I205 and I206 adjacent to N202[50], although information on N202 itself is not yet available. The functional and structural data

suggest that communication between the b_5 binding site and the active site could allosterically favor 17α-hydroxypregnenolone binding in position 2. Optimized positioning of 17α-hydroxypregnenolone for the lyase reaction would be consistent with the observed decrease in the amount of uncoupling for the lyase reaction when b_5 is present[51], increasing the lyase product generated without substantially altering CYP17A1 hydroxylase activity, which is already ~97% coupled[51]. Although we have been unable to replicate these results, phosphorylation of CYP17A1 is also reported to facilitate the lyase reaction[52,53] and could similarly promote a conformation of CYP17A1 that increases 17α-hydroxypregnenolone in position 2 closer to the heme.

In summary, the balance of human mineralocorticoids, glucocorticoids, androgens and estrogens depends on the interactions of CYP17A1 with its four different steroidal substrates. While structural information has previously been lacking, the current set of X-ray structures establishes that each of these substrates binds in the CYP17A1 active site with the site(s) of metabolism oriented toward the heme, the α face packed against the I helix, and with the C3 keto or alcohol substitutent hydrogen bonding to Asn202 in the F helix. Complexes with the hydroxylase substrates progesterone and pregnenolone demonstrate primary binding modes consistent with production of the observed 17α-hydroxy major metabolites, while the structural and functional effects of the A105L mutation suggest a minor alternate orientation not seen in the current structure, but that would be consistent with the 16α-hydroxylation observed for progesterone but not pregnenolone. Comparison of complexes between the poor lyase substrate 17α-hydroxyprogesterone and the efficient lyase substrate 17α-hydroxypregnenolone reveal that only 17α-hydroxypregnenolone is also observed positioned closer to the heme without hydrogen bonding to Asn202. This latter position, termed position 2, is consistent with spectroscopic

evidence suggesting that 17α-hydroxypregnenolone hydrogen bonds differently to the proposed peroxy catalytic intermediate compared to its Δ4-3keto counterpart, resulting in C-C bond cleavage only for 17α-hydroxypregnenolone. Finally, cytochrome b_5 binding to CYP17A1 is known to have an allosteric effect on the active site, which would be consistent with favoring 17α-hydroxypregnenolone localization nearer the heme in position 2 and potentially decreasing nonproductive uncoupling of the catalytic cycle. In aggregate, the set of structures herein provide a structural basis for the regioselectivity and substrate specificity of the hydroxylation reaction and the substrate specificity of the lyase reaction, as well as providing potential mechanism for the allosteric effects of cytochrome b_5 on the lyase reaction. Providing such a structural basis for understanding key reactions at the crossroads of human steroidogenesis should improve our ability to modulate physiological status in diseases ranging from sexual development, fertility and hormone-responsive breast and prostate cancer, to immune and stress responses and blood pressure.

ACKNOWLEDGEMENTS

Initial pregnenolone hydroxylase and 17,20-lyase assay development was performed by Patrick Porubsky. Unpublished CYP17A1 wild type binding data was provided by Dr. Natasha DeVore.

REFERENCES

(1) Miller, W. L.; Auchus, R. J. *Endocr. Rev.* **2011**, *32*, 81.
(2) Gilep, A. A.; Sushko, T. A.; Usanov, S. A. *Biochim. Biophys. Acta* **2011**, *1814*, 200.
(3) Edwards, B. K.; Noone, A. M.; Mariotto, A. B.; Simard, E. P.; Boscoe, F. P.; Henley, S. J.; Jemal, A.; Cho, H.; Anderson, R. N.; Kohler, B. A.; Eheman, C. R.; Ward, E. M. *Cancer* **2013**.
(4) Ferraldeschi, R.; de Bono, J. *Cancer J* **2013**, *19*, 34.
(5) de Bono, J. S.; Logothetis, C. J.; Molina, A.; Fizazi, K.; North, S.; Chu, L.; Chi, K. N.; Jones, R. J.; Goodman, O. B., Jr.; Saad, F.; Staffurth, J. N.; Mainwaring, P.; Harland, S.; Flaig, T. W.; Hutson, T. E.; Cheng, T.; Patterson, H.; Hainsworth, J. D.; Ryan, C. J.; Sternberg, C. N.; Ellard, S. L.; Flechon, A.; Saleh, M.; Scholz, M.; Efstathiou, E.; Zivi, A.; Bianchini, D.; Loriot, Y.; Chieffo, N.; Kheoh, T.; Haqq, C. M.; Scher, H. I. *N. Engl. J. Med.* **2011**, *364*, 1995.
(6) Auchus, M. L.; Auchus, R. J. *J. Investig. Med.* **2012**, *60*, 495.
(7) Loriot, Y.; Bianchini, D.; Ileana, E.; Sandhu, S.; Patrikidou, A.; Pezaro, C.; Albiges, L.; Attard, G.; Fizazi, K.; De Bono, J. S.; Massard, C. *Ann. Oncol.* **2013**, *24*, 1807.
(8) DeVore, N. M.; Scott, E. E. *Nature* **2012**, *482*, 116.
(9) Pia, A.; Vignani, F.; Attard, G.; Tucci, M.; Bironzo, P.; Scagliotti, G.; Arlt, W.; Terzolo, M.; Berruti, A. *Cancer Treat. Rev.* **2013**, *39*, 966.
(10) Attard, G.; Reid, A. H.; Auchus, R. J.; Hughes, B. A.; Cassidy, A. M.; Thompson, E.; Oommen, N. B.; Folkerd, E.; Dowsett, M.; Arlt, W.; de Bono, J. S. *J. Clin. Endocrinol. Metab.* **2012**, *97*, 507.
(11) Ogo, A.; Haji, M.; Ohashi, M.; Nawata, H. *Mol. Cell. Endocrinol.* **1991**, *80*, 83.
(12) Maitra, A.; Shirwalkar, H. *Indian J Exp Biol* **2003**, *41*, 701.
(13) Qin, K. N.; Rosenfield, R. L. *Mol Cell Endocrinol* **1998**, *145*, 111.
(14) Miller, W. L. *Mol. Cell. Endocrinol.* **2002**, *198*, 7.
(15) Strauss, J. F., 3rd *Ann. N. Y. Acad. Sci.* **2003**, *997*, 42.
(16) Groves, J. T.; McClusky, G. A.; White, R. E.; Coon, M. J. *Biochem. Biophys. Res. Commun.* **1978**, *81*, 154.
(17) Akhtar, M.; Corina, D.; Miller, S.; Shyadehi, A. Z.; Wright, J. N. *Biochemistry* **1994**, *33*, 4410.
(18) Auchus, R. J.; Lee, T. C.; Miller, W. L. *J. Biol. Chem.* **1998**, *273*, 3158.
(19) Swart, P.; Swart, A. C.; Waterman, M. R.; Estabrook, R. W.; Mason, J. I. *J. Clin. Endocrinol. Metab.* **1993**, *77*, 98.
(20) Arlt, W.; Martens, J. W.; Song, M.; Wang, J. T.; Auchus, R. J.; Miller, W. L. *Endocrinology* **2002**, *143*, 4665.
(21) Swart, A. C.; Storbeck, K. H.; Swart, P. *J. Steroid Biochem. Mol. Biol.* **2010**, *119*, 112.
(22) Sohl, C. D.; Guengerich, F. P. *J. Biol. Chem.* **2010**, *285*, 17734.
(23) Fluck, C. E.; Miller, W. L.; Auchus, R. J. *J. Clin. Endocrinol. Metab.* **2003**, *88*, 3762.
(24) Guengerich, F. P. *J Biochem. Mol. Toxicol.* **2007**, *21*, 163.

(25) Gregory, M. C.; Denisov, I. G.; Grinkova, Y. V.; Khatri, Y.; Sligar, S. G. *J. Am. Chem. Soc.* **2013**, *135*, 16245.
(26) Gregory, M.; Mak, P. J.; Sligar, S. G.; Kincaid, J. R. *Angew. Chem. Int. Ed. Engl.* **2013**, *52*, 5342.
(27) Katagiri, M.; Kagawa, N.; Waterman, M. R. *Arch. Biochem. Biophys.* **1995**, *317*, 343.
(28) Lee-Robichaud, P.; Wright, J. N.; Akhtar, M. E.; Akhtar, M. *Biochem. J* **1995**, *308 (Pt 3)*, 901.
(29) Onoda, M.; Hall, P. F. *Biochem. Biophys. Res. Commun.* **1982**, *108*, 454.
(30) Idkowiak, J.; Randell, T.; Dhir, V.; Patel, P.; Shackleton, C. H.; Taylor, N. F.; Krone, N.; Arlt, W. *J. Clin. Endocrinol. Metab.* **2012**, *97*, E465.
(31) Kok, R. C.; Timmerman, M. A.; Wolffenbuttel, K. P.; Drop, S. L.; de Jong, F. H. *J. Clin. Endocrinol. Metab.* **2010**, *95*, 994.
(32) Naffin-Olivos, J. L.; Auchus, R. J. *Biochemistry* **2006**, *45*, 755.
(33) Auchus, R. J.; Miller, W. L. *Mol Endocrinol* **1999**, *13*, 1169.
(34) Schappach, A.; Holtje, H. D. *Pharmazie* **2001**, *56*, 435.
(35) Haider, S. M.; Patel, J. S.; Poojari, C. S.; Neidle, S. *J. Mol. Biol.* **2010**, *400*, 1078.
(36) Lin, D.; Zhang, L. H.; Chiao, E.; Miller, W. L. *Mol. Endocrinol.* **1994**, *8*, 392.
(37) Laughton, C. A.; Neidle, S.; Zvelebil, M. J.; Sternberg, M. J. *Biochem. Biophys. Res. Commun.* **1990**, *171*, 1160.
(38) Kabsch, W. *Acta Crystallogr., Sect. D: Biol. Crystallogr.* **2010**, *66*, 125.
(39) McCoy, A. J.; Grosse-Kunstleve, R. W.; Adams, P. D.; Winn, M. D.; Storoni, L. C.; Read, R. J. *J. Appl. Crystallogr.* **2007**, *40*, 658.
(40) Emsley, P.; Lohkamp, B.; Scott, W. G.; Cowtan, K. *Acta Crystallogr., Sect. D: Biol. Crystallogr.* **2010**, *66*, 486.
(41) Adams, P. D.; Afonine, P. V.; Bunkoczi, G.; Chen, V. B.; Davis, I. W.; Echols, N.; Headd, J. J.; Hung, L. W.; Kapral, G. J.; Grosse-Kunstleve, R. W.; McCoy, A. J.; Moriarty, N. W.; Oeffner, R.; Read, R. J.; Richardson, D. C.; Richardson, J. S.; Terwilliger, T. C.; Zwart, P. H. *Acta Crystallogr., Sect. D: Biol. Crystallogr.* **2010**, *66*, 213.
(42) Kleywegt, G. J.; Jones, T. A. *Acta Crystallogr., Sect. D: Biol. Crystallogr.* **1994**, *50*, 178.
(43) Schrodinger, LLC 2010.
(44) Yoshimoto, F. K.; Zhou, Y.; Peng, H. M.; Stidd, D.; Yoshimoto, J. A.; Sharma, K. K.; Matthew, S.; Auchus, R. J. *Biochemistry* **2012**, *51*, 7064.
(45) Nakajin, S.; Hall, P. F. *J. Biol. Chem.* **1981**, *256*, 3871.
(46) Schlichting, I.; Berendzen, J.; Chu, K.; Stock, A. M.; Maves, S. A.; Benson, D. E.; Sweet, R. M.; Ringe, D.; Petsko, G. A.; Sligar, S. G. *Science* **2000**, *287*, 1615.
(47) Mak, P. J.; Gregory, M. C.; Sligar, S. G.; Kincaid, J. R. *Biochemistry* **2013**.
(48) Akhtar, M. K.; Kelly, S. L.; Kaderbhai, M. A. *J. Endocrinol.* **2005**, *187*, 267.
(49) Estrada, D. F.; Laurence, J. S.; Scott, E. E. *J. Biol. Chem.* **2013**, *288*, 17008.
(50) Estrada, D. F.; Skinner, A. L.; Laurence, J. S.; Scott, E. E. *J. Biol. Chem.* **2014**.
(51) Khatri, Y.; Gregory, M. C.; Grinkova, Y. V.; Denisov, I. G.; Sligar, S. G. *Biochem. Biophys. Res. Commun.* **2014**, *443*, 179.
(52) Zhang, L. H.; Rodriguez, H.; Ohno, S.; Miller, W. L. *Proc. Natl. Acad. Sci. U. S. A.* **1995**, *92*, 10619.

(53) Tee, M. K.; Miller, W. L. *J. Biol. Chem.* **2013**, *288*, 23903.

Chapter 4.

Structures of Cytochrome P450 17A1 with A Ring-Modified Steroidal Inhibitors

INTRODUCTION

The first compounds designed to inhibit CYP17A1, a required enzyme in androgen biosynthesis and therefore a target for the treatment of prostate cancer, were logically based on the pregnenolone substrate of this enzyme. Effective inhibitors were developed by incorporation of nitrogen heterocycle substituents at carbon 17 of the steroidal scaffold, which is now known to coordinate the heme iron of CYP17A1[1]. The FDA-approved abiraterone incorporates a pyridine ring at this position. Galeterone, currently in Phase III clinical trials, substitutes a benzimidazole. The design of these inhibitors was guided by structure activity relationships to optimize the type of heterocycle[2], the configuration of the heterocycle[2,3], and the oxidation state of the D ring[4]. Although these early efforts were more focused on the heterocycles that interact with the heme iron directly, more recent studies have explored structure activity relationships on other parts of the steroidal scaffold.

Variations in the configurations of A and B rings are of particular interest because the natural substrates of CYP17A1 vary in these rings. Abiraterone and galeterone share the 3β-OH, Δ5 configuration with pregnenolone. However, human CYP17A1 also turns over progestagens with different A ring configurations, and A ring configuration can strongly influence the efficiency of the reactions performed on the other end of the steroid (as discussed more thoroughly in Chapter 3). Progesterone (a 3-keto, Δ4 progestagen) is a comparable substrate to pregnenolone for the CYP17A1-mediated hydroxylase reaction. However, the 17-hydroxylated progesterone product is a much poorer substrate for the subsequent 17,20 lyase reaction of

human CYP17A1 compared to its 3β-OH, Δ5 analog, 17α-hydroxypregnenolone[5]. Reduction of pregnenolone's Δ5 double bond and projection of the hydroxyl group on carbon 3 toward the α-face of the steroid results in allopregnanolone. Allopregnenolone is an endogenous progestagen that is also a substrate for 17α-hydroxylation by CYP17A1. Additionally, the 17α-hydroxyallopregnanolone product has been reported to subsequently undergo the 17,20 lyase reaction more efficiently than 17α-hydroxypregnenolone[6]. CYP17A1-mediated hydroxylation and lyase reactions on allopregnanalone and 17α-hydroxyallopregnanolone are components of the so-called "backdoor" route to androgen biosynthesis described in Chapter 1.

Several different A ring configurations have been explored in the context of CYP17A1 inhibition by steroidal compounds. Reduction of the Δ5 double bond in galeterone (while maintaining the 3β stereochemistry of the hydroxyl group) is reported to result in a significantly less potent inhibitor of CYP17A1-mediated 17,20-lyase activity[7], but there are currently no reports of analogs with A configurations that more closely resemble that of progesterone (3-keto, Δ4) or allopregnanolone (3α-OH, 5α). Recently, however, analogs of abiraterone with various A ring configurations (Table 4.1) were examined for CYP17A1 binding affinity and inhibition of progesterone hydroxylation in the Auchus lab, including the 3-keto, Δ4 analog (1), the 3-keto, 5α analog (2), and the 3α-OH, 5α analog (3)[8]. Notably, compounds (1) and (3) have A-ring configurations based on CYP17A1 substrates progesterone and allopregnanolone, respectively. All three compounds demonstrated binding affinity and potency for progesterone hydroxylation comparable to abiraterone[8]. Moreover, compound (1) was recently identified as a metabolite of abiraterone in human patients receiving abiraterone as treatment for prostate cancer[9]. *In vivo*, patients convert small amounts of abiraterone to (1) via 3β-hydroxysteroid dehydrogenase[9]. Importantly, (1) was shown to inhibit not only CYP17A1, but two other enzymes required for

androgen biosynthesis, 3β-hydroxysteroid dehydrogenase and 5α-reductase. Finally, (1) also acts as a very effective androgen receptor antagonist, equipotent to a specific androgen receptor antagonist used clinically, enzalutamide[9]. This four-way inhibition of androgen biosynthesis potentially represents a significantly improved multi-target approach for treatment of prostate cancer. Long-term inhibition of CYP17A1, or any single target approach, can result in resistance to treatment[10]. Therefore an agent such as (1) that interferes with androgen biosynthesis at multiple steps in the pathway could minimize resistance and improve overall survival, especially if undesirable off-target effects on enzymes such as CYP21A2 can be simultaneously avoided.

Table 4.1: Analogs of abiraterone with A-ring modifications with reported affinities for CYP17A1 and K_i values for inhibition of progesterone hydroxylation.

Inhibitor	Reported K_d (nM)[8]	Reported K_i (nM)[8]
Abiraterone 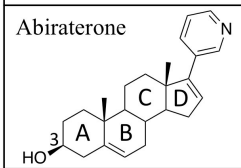	2.6 ± 3.2	27
(1) 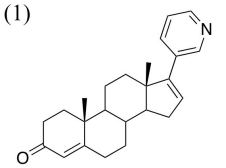	0.1 ± 0.4	22
(2) 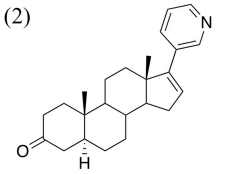	0.7 ± 2.8	7
(3) 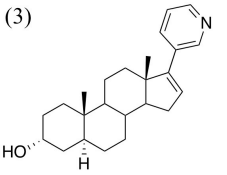	0.6 ± 1.3	14

Although inhibitors (1), (2), and (3) are reported to bind and effectively inhibit CYP17A1, there have been no reported structures of CYP17A1 in complex with any of them.

All three inhibitors share substantial structural similarity with abiraterone, and therefore were proposed to adopt the same orientation and engage in the same interactions with the CYP17A1 active site as abiraterone, for which a structure has previously been reported[1]. To examine this hypothesis, CYP17A1 was crystallized in complex with compounds (1), (2), and (3) and the X-ray crystal structures solved at resolutions of 2.7, 2.0, and 2.4 Å, respectively. The structures do indeed indicate that compounds (1), (2), and (3) bind to CYP17A1 in the same orientation as abiraterone, and make similar contacts with the active site of CYP17A1. Such findings support previous studies comparing the affinity and potency of CYP17A1 inhibition for these inhibitors compared to abiraterone. Furthermore, the 2.0 Å structure of CYP17A1 with inhibitor (2) is the highest resolution structure of the enzyme to date, and supports a peripheral ligand binding site that had not been clearly defined in previous CYP17A1 structures.

METHODS

Protein Expression and Purification

CYP17A1 was expressed and purified without ligand as described in Chapter 2.

Crystallization, Data Collection, and Structure Determination

CYP17A1 was co-crystallized with inhibitors (1), (2), and (3) via hanging drop vapor diffusion. CYP17A1 (30 mg/mL) in buffer containing 50 mM Tris-HCl, pH 7.4, 20% glycerol, 100 mM glycine, 500 mM NaCl, 0.5% (v/v) Emulgen-913, with 10 μM inhibitor (1) or (3), or 20 μM (2) was set up in a 1:1 ratio with precipiant to form 2 μL drops. Drops were equilibrated against 750 μL precipitant containing 175 mM Tris HCl, pH 8.5, 30% PEG-3350, 300 mM $LiSO_4$, and 3% glycerol. Crystals were cryoprotected in a 7:3 mixture of mother liquor to 80% glycerol and flash cooled in liquid nitrogen.

Data were collected on beamline 14-1 and 12-2 at the Stanford Synchrotron Radiation Lightsource. All crystallographic data were processed using XDS[11]. Statistics for data collection and refinement are shown in Table 4.2. Structures were solved by molecular replacement in Phaser[12] at the corresponding resolution cutoff for each structure (see Table 4.2) and using a previous structure of CYP17A1 with heme cofactor (PDB ID: 3SWZ[1]) as a search model. Model building and iterative refinement were performed using COOT[13] and PHENIX[14], respectively. Ligand coordinates were generated using eLBOW in PHENIX[14]. Simulated-annealing composite omit maps were calculated in PHENIX[14]. Probe-occupied active site void volumes were calculated using VOIDOO[15] (Probe radius of 1.4 Å, grid spacing of 0.33). Overlays between CYP17A1 structures were generated in COOT[13] using the secondary structure matching algorithm. Overlays between CYP17A1 and CYP3A4 or CYP21A2 were generated in COOT[13] using the least squares fit to overlay hemes. Figures were created using PyMOL[16].

Table 4.2: Crystallographic data collection and refinement statistics for CYP17A1 with abiraterone A-ring analogs.

	CYP17A1/(1)	**CYP17A1/(2)**	**CYP17A1/(3)**
Data Collection			
Beamline	SSRL 12-2	SSRL 12-2	SSRL 14-1
Space group	$P2_12_12_1$	$P2_12_12_1$	$P2_12_12_1$
Cell dimensions: a, b, c (Å)	90.35,152.98,168.50	85.72, 151.18, 169.94	89.76, 153.18, 168.88
Molecules/a.u.	4	4	4
Resolution (Å)*	39.81-2.70 (2.85 – 2.75)	38.68 – 2.00 (2.11-2.00)	39.29 - 2.39 (2.52-2.39)
Total reflections*	432,291 (58,652)	1,503,586 (191,079)	683,522 (97,537)
Unique reflections*	64,672 (9,236)	146,679 (20,040)	92,392 (13,193)
Redundancy*	6.7 (6.4)	10.3 (9.5)	7.4 (7.4)
R_{pim}*	0.062 (0.554)	0.066 (0.717)	0.067 (0.629)
$<I/\sigma(I)>$*	12.9 (1.7)	8.5 (1.5)	11.5 (1.5)
Completeness*	99.7 (98.4)	98.8 (93.5)	99.8 (97.7)
Refinement			
Resolution (Å)	39.81-2.70	38.68-2.00	39.29-2.40
No. reflections	64,546	144,568	92,110
R/R_{free} (%)	18.82/24.88	18.46/24.23	18.95/24.51
Ramachandran (%)			
Favored	96.50	97.41	96.32
Allowed	3.28	2.43	3.57
Outliers	0.22	0.16	0.11
Wilson B Factor ($Å^2$)	52.76	27.91	41.13
No. Atoms/B Factors ($Å^2$)			
Protein	14,905 / 63.09	14,872 / 39.27	15,015 / 47.13
Ligand	104 / 42.07	156 / 45.87	104 / 34.20
Heme	172 / 46.20	172 / 26.75	172 / 31.51
Water	91 / 43.47	778 / 37.62	339 / 35.97
RMSD bonds (Å)	0.009	0.008	0.007
RMSD angles (°)	1.251	1.130	1.130
Coordinate error (maximum-likelihood based) (Å)	0.39	0.27	0.34
Average bond angles/distances			
N/O_{N202}-O3 (Å)	2.70 ± 0.10	2.86 ± 0.08	2.67 ± 0.04
$\angle C3\text{-}O3\text{-}N/O_{N202}$ (°)	130 ± 20	130 ± 3	95 ± 7

*Statistics for highest resolution shell are shown in parentheses.

RESULTS

The crystal structures of CYP17A1 co-crystallized with each of the three compounds were determined in the same space group ($P2_12_12_1$) as previous structures of CYP17A1[1,17]. The four molecules occupying the asymmetric unit also had conformations consistent with previous structures of CYP17A1, with two sets of similar copies of the enzyme. Molecules A and B demonstrate high similarity to one another (RMSD over all Cα ranges from 0.18 to 0.62 Å), while molecules C and D are also similar to each other (RMSD over all Cα ranges from 0.27 to 0.9 Å), but there are some greater disparities between the conformations of molecules A and B compared to molecules C and D (average RMSD over all Cα = 1.26 ± 0.06 Å). These differences in protein backbone are very similar to those of all other CYP17A1 structures described to date regardless of the ligand[17].

For all three complexes, clearly defined electron density was apparent in the active sites of all four copies of the protein, and was consistent between copies of the protein. Inhibitors (1), (2), and (3) share a similar orientation within the CYP17A1 active site compared to one another and abiraterone[1] (Figure 4.1). The α-face of the steroid lies flat against the I helix at ~60° angle from the plane of the heme. Consistent with Type II spectral shifts observed during binding studies,[8] the heteroatom of the pyridine ring incorporated into inhibitors (1), (2), and (3) coordinates the heme iron, as also observed previously with abiraterone[1].

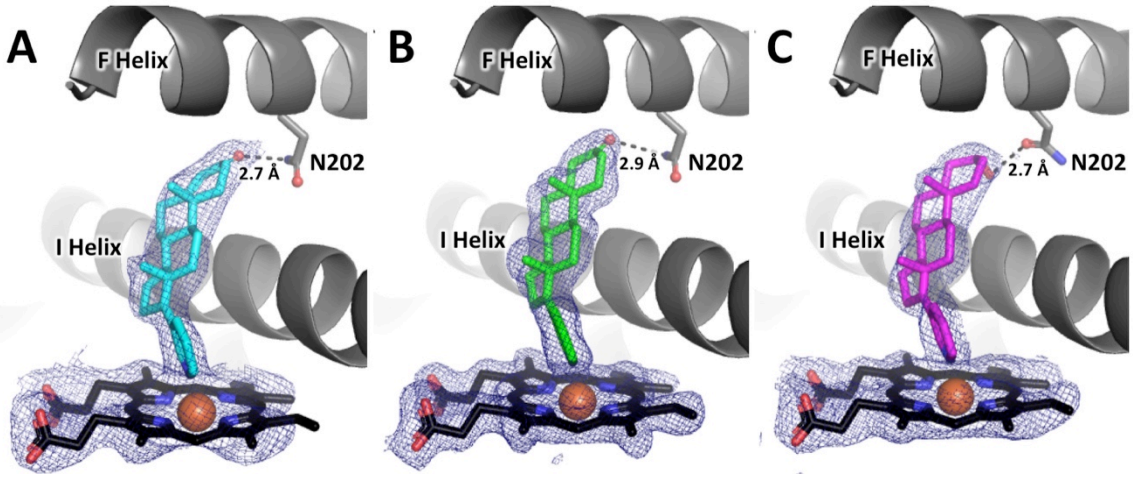

Figure 4.1: Electron density for inhibitors (1) in panel A, (2) in panel B, and (3) in panel C support a binding mode similar to abiraterone for all three. Direct contacts between C3 substituents to N202, as well as between the pyridine nitrogen and the heme iron are conserved. Distances shown are average distances among the all four molecules of CYP17A1 in each structure. Maps shown are simulated annealing composite omit maps contoured to 1.0 σ.

On the steroid A ring, C3 substituent hydrogen bonding to asparagine 202 (N202) in the F helix is conserved among the three inhibitors and abiraterone. For inhibitors (1) and (2), which have a ketone as a C3 substituent, N202 is implied to act as a hydrogen bond donor. In contrast, N202 may either be the hydrogen bond donor or acceptor to inhibitor (3), which has a C3 hydroxyl substituent. The average distance between C3 substituent and N202 among the four molecules of CYP17A1 is relatively consistent between ligands (2.6 ± 0.1 Å, 2.86 ± 0.08 Å, and 2.66 ± 0.04 Å for inhibitors (1), (2), and (3), respectively). The angle between the C3 substituent and the participating carbon or nitrogen of N202 varies depending on the conformation adopted by the A ring. The A rings of abiraterone and inhibitor (3) are completely saturated and both inhibitors are sp^3 hybridized at carbon 3. The A ring adopts the chair conformation as a result. In both axial and equatorial positions, the C3 alcohol adopts a ~95° bond angle from the heteroatom of N202 participating in a hydrogen bond. For inhibitors (1) and (2) with sp^2 hybridization at C3, the A ring takes on a conformation closer to that of a half-chair.

Consequently, the C3 substituent is projected more directly at N202 and forms an ~130° degree angle with the nitrogen of that residue.

Although direct contacts with the protein are largely conserved among the three inhibitors, substantial differences in the A ring configuration affect indirect interactions of these inhibitors with active site waters (Figure 4.2). Projection of the hydroxyl substituent from the α-face of the saturated A ring of inhibitor (3) allows this hydroxyl to interact with water molecule A, which is in turn engaged in hydrogen bonds with the side chain of residue arginine 239 (R239) on the G helix and the backbone carbonyl of glycine 297 (G297) in the I helix (Figure 4.2A). This water is also hydrogen bonded to an additional water (water B), which is hydrogen bonded to tyrosine 201 (Y201) on the F helix, forming a hydrogen bond network. The ketone substituent of the 3-keto, Δ4 inhibitor (1) also participates in a hydrogen bond with this water (Figure 4.3A) in some copies of this complex, although in others the water molecule lies outside hydrogen bonding distance or is not observed. It is important to note that structures of CYP17A1 with A-ring modified inhibitors span a range of resolutions from 2.0-2.7 Å, which can affect visualization of water molecules between structures. This is especially apparent in comparisons with the lowest resolution structure, the complex of CYP17A1 with inhibitor (1).

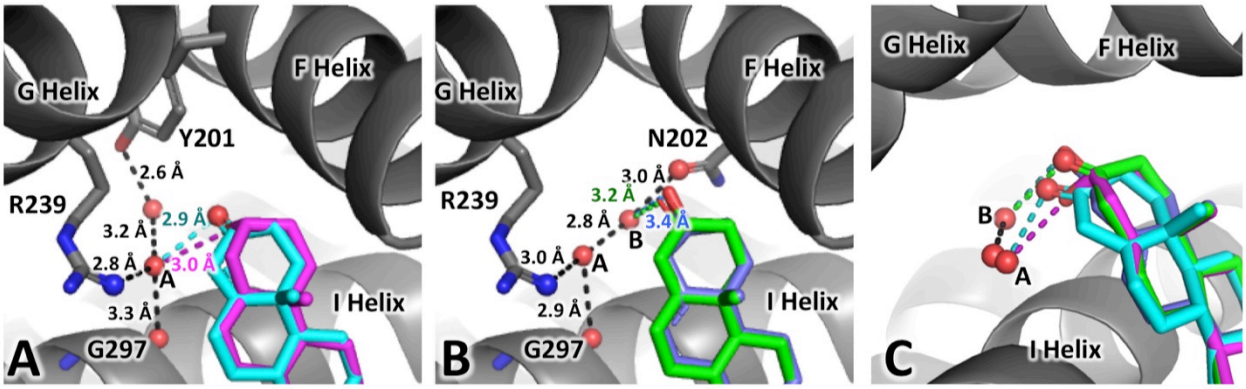

Figure 4.2: Analogs of abiraterone with various modifications to the A ring participate in different hydrogen bond networks. A) The hydrogen bond network surrounding compound (1, 3-keto,Δ4 analog) (shown in cyan sticks) is similar to that of (3, 3α-OH analog) (shown in magenta sticks). B) The hydrogen bond network of inhibitor (2, 3-keto analog) (green sticks) is most similar to that of abiraterone (light blue sticks). C) Differences in the A ring configuration affect whether the C3 substituent interacts with water A or B.

In contrast, the 3-keto group of inhibitor (2), with the A and B rings saturated, does not participate in a direct hydrogen bond with water A. Instead, the 3-keto substituent of inhibitor (2) lies within weak hydrogen bonding distance (average bond length among four molecules of CYP17A1 = 3.5 ± 0.3 Å) of water B, which itself participates in a larger network that includes N202 directly, as well as other residues (side chains of Y201 and R239 and the backbone carbonyl of G297). This hydrogen bonding network is most similar to that observed in the structure of CYP17A1 with abiraterone (Figure 4.2B). Projection of the C3 substitutent above the plane of the ring by abiraterone and inhibitor (2) seems to favor hydrogen bonding to water B, whereas projection of the C3 substituent below the plane of the ring by inhibitors (1) and (3) facilitates interaction with water A (Figure 4.2C).

The structure of CYP17A1 with inhibitor (2) is the highest resolution structure of this enzyme to date, which allows us to observe less-ordered elements and lower occupancy components of this complex than previous structures of ligand-bound CYP17A1. Most structures of CYP17A1 to date include unmodeled electron density in two of the four molecules

of the structure in a lipophilic region near the N-terminal β strands and the F/G loop (Figure 4.3A). There are no apparent hydrogen-bonding contacts with polypeptide to facilitate modeling a chain of waters, and the density was not clear enough to model any of the known components of the crystallization solution. This density is best defined in the 2.0 Å structure of CYP17A1 with inhibitor (2), and is consistent in length and planarity to the steroidal scaffold of the inhibitor (Figure 4.3B). Inhibitor (2) was modeled with the pyridine ring oriented either toward the interior of the protein or toward the solvent exposed surface (Figure 4.3C). The electron density maps and a 0.32% decrease in Rfree following refinement suggested that the pyridine ring is better modeled with the pyridine ring projected toward the interior of the protein. An alternate scenario in which both orientations are simultaneously present at partial occupancy was explored, but was a poor fit to the maps following a round of refinement. Thus, the final model of inhibitor (2) in the peripheral binding site has the pyridine ring oriented toward the interior of the binding pocket (Figure 4.3B)

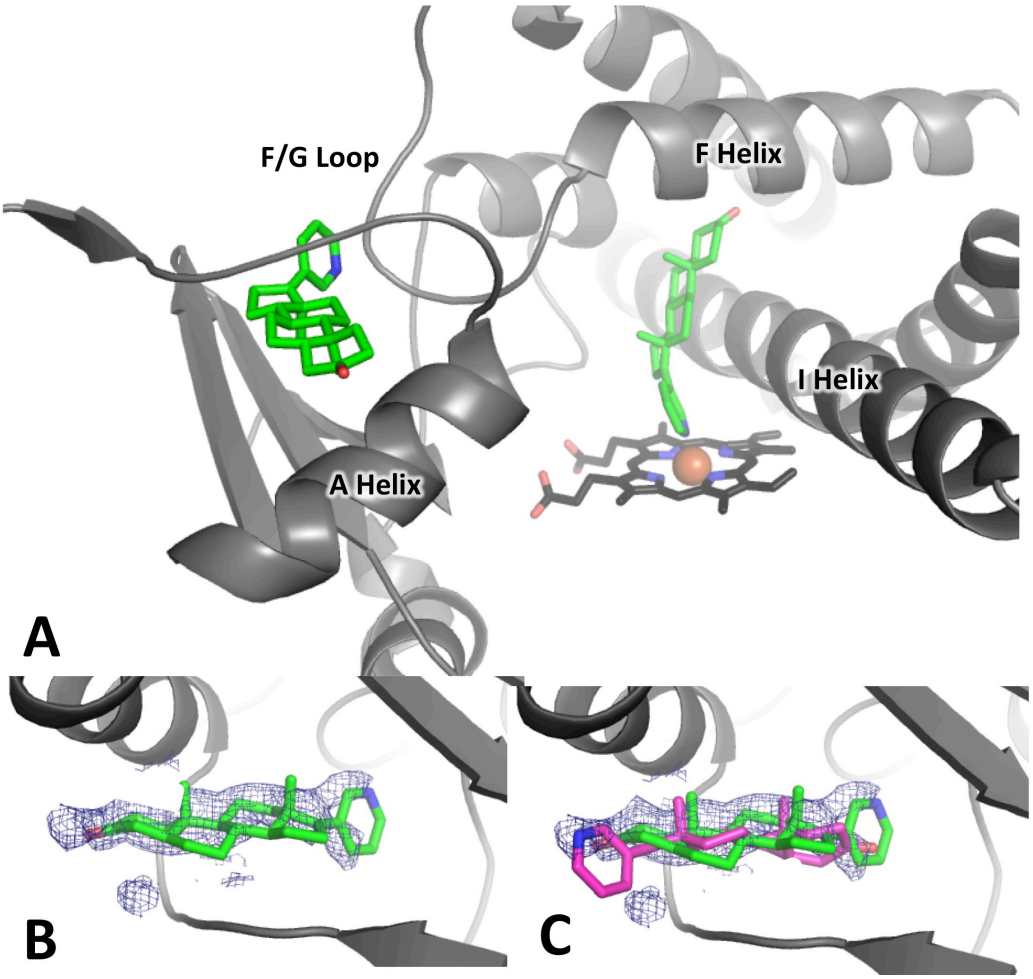

Figure 4.3: Peripheral steroid binding site observed in structure of CYP17A1 with inhibitor (2). A) Locations of inhibitor (2) (shown in green sticks) binding sites in CYP17A1 with respect to heme (shown in black sticks). B) Inhibitor (2) (green sticks) modeled into electron density (shown as blue mesh) at peripheral site.. C) Inhibitor (2) modeled into the peripheral binding site in the orientation modeled in the final structure (green sticks) as well as the alternate orientation projecting the pyridine ring into bulk solvent (magenta sticks). Map shown in panels B and C is composite omit map with simulated annealing contoured to 0.8 σ.

DISCUSSION

Analogs of abiraterone with modifications to the A ring of the steroid nucleus have previously been demonstrated to have similar affinity for CYP17A1 as abiraterone and are reported to be equipotent inhibitors of progesterone hydroxylation[8]. In the current work, the X-ray crystal structures of three such analogs in complex with CYP17A1 demonstrate that these inhibitors bind within CYP17A1 active site very similarly to abiraterone.

Direct contacts with the enzyme, specifically coordination of the pyridine nitrogen to the heme iron and the hydrogen bond between the C3 substituent and N202, were maintained among the three inhibitors. The most substantial differences among the structures of CYP17A1 with A-ring modified analogs were different interactions between the active site water network and the inhibitors.

In the structure of CYP17A1 with 3-hydroxy, Δ5 inhibitor abiraterone, the 3-hydroxy substituent of the inhibitor interacts with an active site water A, which in turn hydrogen bonds to water B, a participant in hydrogen bonds with R239 and the backbone of G297. Inhibitor (2), for which the A ring can also adopt the chair conformation, also participates in a weak hydrogen bond with the same water. In contrast, the 3α-hydroxy substituent of inhibitor (3) lies in an axial position where it can no longer interact with water molecule A, but is placed within hydrogen bonding distance of water molecule B. The Δ4 double bond of inhibitor (2) leads to a flattening of the A-ring, and consequently the 3-keto-substituent interacts with water molecule B in some copies of the structure.

Interaction of C3 substituents with different water molecules demonstrates the role of A ring configuration on where in the active site the oxygen on C3 is projected. Since this oxygen is part of one of the few functional groups available for modification on the steroid, the direction in which it is projected could be crucial in designing inhibitors to access particular active site features. For example, the CYP17A1 active site features a pocket that extends over the I helix (Figure 4.4), which is not observed in other steroidogenic cytochrome P450s such as CYP21A2 (as described in more detail in Chapter 7). Design of inhibitors that extend over the I helix may therefore demonstrate more selectivity for CYP17A1 compared to CYP21A2. Building upon the 3α-hydroxyl group of inhibitor (3), which runs parallel to and is projected over the I helix, might

be more effective in accessing this pocket than building upon the corresponding 3β-hydroxyl group in abiraterone, which is projected toward the F helix.

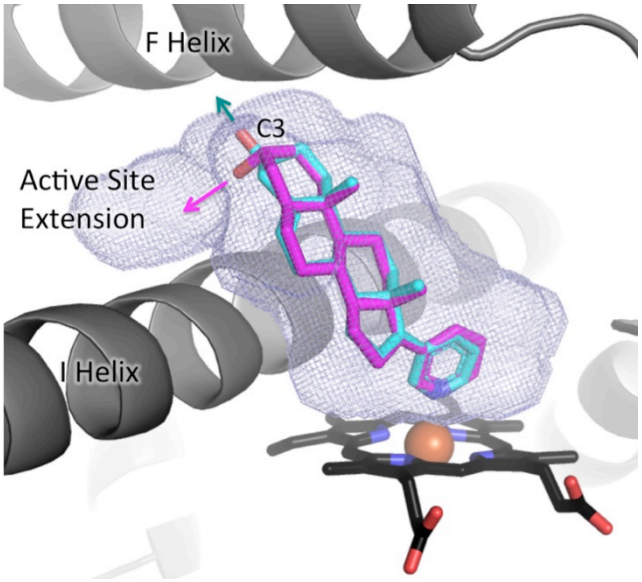

Figure 4.4: The C3 hydroxyl substituent of inhibitor (3) shown in magenta points toward an extension of the CYP17A1 active site, whereas the C3 hydroxyl substituent of abiraterone (cyan) is projected into the F helix. Further functionalization of the C3 hydroxyl group of inhibitor (3) may therefore be a strategy for accessing this active site pocket.

Differences in A ring configuration and therefore hydrogen-bonding to the active site water network do not appear to affect the potency of progesterone 17α-hydroxyase inhibition[8], though all three A-ring modified inhibitors have yet to be compared for inhibition of the 17,20-lyase reaction. However, changes to the A ring configuration of abiraterone do appear to have a significant effect on the compound's potency toward other prostate cancer targets. This was recently demonstrated by studies that identified inhibitor (1) as an effective inhibitor of 3β-hydroxysteroid dehydrogenase and 5α-reductase, both of which are necessary to generate dihydrotestosterone, and a much more potent androgen receptor antagonist than abiraterone[9]. The structure of CYP17A1 with inhibitor (1), as well as the two other analogs of abiraterone, support binding and inhibition data that suggest changes to the A-ring do not substantially affect interactions of these inhibitors with CYP17A1. Besides inhibitor (1), inhibitors (2) and (3)

should also be evaluated against other prostate cancer targets, as these compounds could also demonstrate improved capabilities as multi-targeting agents for the treatment of advanced stage prostate cancer.

In addition to revealing interactions of A-ring modified inhibitors with the active site of CYP17A1, the high resolution structure of CYP17A1 with inhibitor (2), solved to 2.0 Å, provides insight into a potential peripheral ligand binding site. Electron density near the N-terminal beta sheet region, A helix, and F/G loop has been observed in some molecules of previous CYP17A1 crystal structures, but was too ambiguous to permit the modeling of an additional ligand. At 2.0 Å resolution, the map more strongly suggests this density is actually a steroid at partial occupancy. Although additional steroid binding sites had not been previously reported for CYP17A1, crystal structures of other cytochrome P450 enzymes have shown steroids interacting with similar regions of the enzyme. One of the first structures of CYP3A4 revealed that progesterone, the intended ligand, was not located in the active site, but instead bound to a shallow pocket formed in the F/G loop (Figure 4.5A)[18]. This site has also been identified through fluorescence energy resonance transfer, and is hypothesized to participate in cooperative ligand binding by inducing a conformational change in CYP3A4[19]. The structure of the steroidogenic bovine CYP21A2 revealed a second copy of the substrate 17α-hydroxyprogesterone in a site near the N-terminal β strands and the F′ helix[20] (Figure 4.5B). This site lies between the active site of the enzyme and bulk solvent, suggesting that this channel may be a route for substrate access. The peripheral ligand in the structure of CYP17A1 with inhibitor (2) interacts with very similar structural elements of the enzyme. However, the conformation of the F/G region in bovine CYP21A2 is so dissimilar from that of human CYP17A1 (Figure 4.5C), that the peripheral copy of ligand is nearly 20 Å from the active site

ligand compared to ~10 Å in the bovine CYP21A2 structure. A more recent structure of human CYP21A2 with progesterone also identified a second binding site in the the same region of the human form of the enzyme, albeit at lower occupancy[21]. Whether or not this second, partially-occupied binding site is an artifact of crystallization or functionally relevant is unknown, as the role of a peripheral binding site in CYP17A1 function has yet to be explored. It is tempting to suggest that binding interactions at this secondary site, near elements suggested to be responsible for enzyme opening and closing, might affect the processivity of CYP17A1 and thus provide opportunities for lyase-selective inhibition. Cytochrome b_5, which binds to a site on the proximal face of the enzyme, is known to allosterically and selectively augment the CYP17A1-mediated 17,20-lyase reaction but not 17α-hydroxylation and has been shown to modulate the conformation of residues in the F and G helices[22]. Thus allosteric influences on CYP17A1 function are not only possible, but may suggest a new strategy for selective inhibition of the 17,20-lyase reaction. Retrospective analysis of this peripheral binding site may be particularly informative for CYP17A1 with *R*-orteronel, which demonstrates the most selectivity toward 17,20-lyase inhibition in our studies (*vide infra*, Chapter 6).

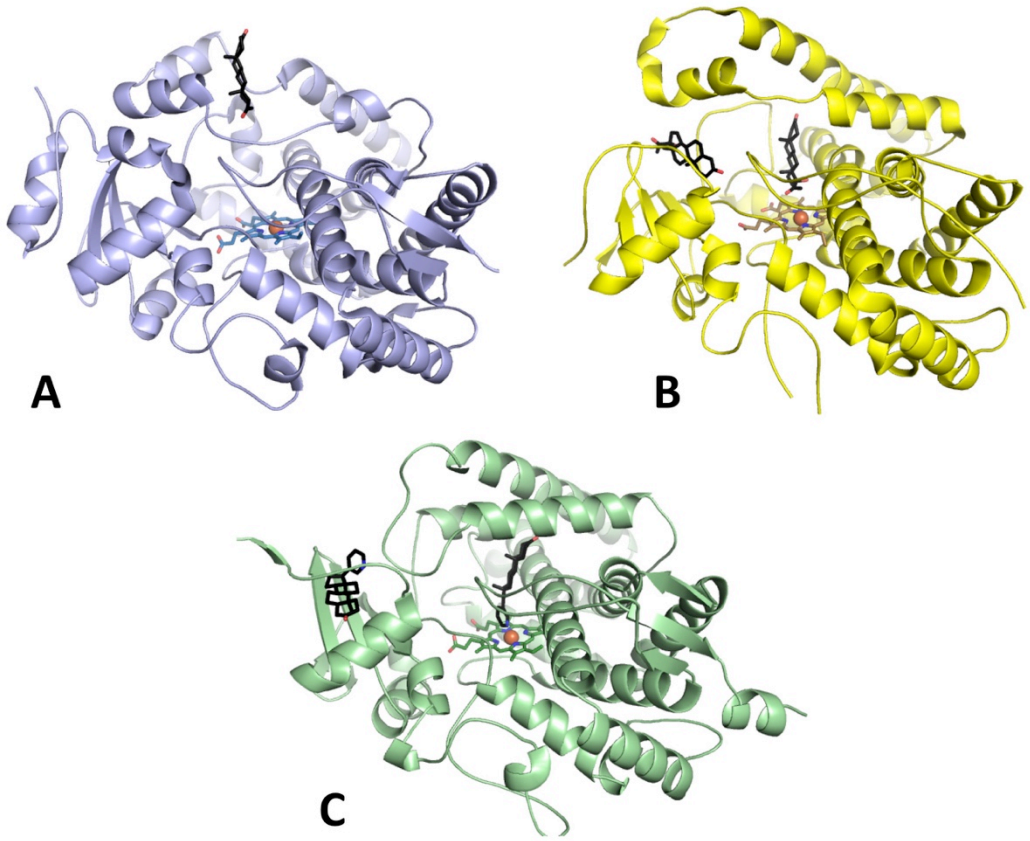

Figure 4.5: Steroids (all shown in black sticks) bind in different peripheral sites in cytochrome P450 enzymes A) human CYP3A4 with progesterone B) bovine CYP21A2 with 17α-hydroxyprogesterone, and C) human CYP17A1 with inhibitor 2.

In conclusion, the crystal structure of CYP17A1 with A-ring modified analogs of abiraterone demonstrate that these inhibitors make similar direct interactions with CYP17A1. Changes in the conformation of the A ring do affect indirect interactions with the active site by changing which active site waters participate in hydrogen bonds with an inhibitor. Additionally, the high resolution structure of CYP17A1 with inhibitor (2) demonstrates a likely peripheral ligand binding site, which may be relevant to the function of CYP17A1, a crucial target in the treatment of advanced prostate cancer.

AKNOWLEDGEMENTS

Inhibitors (1), (2), and (3) were synthesized by Maria Garrido and Francis Yoshimoto in the lab of Dr. Richard Auchus.

REFERENCES

(1) DeVore, N. M.; Scott, E. E. *Nature* **2012**, *482*, 116.
(2) Handratta, V. D.; Vasaitis, T. S.; Njar, V. C.; Gediya, L. K.; Kataria, R.; Chopra, P.; Newman, D., Jr.; Farquhar, R.; Guo, Z.; Qiu, Y.; Brodie, A. M. *J. Med. Chem.* **2005**, *48*, 2972.
(3) Potter, G. A.; Barrie, S. E.; Jarman, M.; Rowlands, M. G. *J. Med. Chem.* **1995**, *38*, 2463.
(4) Jarman, M.; Barrie, S. E.; Llera, J. M. *J. Med. Chem.* **1998**, *41*, 5375.
(5) Fluck, C. E.; Miller, W. L.; Auchus, R. J. *J. Clin. Endocrinol. Metab.* **2003**, *88*, 3762.
(6) Gupta, M. K.; Guryev, O. L.; Auchus, R. J. *Arch. Biochem. Biophys.* **2003**, *418*, 151.
(7) Bruno, R. D.; Vasaitis, T. S.; Gediya, L. K.; Purushottamachar, P.; Godbole, A. M.; Ates-Alagoz, Z.; Brodie, A. M.; Njar, V. C. *Steroids* **2011**, *76*, 1268.
(8) Garrido, M.; Peng, H. M.; Yoshimoto, F. K.; Upadhyay, S. K.; Bratoeff, E.; Auchus, R. J. *J. Steroid Biochem. Mol. Biol.* **2014**, *143*, 1.
(9) Li, Z.; Bishop, A. C.; Alyamani, M.; Garcia, J. A.; Dreicer, R.; Bunch, D.; Liu, J.; Upadhyay, S. K.; Auchus, R. J.; Sharifi, N. *Nature* **2015**.
(10) Cai, C.; Chen, S.; Ng, P.; Bubley, G. J.; Nelson, P. S.; Mostaghel, E. A.; Marck, B.; Matsumoto, A. M.; Simon, N. I.; Wang, H.; Chen, S.; Balk, S. P. *Cancer Res.* **2011**, *71*, 6503.
(11) Kabsch, W. *Acta Crystallogr., Sect. D: Biol. Crystallogr.* **2010**, *66*, 125.
(12) McCoy, A. J.; Grosse-Kunstleve, R. W.; Adams, P. D.; Winn, M. D.; Storoni, L. C.; Read, R. J. *J. Appl. Crystallogr.* **2007**, *40*, 658.
(13) Emsley, P.; Lohkamp, B.; Scott, W. G.; Cowtan, K. *Acta Crystallogr., Sect. D: Biol. Crystallogr.* **2010**, *66*, 486.
(14) Adams, P. D.; Afonine, P. V.; Bunkoczi, G.; Chen, V. B.; Davis, I. W.; Echols, N.; Headd, J. J.; Hung, L. W.; Kapral, G. J.; Grosse-Kunstleve, R. W.; McCoy, A. J.; Moriarty, N. W.; Oeffner, R.; Read, R. J.; Richardson, D. C.; Richardson, J. S.; Terwilliger, T. C.; Zwart, P. H. *Acta Crystallogr., Sect. D: Biol. Crystallogr.* **2010**, *66*, 213.
(15) Kleywegt, G. J.; Jones, T. A. *Acta Crystallogr., Sect. D: Biol. Crystallogr.* **1994**, *50*, 178.
(16) Schrodinger, LLC 2010.
(17) Petrunak, E. M.; DeVore, N. M.; Porubsky, P. R.; Scott, E. E. *J. Biol. Chem.* **2014**, *289*, 32952.
(18) Williams, P. A.; Cosme, J.; Vinkovic, D. M.; Ward, A.; Angove, H. C.; Day, P. J.; Vonrhein, C.; Tickle, I. J.; Jhoti, H. *Science* **2004**, *305*, 683.
(19) Davydov, D. R.; Rumfeldt, J. A.; Sineva, E. V.; Fernando, H.; Davydova, N. Y.; Halpert, J. R. *J. Biol. Chem.* **2012**, *287*, 6797.

(20) Zhao, Y.; White, M. A.; Muralidhara, B. K.; Sun, L.; Halpert, J. R.; Stout, C. D. *J. Biol. Chem.* **2006**, *281*, 5973.
(21) Pallan, P. S.; Wang, C.; Lei, L.; Yoshimoto, F. K.; Auchus, R. J.; Waterman, M. R.; Guengerich, F. P.; Egli, M. *J. Biol. Chem.* **2015**, *290*, 13128.
(22) Estrada, D. F.; Skinner, A. L.; Laurence, J. S.; Scott, E. E. *J. Biol. Chem.* **2014**, *289*, 14310.

Chapter 5.

Evaluation of Cytochrome P450 17A1 (CYP17A1) Function with Clinically Observed Mutations

INTRODUCTION

Cytochrome P450 17A1 (CYP17A1) is necessary for the biosynthesis of both androgens and corticosteroids. Impairment of CYP17A1 function is desirable for patients with hormone-dependent prostate cancer since inhibition of androgen biosynthesis can halt tumor growth and progression. For otherwise healthy individuals, however, suppression of CYP17A1 function as a consequence of missense mutations in the enzyme prevents production of sex steroids required for normal development[1]. In both populations, impaired CYP17A1 function can manifest as high blood pressure and fluid retention, as a consequence of secondary mineralocorticoid excess[1-3]. Unlike androgen deprivation, which is useful for the treatment of prostate cancer, the corticosteroid-related symptoms of CYP17A1 impairment are generally detrimental. Ideally, therapeutic inhibition of CYP17A1 to treat prostate cancer would affect only androgen production, but have minimal effects on the production of corticosteroids.

More than 50 mutations of CYP17A1 have been observed in human patients with varying effects on steroid biosynthesis, altering levels of circulating androgens and estrogens, as well as 17-hydroxysteroids and glucocorticoids[4,5]. Most patients in which CYP17A1 mutations are identified present with symptoms such as ambiguous genitalia or lack of secondary sexual development as a consequence of low levels of circulating androgens and estrogens[1,4]. Hypertension as a result of low cortisol production and the resulting secondary mineralocorticoid excess is often also observed[1].

Inhibitors of CYP17A1 approved to treat prostate cancer have not yet been able to selectively disrupt androgen production without interfering with corticosteroid biosynthesis. However, there is precedent in the literature for selective disruption of androgen production in humans with CYP17A1 deficiency due to missense mutations in the CYP17A1 gene[5]. Two types of CYP17A1 mutations have been observed clinically. The first type of mutations disrupt both androgen production and glucocorticoid production, while the second type appear to only affect the production of androgens. Biochemically, this is the consequence of inhibiting the different reactions performed by CYP17A1, which result in different steroid hormone metabolites. Mutations of CYP17A1 that prevent both androgen production and glucocorticoid production block both 17α-hydroxylation necessary to generate both androgens and glucocorticoids, as well as the 17,20-lyase reaction necessary for biosynthesis of androgens. In contrast, mutations of CYP17A1 that affect androgen production without interrupting glucocorticoid production selectively disrupt the 17,20-lyase reaction while allowing CYP17A1-mediated 17α-hydroxylation to proceed normally. Understanding how some mutations selectively disrupt the 17,20-lyase reaction but allow the 17α-hydroxylase reaction to proceed may be useful to inform strategies for selective inhibition of androgen production by small molecule inhibitors.

Mutations of CYP17A1 that disrupt both hydroxylase and 17,20-lyase reactions are the most widely reported, and may affect crucial aspects of the enzyme including the formation of key secondary structural elements and heme incorporation. Two such examples are D116V and F114V mutations[5]. The D116V mutation was identified in a female patient that presented with lack of sexual development due to insufficient androgen production and low levels of cortisol, indicating both hydroxylase and lyase deficiency[5]. Following identification, the D116V

mutation was demonstrated to indeed result in a loss of both hydroxylase and l7,20-lyase function (38% and ~11% wild type activity, respectively)[5]. The side chain of D116, a solvent exposed residue in the loop between the B′ and C helices, hydrogen bonds to the backbone of residue R96, which in turn interacts with the heme cofactor proprionates (Figure 5.1). Mutation of D116 to a valine would not support such hydrogen bonding to R96 and may therefore indirectly affect heme incorporation, which would prevent all CYP17A1 catalysis[6]. However, the proximity of D116 to the B′ helix could also make mutation of this residue deleterious to formation of this crucial element of the CYP17A1 structure. Some mutations that affect both hydroxylase and 17,20-lyase turnover line the CYP17A1 active site directly. Originally identified in a 17 year-old female patient that presented with lack of secondary sexual development and hypertension[5], mutation of active site residue F114 to a valine is reported to demonstrate less than 10% of the progesterone hydroxylase activity of the wild type enzyme[5,7]. Also located in the B′/C loop, the side chain of F114 is directed toward the protein interior and lies only ~4 Å from steroidal substrates and inhibitors in previous structures of CYP17A1[6,8]. Mutation to the smaller hydrophobic valine would certainly affect active site topography and potentially the binding of hydroxylase and lyase substrates. Alternatively, as proposed for the D116V mutation, dual hydroxylase/17,20-lyase deficiency observed for F114V could be the result of substitution of a substitution at this position which disrupts the formation of adjacent secondary structural elements such as the B′ helix (Figure 5.1).

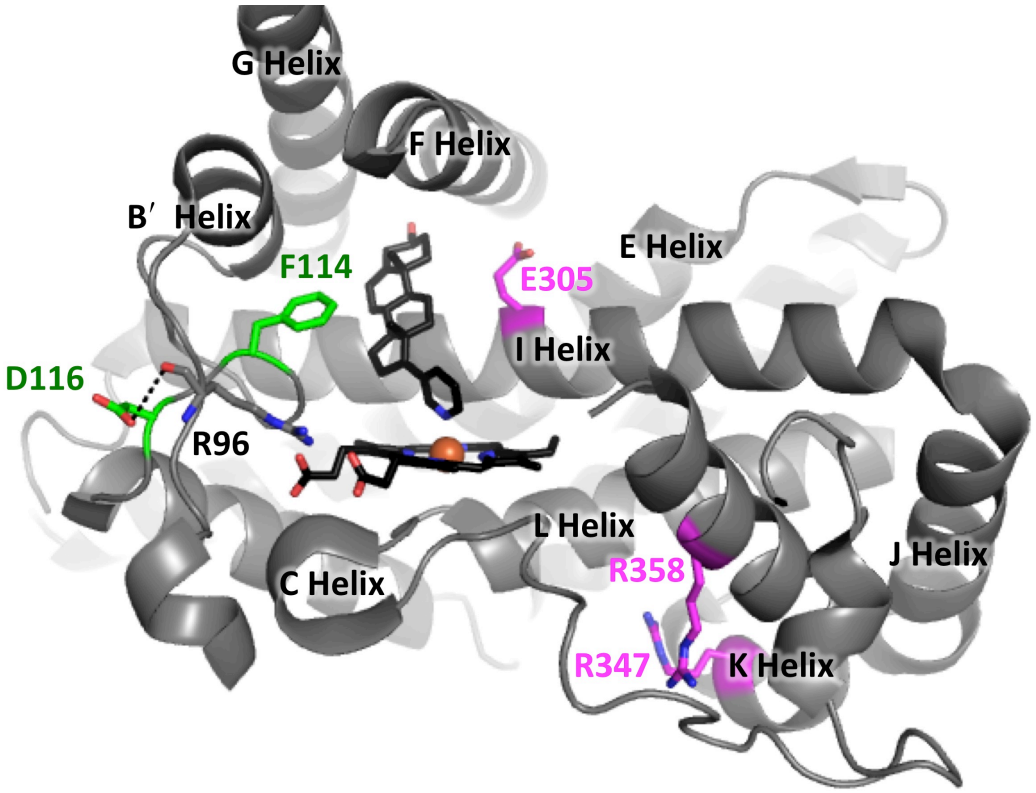

Figure 5.1: Location of CYP17A1 residues whose mutation is reported to affect 17α-hydroxylase and 17,20-lyase activity (green) or only 17,20-lyase activity (magenta).

Mutations of CYP17A1 that disrupt the 17,20-lyase reaction more substantially than the hydroxylase reaction are rarer than those which impact both reactions equally. Of these mutations, only one is known to occur in the active site. Mutation of a glutamate residue in the I helix (E305) to a glycine was identified in a male patient with a lack of secondary sexual development but with high levels of 17α-hydroxylated metabolites, suggesting selective 17,20-lyases deficiency[9]. Follow-up studies substantiated 17α-hydroxylase activity for both progesterone and pregnenolone. Additionally, although human CYP17A1 enzyme is very inefficient at converting the Δ4 17α-hydroxyprogesterone to its 19-carbon counterpart androstenedione via 17,20-lyase activity[10], this reaction was not further compromised in the E305G variant[9]. However, this mutant failed to produce the major 17,20-lyase product,

dehydroepiandrosterone, at detectable levels[9]. Despite production of small quantities of the Δ4 17,20-lyase product androstenedione, the male patient with E305G mutation presented with a micropenis and gynecomastia[9]. This indicated that the 17α-hydroxyprogesterone turnover by E305G was not sufficient to support normal sexual development[9]. CYP17A1 E305G was expressed in *E. coli* and purified by Dr. Natasha DeVore, a previous lab member, but this mutant enzyme failed to catalyze progesterone hydroxylation in our typical system of reconstituted, purified proteins.

Other mutations reported to selectively disrupt the 17,20-lyase function are located on the proximal face of CYP17A1. This region of the protein is known to generally interact with partner proteins NADPH-cytochrome P450 reductase (CPR) and cytochrome b_5[11,12]. Electron delivery by CPR is necessary for both CYP17A1-mediated reactions. In contrast, cytochrome b_5 augments the 17,20-lyase reaction 10-fold, but has little effect on the 17-hydroxylase reaction[13]. Mutation of basic residues on this face of CYP17A1 had been proposed to interrupt binding to the anionic surface of cytochrome b_5 and therefore selectively disrupt the CYP17A1-mediated 17,20-lyase reaction[14,15].

Mutation of residues R347 and R358 (Figure 5.1) to histidine and glutamine, respectively were identified in patients with severe 17,20-lyase deficiency but normal or elevated levels of 17α-hydroxylated metabolites[16]. Further studies demonstrated that these single site mutations result in only 5% 17,20-lyase activity compared to wild type[16]. However, these mutants retain 65% of wild type 17α-hydroxylase activity. Unlike wild type enzyme, addition of cytochrome b_5 does not appear to augment the 17,20-lyase reaction, which suggests that impairment of the 17,20-lyase reaction by these mutants could be mediated by interrupting the CYP17A1/cytochrome b_5 interaction[14,15]. Moreover, mutation of these residues to conserve

cationic charge results in a partial recovery of 17,20-lyase activity[14], which also implicates binding of anionic partner proteins as the basis for loss in 17,20-lyase activity.

Most studies examining the effect of these mutations have been performed using CYP17A1 in COS-1 cells or yeast microsomes which can contain other enzymes capable of steroid metabolism or electron delivery to cytochromes P450 and varying amounts of redox partner proteins[5,9,15]. Very few studies have kinetically characterized both 17α-hydroxylase or 17,20-lyase reactions for wild type CYP17A1 and relevant mutants. Additionally, most studies have only focused on a single CYP17A1 mutant or a small panel of mutants with similar functional impairment, evaluating either mutants that exhibit no CYP17A1 activity or mutants with selective 17,20-lyase impairment.

The aim of the study described herein was to use purified cytochrome P450 and partner proteins to evaluate the function of a small panel of clinically-observed CYP17A1 mutants that exhibit either 1) both hydroxylase and lyase impairment or 2) selective 17,20-lyase impairment. Kinetic analysis of relevant reactions could help determine a basis for hindered enzymatic activity by CYP17A1 mutants F114V and D116V, confirm the role of cytochrome b_5 in l7,20-lyase-deficient mutants R347H and R358Q, and perhaps even help elucidate whether cytochrome b_5 augments 17,20-lyase activity via electron transfer or allosteric effects on CYP17A1 conformation.

The mutants reported with combined hydroxylase/17,20-lyase deficiencies, F114V and D116V, were expressed in *E. coli*, but were not stable enough to permit isolation. This suggested that the native residues at these positions are necessary for protein stability. In contrast, the R347H and R358Q mutants, reported to be selectively lyase-deficient, were successfully purified from *E. coli*. Both enzymes were subsequently evaluated for conversion of

progesterone to 17α-hydroxyprogesterone. R347H did not bind or turn over progesterone, while R358Q was substantially less active than the wild type enzyme,. R358Q was also evaluated for 17,20-lyase turnover, and produced levels of DHEA at lower levels compared to wild type enzyme in the presence of cytochrome b_5, suggesting that lyase deficiency resulting from mutation of this residue is the result of decreased interactions between CYP17A1 and redox partner proteins. However, both of the latter mutants demonstrated substantial deficiencies in progesterone hydroxylation compared to wild type, suggesting that R358Q and R347H are not selectively lyase-deficient as reported previously[15,16].

METHODS

Mutagenesis

Site-directed mutagenesis was performed using the pCW/CYP17A1Δ19H plasmid to generate CYP17A1 mutants F114V, D116V, R347H, and R358Q as described in Chapter 2.

Expression and Purification of Wild Type CYP17A1 and CYP17A1 Mutants

CYP17A1 wild type enzyme and all four mutants were expressed in the absence of ligand as described in Chapter 2. In addition to expression in the absence of ligand, the unstable F114V mutant was also expressed at a separate time in the presence of 50 μM progesterone since the presence of ligand can aid in the stabilization of these enzymes.

CYP17A1 wild type enzyme was purified as described in Chapter 2. CYP17A1 R347H and R358Q mutant enzymes were purified in the absence of ligand through CM sepharose chromatography as described in Chapter 2. Purification was performed for CYP17A1 F114V and D116V mutant enzymes expressed in the absence of ligand through Ni-NTA affinity

chromatography as described in Chapter 2. CYP17A1 F114V expressed in the presence of 50 μM progesterone was purified through Ni-NTA affinity chromatography as described in Chapter 2, but with 50 μM progesterone in all purification buffers in an effort to enhance protein stability.

CYP17A1 R358Q was quantified via carbon monoxide spectral shift as described in Chapter 2, but since the reduced form of this mutant was unstable in the absence of ligand resulting in a spectral shift to 420 nm, the enzyme was also quantified in the presence of 50 μM progesterone.

Assays

The progesterone hydroxylation assay was performed as described in Chapter 2 at substrate concentrations varying from 0-200 μM.

The 17,20-lyase assay was performed as described in Chapter 2 using a substrate concentration of 25 μM. One modification is that the reconstituted protein system for reactions run in the absence of cytochrome b_5 contained a 1:4:0 ratio of cytochrome P450 to CPR to cytochrome b_5.

Spectral ligand binding assays were performed as described in Chapter 2 with the progesterone concentration varied from 0 – 11 μM.

RESULTS

Protein Expression and Purification of CYP17A1 Mutants

CYP17A1 mutants were all expressed in *E. coli* and purification attempted according to the same protocol used to express wild type enzyme. However, the yield and stability of these

mutant proteins varied substantially between CYP17A1 mutants. The combined 17α-hydroxylase/17,20-lyase deficient mutants CYP17A1 F114V and D116V demonstrated a small amount cytochrome P450 immediately following detergent extraction as revealed by the reduced carbon monoxide difference spectrum (Figure 5.2), albeit much less than wild type at the same stage in purification. Following affinity chromatography, the elution fractions for CYP17A1 D116V demonstrated little absorbance based on the absolute spectrum of the protein, indicating the presence of very little heme-containing protein. The heme Soret peak λ_{max} was observed at 405-407 nm, which is more consistent with free heme cofactor than heme coordinated to thiolate. Following seven-fold concentration, the reduced carbon monoxide difference spectrum of these elution fractions demonstrated a very small amount of the inactive P420 form (Figure 5.3A). Although the nature of the protein absorbing at 420 nm, commonly referred to as "P420", is not fully understood, this species is generally considered to be a form of the enzyme unstable under reducing conditions. The difference spectrum was also recorded in the presence of 50 μM progesterone as a potential stabilizing ligand, but still did not result in significant absorbance at 450 nm (Figure 5.3B).

Affinity chromatography of CYP17A1 F114V yielded similar results with the heme Soret peak λ_{max} at 408-413 nm in the initial absolute spectrum and very little absorbance demonstrated by any of the affinity chromatography elution fractions. The carbon monoxide difference spectrum of the affinity chromatography elution fractions exhibited only a small peak at 420 nm, also similar to that of the D116V mutant.

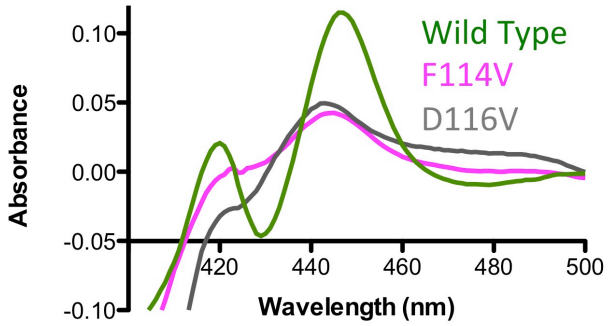

Figure 5.2: Reduced carbon monoxide difference spectra of F114V (magenta) and D116V (gray) mutants following detergent extraction demonstrate a small absorbance peak at 450 nm. Reduced carbon monoxide spectrum of wild type enzyme (green) at the same stage of purification shown for comparison.

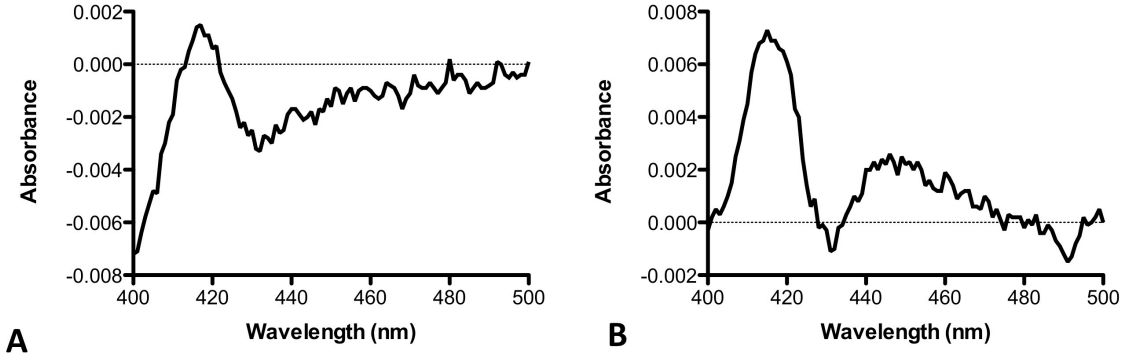

Figure 5.3: Carbon monoxide difference spectra of D116V in the absence of ligand (panel A) and presence of 50 μM progesterone (panel B) mainly demonstrate a shift to 420 nm.

CYP17A1 F114V had previously been successfully expressed and purified in the same strain of *E. coli* by another lab member, Dr. D. Fernando Estrada, when the tight-binding CYP17A1 inhibitor abiraterone was present in both expression media and purification buffers. This suggests that the presence of this ligand improves the stability of the protein. Since the presence of abiraterone precludes functional studies of the mutant, expression and purification of CYP17A1 F114V was attempted in the presence of 50 μM progesterone substrate instead. The outcome of this expression and attempted isolation of the mutant was similar to that in the absence of ligand. The affinity chromatography elution demonstrated no significant absorbance

at 417 nm and the reduced carbon monoxide difference spectrum revealed only a peak at 420 nm very similar to D116V.

Purification of CYP17A1 R358Q through CM sepharose chromatography yielded ~5 mg/L expression culture based on the absolute spectrum of the purified protein, which is similar to the amount of wild type enzyme usually isolated at this stage, an average of 7 ± 2 mg/L. The reduced carbon monoxide spectrum of CYP17A1 R358Q featured very little protein with a λ_{max} at 450 nm approximately one minute after treatment with carbon monoxide, and instead resulted in absorbance at 420 nm (Figure 5.4A, light blue). After eight minutes, essentially all available protein had shifted to a λ_{max} at 420 nm, leaving no absorbance at 450 nm (Figure 5.24, dark blue). In an effort to better stabilize the CYP17A1 R358Q under reducing conditions, a reduced carbon monoxide spectrum was obtained in the presence of substrate progesterone (50 µM). The resulting difference spectrum yielded only a λ_{max} of 450 nm (Figure 5.4A, red), similar to wild type CYP17A1, indicating that the R358Q mutant can be stabilized in the presence of substrate.

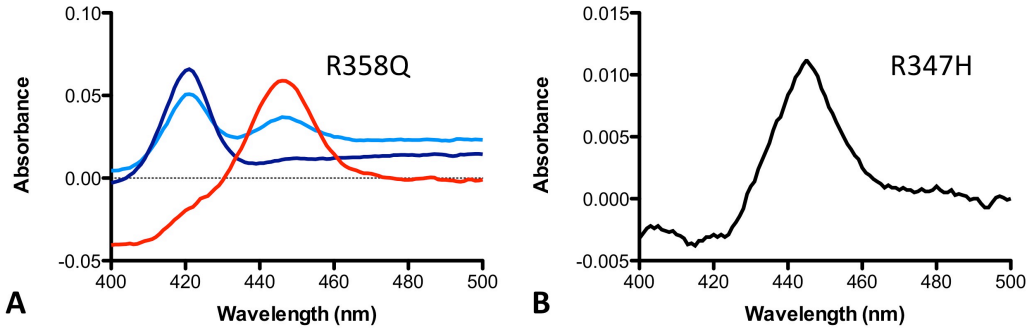

Figure 5.4: Carbon monoxide difference spectra of CYP17A1 mutants reported to be selectively 17,20-lyase deficient. A) In the absence of ligand, the spectrum of R358Q exhibits some absorbance at 450 nm at ~1 minute (light blue), but after 8 minutes is entirely shifted to 420 nm (dark blue). However, when this spectrum is collected in the presence of 50 µM progesterone, the λ_{max} is observed at 450 nm after 10 minutes (red) similar to wild type CYP17A1. B) The λ_{max} of R347H is shifted to 450 nm even in the absence of ligand, consistent with active cytochrome P450 protein.

CYP17A1 R347H, which features a modification to a similar region of the enzyme as R358Q, was isolated at about $1/10^{th}$ the quantity seen for wild type enzyme. Following cation exchange chromatography, CYP17A1 R347H yielded only 0.42 mg / L expression media. The protein that was isolated, however, demonstrated a carbon monoxide difference spectrum with a λ_{max} of 450 nm (Figure 5.4B). This indicated that the purified protein was stable similar to wild type enzyme under reducing conditions, even in the absence of ligand.

Progesterone Hydroxylation by Reported Lyase-Deficient Mutants

Both mutants CYP17A1 R347H and R358Q, reported to be selectively lyase deficient, were evaluated for progesterone hydroxylation. The R347H mutant demonstrated no production of the major CYP17A1 metabolite 17α-hydroxyprogesterone at substrate concentrations as high as 200 μM. To determine whether the lack of progesterone hydroxylase activity by R347H resulted from a failure to bind substrate or an inability to perform catalysis, binding of progesterone to R347H was monitored via spectral shift binding assay as described in Chapter 2. At a progesterone concentration of 11 μM, no shift in spectrum was observed for the R347H mutant. This indicated impaired binding of the substrate compared to wild type CYP17A1, which is saturated with the same ligand at 1 μM under the same conditions.

In contrast, the R358Q mutant protein demonstrated turnover of progesterone to 17α-hydroxyprogesterone. The R358Q mutant demonstrated a two-fold increase in K_m compared to wild type enzyme, which may not be significant when considering the error of measurement. In contrast, its k_{cat} was over 25-fold lower than that of wild type CYP17A1, resulting in a significant drop in catalytic efficiency (Table 5.1).

Table 5.1: Kinetic constants for progesterone 17α-hydroxylation by CYP17A1 wild type and R358Q mutant.

Enzyme	K_m **(μM)**	k_{cat} **(min^{-1})**	k_{cat}/K_m **(μM^{-1} min^{-1})**
Wild type	10 ± 2	1.01 ± 0.05	0.0960
R358Q	20 ± 5	0.039 ± 0.003	0.0195

17,20-Lyase Catalysis by R358Q

Since the 17,20-lyase activity of CYP17A1 of R358Q is reported to be extremely low[16], full kinetic analysis of the enzyme was not performed. Instead, 17,20-lyase activity of the R358Q mutant was evaluated alongside wild type CYP17A1 at 25 μM 17α-hydroxypregnenolone, which corresponds to saturation of wild type enzyme. Measurements were made in both the presence and absence of cytochrome b_5 (Table 5.2) to validate whether or not the R358Q mutant performs the 17,20-lyase reaction[14,16]. The rate of 17,20-lyase turnover by R358Q in the absence of cytochrome b_5 (0.011 ± 0.001 pmol product/min/pmol cytochrome P450) was 2-fold lower than wild type CYP17A1 under the same conditions (0.023 ± 0.003 pmol product/min/pmol cytochrome P450). A slight increase in 17,20-lyase turnover by the R358Q mutant was observed in the presence of cytochrome b_5 (0.019 ± 0.002 pmol product/min/pmol cytochrome P450). By comparison, wild-type CYP17A1 demonstrated the expected eight-fold increase in 17,20-lyase turnover in the presence of cytochrome b_5. The net result is that in the presence of cytochrome b_5, the lyase activity of R358Q is ten-fold lower than wild type evaluated under the same conditions. Thus, compared to wild type enzyme, the R358Q mutant exhibits substantial deficiency in both hydroxylase and 17,20-lyase catalysis.

Table 5.2: 17α-hydroxypregnenolone 17,20-lyase turnover by CYP17A1 wild type and R358Q mutant in the presence and absence of cytochrome b_5.

Enzyme	**17,20-Lyase turnover (min^{-1})**	
	- cytochrome b_5	**+ cytochrome b_5**
Wild type	0.023 ± 0.009	0.19 ± 0.03
R358Q	0.011 ± 0.001	0.019 ± 0.003

DISCUSSION

Different mutations of CYP17A1 have been reported in the literature to either disrupt both 17α-hydroxylase and 17,20-lyase reactions performed by the enzyme[5] or to selectively prevent 17,20-lyase turnover while retaining the ability to perform the 17α-hydroxylase reaction[9,16]. Although the structure of CYP17A1 has been determined in the presence of both inhibitors and substrates, the inability of such studies to capture the dynamics of the enzyme or its interactions with essential partner proteins does not necessarily inform the basis for loss in activity associated with mutation of these residues. An understanding of how such mutations affect CYP17A1 structure, function, and interaction with partner proteins can be useful in designing inhibitors of the enzyme intended to halt androgen production and treat hormone-dependent prostate cancer. This is especially true of mutations that selectively disrupt 17,20-lyase activity and androgen biosynthesis, but allow the production of 17α-hydroxylated products that act as glucocorticoid precursors. Selective 17,20-lyase inhibition is expected to achieve the desired androgen ablation effects in prostate cancer patients with reduced corticosteroid-mediated side effects. The aim of the study described herein was to functionally characterize clinical mutants of CYP17A1 *in vitro*.

Two of the mutations evaluated, F114V and D116V, are located in the loop region between B′ and C helices and are reported to result in loss of both 17α-hydroxylase and 17,20-lyase activity[5]. Although both proteins seemed to express at low levels in *E. coli*, the F114V and D116V mutants appeared to be much less stable than wild type enzyme purified under the same conditions. Purification of the F114V and D116V mutants by affinity chromatography, which yields substantial wild type enzyme, resulted in very little heme-containing protein. The protein that was isolated did not produce the characteristic cytochrome P450 spectrum with λ_{max} at 450

nm when bound to carbon monoxide in the reduced state (Table 5.3). This suggests that the F114V and D116V mutations may both affect the folding and/or stability of catalytically active CYP17A1. As discussed in the introduction, the side chain of residue D116 participates in a hydrogen bond with R96, which in turn interacts with the heme cofactor. Therefore mutation of this residue to valine could affect incorporation or retention of the heme necessary for catalysis and/or destabilize adjacent structural elements, such as the B′ helix. The B′ helix comprises part of the active site and is known to be a relatively dynamic region of cytochrome P450 enzymes[17]. The heme Soret peak λ_{max} of 405-407 nm is consistent with the presence of some free heme cofactor, suggesting poor heme incorporation or retention, but poor yields of D116V prevented us from further characterizing the loss in enzymatic activity due to this substitution.

Table 5.3: Summary of CYP17A1 mutant evaluation.

Mutation	**Purification**			**Function Compared to Wild Type**	
	Yield (mg / L culture)	**Absolute Spectrum λ_{max} (nm)***	**Reduced CO difference spectrum**	**Hydroxylase**	**Lyase**
Wild Type	7 ± 2	416-419	Mostly P450	--	--
F114V	Very low	408-413	Mostly P420	ND§	ND§
D116V	Very low	405-407	Mostly P420	ND§	ND§
R347H	0.42**	420	P450	No product detected⌘	ND§
R358Q	5**	416	P450 in presence of substrate	2x ↑ K_m, 25x↓ k_{cat}	2x ↓ activity $-b_5$ 10x ↓ activity $+b_5$

*Range indicates values from multiple purifications
**Standard error not determined as values reflect yield from a single expression and purification
§Not determined
⌘Titration with substrate did not produce spectral shift

As with D116V, very little heme protein was purified from *E. coli* transformed with plasmid containing the F114V mutation, and the protein that was isolated did not demonstrate a spectrum with a peak at 450 nm in the reduced, carbon-monoxide bound state (Table 5.3). Also similar to D116V, the Soret peak λ_{max} for isolated F114V (408-413) was lower than wild type, potentially indicating the presence of free heme. This similarly suggests disruption of protein folding and stability and/or a problem with heme incorporation. The lack of stable protein prevented further investigation into the loss of function associated with the F114V mutation. While the presence of progesterone in expression media and purification buffers to improve stabilization did not permit the isolation of this mutant protein in higher yields, addition of abiraterone in previous studies did permit isolation of inhibitor-bound F114V in significant quantities. Abiraterone interacts with the CYP17A1 active site by simultaneously coordinating to the heme iron and hydrogen bonding residue asparagine 202, whereas progesterone only interacts with asparagine 202. Consequently, abiraterone binds wild type CYP17A1 with a reported K_d < 100 nM and therefore much higher affinity than progesterone (K_d = 230 ± 10 nM)[6]. This suggests that a heme-coordinating, and therefore tight-binding ligand in the CYP17A1 active site overcomes the destabilizing effects of a smaller residue substituted for phenylalanine in this position. Residue F114 is only separated from D116 by a single residue, but instead of being projected toward the exterior of the protein, the side chain of F114 faces inward, comprising a part of the CYP17A1 active site. The ζ-carbon of phenylalanine side chain is only ~4 Å from the β-face of steroidal substrates and inhibitors in the X-ray crystal structure with wild type enzyme[6]. Inability to generate significant quantities of the F114V mutant under standard conditions for wild type enzyme suggests that destabilization of this enzyme may be the consequence of packing defects. In summary, the inability to generate stable F114V and D116V

for further analysis is consistent with impaired hydroxylase and lyase turnover resulting from misfolded protein in patients harboring these mutations[5].

In contrast, the R347H and R358Q mutant proteins reported to be selectively deficient in 17,20-lyase turnover demonstrated normal spectral properties for P450 enzymes and could be purified in quantities sufficient to evaluate enzyme catalysis (Table 5.3). Substantial differences in ligand binding and catalytic activity compared to wild type enzyme were observed for both mutants. Mutation of residue R347 to histidine was proposed to selectively prevent 17,20-lyase turnover by interfering with the CYP17A1/cytochrome b_5 interaction[14,15] that significantly augments 17,20-lyase catalysis but does not significantly affect the hydroxylase reaction. However, in our system the R347H mutant did not demonstrate a spectral shift upon titration with progesterone or produce detectable amounts of the 17α-hydroxyprogesterone when evaluated catalytically (Table 5.3). Consequently, R347H did not appear to bind or turn over progesterone. This contrasts with previous reports that R347H retains some pregnenolone hydroxylase activity, albeit with a 3.5-7.5-fold loss in V_{max} compared to wild type enzyme[5,15]. The K_m value for R347H has also been consistently reported as lower than that of wild type enzyme, which suggests higher affinity for the substrate than wild type[5,16]. The aforementioned comparison studies of R347H were performed in COS-1 cells and using a different hydroxylase substrate, making it difficult to determine which experimental parameter leads to such different results. Although the inability of R347H to bind steroidal substrate described herein contradicts previous studies that demonstrate 17α-hydroxylase turnover, the effects of this residue on substrate binding does suggest that changes on the surface of the proximal face of the enzyme can have a significant effect on either the conformation of the active site itself, or on substrate access to the buried active site.

In contrast to the R347H mutant, CYP17A1 R358Q was isolated in quantities similar to wild-type enzyme, and did metabolize the hydroxylase substrate progesterone. However, the 17α-hydroxyprogesterone metabolite was generated with a five-fold loss in catalytic efficiency compared to wild type enzyme (Table 5.3). R358Q had a K_m value within two-fold of the wild type enzyme, but the k_{cat} was 25-fold lower. Positive residues on the proximal face of the enzyme may interact with anionic residues of both cytochrome b_5 and CPR. The binding sites of these partner proteins are not well defined, but are reported to overlap[12]. Since cytochrome b_5 is not present in hydroxylation assays, the simplest explanation for deficient hydroxylase catalysis is that mutation of residue R358 hinders electron transfer by CPR and consequently reduces 17α-hydroxylase activity. The 17,20-lyase activity of the R358Q mutant was lower than that of wild type CYP17A1, even in the presence of cytochrome b_5. Addition of cytochrome b_5 to R358Q in a 4:1 ratio resulted in a very small increase in activity, but not enough to result in substantial 17,20-lyase turnover. Therefore, although deficient 17,20-lyase turnover in the R358Q mutant may be partially the result of reduced cytochrome b_5 binding, this residue likely plays a role in electron transfer by CPR as well. At a minimum, it is clear that the R358Q mutation substantially impacts both hydroxylase and 17,20-lyase activities, and not just hydroxylation as previously reported[15,16].

In the past, *in vitro* follow-up studies have revealed that several other mutations initially reported to selectively block 17,20-lyase activity actually caused combined hydroxylase/17,20-lyase deficiencies[18,19] or were actually the result of functional deficiency of CYP17A1 redox partners[20]. 17α-hydroxylase deficiencies demonstrated by R347H and R358Q as a part of this study similarly reflect less selective 17,20-lyase impairment than previously reported. Such

discrepancies make evaluation of mutant proteins in a controlled setting very important for determining their molecular basis.

The analysis of purified CYP17A1 R347H and R358Q proteins in this study supports important roles for these residues in catalysis. Cationic residues on the proximal face of the enzyme appear to play a substantial and complex role in ligand binding and electron transfer, as well as binding of cytochrome b_5 in the case of R358Q. In contrast, CYP17A1 with mutations of residues on the loop between the B′ and C helices demonstrated decreased stability, likely the consequence of improper folding, poor stability, and/or impaired heme incorporation. Overall, these studies highlight the necessity of evaluating mutant proteins in a controlled system to better understand the functional basis of deficiencies reportedly related to mutations identified in patients.

REFERENCES

(1) Auchus, R. J. *Endocrinol. Metab. Clin. North Am.* **2001**, *30*, 101.
(2) Attard, G.; Reid, A. H.; Auchus, R. J.; Hughes, B. A.; Cassidy, A. M.; Thompson, E.; Oommen, N. B.; Folkerd, E.; Dowsett, M.; Arlt, W.; de Bono, J. S. *J. Clin. Endocrinol. Metab.* **2012**, *97*, 507.
(3) Fizazi, K.; Scher, H. I.; Molina, A.; Logothetis, C. J.; Chi, K. N.; Jones, R. J.; Staffurth, J. N.; North, S.; Vogelzang, N. J.; Saad, F.; Mainwaring, P.; Harland, S.; Goodman, O. B., Jr.; Sternberg, C. N.; Li, J. H.; Kheoh, T.; Haqq, C. M.; de Bono, J. S.; Investigators, C.-A.-. *Lancet Oncol.* **2012**, *13*, 983.
(4) Auchus, R. J.; Miller, W. L. In *Cytochrome P450: Structure, Mechanism, and Biochemistry*; 4th ed.; Ortiz de Montellano, P., Ed.; Springer: New York, 2015; Vol. II, p 851.
(5) Van Den Akker, E. L.; Koper, J. W.; Boehmer, A. L.; Themmen, A. P.; Verhoef-Post, M.; Timmerman, M. A.; Otten, B. J.; Drop, S. L.; De Jong, F. H. *J. Clin. Endocrinol. Metab.* **2002**, *87*, 5714.
(6) DeVore, N. M.; Scott, E. E. *Nature* **2012**, *482*, 116.
(7) Yang, J.; Cui, B.; Sun, S.; Shi, T.; Zheng, S.; Bi, Y.; Liu, J.; Zhao, Y.; Chen, J.; Ning, G.; Li, X. *J. Clin. Endocrinol. Metab.* **2006**, *91*, 3619.
(8) Petrunak, E. M.; DeVore, N. M.; Porubsky, P. R.; Scott, E. E. *J. Biol. Chem.* **2014**, *289*, 32952.

(9) Sherbet, D. P.; Tiosano, D.; Kwist, K. M.; Hochberg, Z.; Auchus, R. J. *J. Biol. Chem.* **2003**, *278*, 48563.
(10) Fluck, C. E.; Miller, W. L.; Auchus, R. J. *J. Clin. Endocrinol. Metab.* **2003**, *88*, 3762.
(11) Waskell, L.; Kim, J. P. In *Cytochrome P450: Structure, Mechanism, and Biochemistry*; 4th ed.; Ortiz de Montellano, P., Ed.; Springer: New York, 2015; Vol. I, p 33.
(12) Estrada, D. F.; Laurence, J. S.; Scott, E. E. *J. Biol. Chem.* **2013**, *288*, 17008.
(13) Auchus, R. J.; Lee, T. C.; Miller, W. L. *J. Biol. Chem.* **1998**, *273*, 3158.
(14) Lee-Robichaud, P.; Akhtar, M. E.; Wright, J. N.; Sheikh, Q. I.; Akhtar, M. *J. Steroid Biochem. Mol. Biol.* **2004**, *92*, 119.
(15) Geller, D. H.; Auchus, R. J.; Miller, W. L. *Mol. Endocrinol.* **1999**, *13*, 167.
(16) Geller, D. H.; Auchus, R. J.; Mendonca, B. B.; Miller, W. L. *Nat. Genet.* **1997**, *17*, 201.
(17) Poulos, T. L.; Johnson, E. F. In *Cytochrome P450: Structure, Mechanism, and Biochemistry*; 4th ed.; Ortiz de Montellano, P., Ed.; Springer: New York, 2015; Vol. I, p 3.
(18) Gupta, M. K.; Geller, D. H.; Auchus, R. J. *J. Clin. Endocrinol. Metab.* **2001**, *86*, 4416.
(19) Yanase, T.; Waterman, M. R.; Zachmann, M.; Winter, J. S.; Simpson, E. R.; Kagimoto, M. *Biochim. Biophys. Acta* **1992**, *1139*, 275.
(20) Hershkovitz, E.; Parvari, R.; Wudy, S. A.; Hartmann, M. F.; Gomes, L. G.; Loewental, N.; Miller, W. L. *J. Clin. Endocrinol. Metab.* **2008**, *93*, 3584.

Chapter 6.

Evaluation and Comparison of Clinically-Relevant Inhibitors of Cytochrome P450 17A1 (CYP17A1)

INTRODUCTION

The role of cytochrome P450 17A1 (CYP17A1) in human androgen biosynthesis makes inhibition of this enzyme an emerging strategy for the treatment of castration-resistant prostate cancer in contrast to traditional androgen-deprivation therapy. As discussed in previous chapters, CYP17A1 mediates two successive reactions relevant to steroid biosynthesis, the hydroxylation of 21-carbon progestagens followed by a carbon-carbon bond cleavage reaction to generate 19-carbon androgens. The 17-hydroxylase reaction is necessary for both androgen and glucocorticoid synthesis, whereas the second carbon-carbon bond cleavage (17,20-lyase) reaction is only required for androgen biosynthesis.

Although the clinical success of abiraterone in treating prostate cancer has validated CYP17A1 as a target for this disease state, a variety of corticosteroid-related side effects including hypertension and peripheral edema have been attributed to off-target inhibition of the 17-hydroxylase reaction. Consequently, there has been a growing interest in developing CYP17A1 inhibitors that selectively inhibit the 17,20-lyase reaction while allowing CYP17A1-mediated 17-hydroxylation to proceed with minimal interference. A number of CYP17A1 inhibitors have entered clinical trials since the discovery of abiraterone, some reportedly showing selectivity for inhibition of the 17,20-lyase reaction (Table 5.1).

Table 6.1: Reported IC_{50} values for inhibitors of CYP17A1 that have undergone clinical trials.

Inhibitor	**FDA Approval Status**	**Reported 17,20-Lyase IC_{50} (nM)**	**Reported 17α-Hydroxylase IC_{50} (nM)**	**Reported 17,20-Lyase Selectivity**
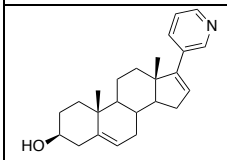 Abiraterone	Approved	2.9 - 800[1-4]	1.5 - 72[1,3-6]	0.1 to 1.4-fold[1,3,4]
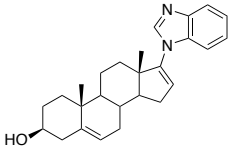 Galeterone	Phase III Clinical Trials	47-300[2,7]	N/R*	N/R*
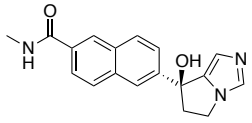 (*S*)-Orteronel	Discontinued after Phase III Clinical Trials	19-140[3,8]	760[3]	5-fold[3]
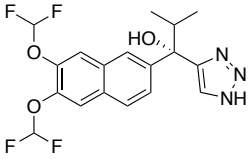 (*S*)-VT-464	Phase II Clinical Trials	69[4]	690[4]	10-fold[4]

*Value not reported in literature.

CYP17A1 inhibition is typically evaluated as the half-maximal inhibitory concentration (IC_{50}), or the concentration at which the inhibitor reduces a CYP17A1-mediated reaction to half of its maximal activity. This value is useful for comparing potency between inhibitors, and in the case of CYP17A1 is also used to compare potency of inhibition for a single inhibitor between different reactions (17α-hydroxylase vs. lyase). The apparent IC_{50} value can vary widely depending on experimental conditions, as demonstrated by the reports of abiraterone's IC_{50} for the 17,20-lyase reaction, which ranges over three orders of magnitude (Table 6.1).

There are multiple factors that contribute to such variability. Included among them are the concentration of substrate and the mode of inhibition (competitive, non-competitive, or uncompetitive). For example, low concentrations of substrate bias inhibition studies toward

competitive inhibitors, whereas high concentrations of substrate are associated with a bias toward uncompetitive inhibitors[9]. Bias related to inhibitor modality can be reduced by using a substrate concentration equivalent the Michaelis-Menten constant for a particular reaction[9]. Unfortunately, such kinetic considerations have often not been taken into account when evaluating CYP17A1 inhibitors.

To complicate matters further, CYP17A1 requires the partner proteins NADPH-cytochrome P450 reductase and cytochrome b_5 for catalysis, and the system in which these partner proteins are produced and incorporated with CYP17A1 vary. Almost all inhibitor evaluations use human CYP17A1 and partner proteins produced recombinantly in *E. coli* or yeast, but the preparation and purity of such enzyme system components vary. Some studies use CYP17A1 and redox partners in whole cells, in which case IC_{50} values reflect not only inhibition of a reaction but also membrane permeability. The majority of *in vitro* inhibitor evaluation are performed using CYP17A1 and partner proteins in microsomes, the fraction of cell lysate that includes cell membrane and membrane-bound components including associated proteins. In whole cell and microsomal systems, it is difficult to accurately measure or control the amount of available CYP17A1 enzyme or the relative amounts of co-expressed partner proteins required for catalysis. A few *in vitro* studies have used purified CYP17A1 and redox partners. Under these conditions, it is easier to control relative amounts of enzyme system components. However, experiments performed with purified proteins may or may not be conducted in the presence of lipid, an essential component for full-length enzyme in microsomal and whole cell systems. The presence of lipid has been known to affect cytochrome P450 turnover, and previous studies have even demonstrated that the type of lipid used can affect catalysis by CYP17A1[10]. Finally, the source (human or rat) of redox partners CRP and cytochrome b_5 can vary between experimental

conditions, which can influence catalytic turnover. In summary, different systems used to measure cytochrome P450 catalysis produce substantial variation in the resultant kinetics. Therefore direct comparisons of CYP450 IC_{50} values evaluated under different conditions are problematic.

In the interest of developing lyase-selective inhibitors of CYP17A1, it has become increasingly common to evaluate candidates for their ability to inhibit the 17α-hydroxylase reactions that contribute to secondary mineralocorticoid excess, in addition to the targeted 17,20-lyase reaction. As discussed earlier, studies comparing inhibition between different reactions are not always performed using kinetically comparable substrate concentrations. It is also often neglected that CYP17A1 has two physiologically relevant substrates for the 17α-hydroxylase reaction, and when evaluating candidates for inhibition of this reaction, usually only one substrate (progesterone or pregnenolone) is evaluated. Although the structure of these substrates differs only in the A-ring of the steroid on the opposite end of the steroid that is catalytically modified by CYP17A1, progesterone and pregnenolone have different affinities for CYP17A1 and are hydroxylated at different rates[11].

Evaluation of compounds for selective inhibition of the 17,20-lyase reaction has focused on two clinical candidates, orteronel and VT-464. Both inhibitors are nonsteroidal, in contrast to abiraterone and galeterone, but still include a nitrogen-containing heterocycle capable of coordinating the heme iron. Such coordination is seemingly at odds with the reported selectivity profiles for these inhibitors. It is logical to expect that coordination of the heme iron should prevent all catalysis by CYP17A1 equally, but in the absence of structural information about interactions between reported lyase-selective non-steroidal inhibitors and CYP17A1, the

mechanism for selective inhibition of the 17,20-lyase versus either 17α-hydroxylase reaction remains unclear.

One possible mechanism for selective inhibition of the 17,20-lyase reaction over 17α-hydroxylation is interference with CYP17A1 processivity, the capacity of CYP17A1 to perform the 17,20-lyase reaction following the 17α-hydroxylase reaction without releasing the intermediate product from the active site. Studies with zebra fish CYP17A1[12] have demonstrated that the Δ4 17α-hydroxyprogesterone is more likely than its Δ5 counterpart 17α-hydroxypregnenolone to dissociate from the active site prior to 17,20-lyase turnover. Differences in IC_{50} values between hydroxylase and lyase reactions are not observed with Δ5 steroids in which the hydroxylase product is less likely to leave the active site (Figure 6.1A). In contrast, a 10-fold difference is observed between progesterone hydroxylase and 17α-hydroxyprogesterone 17,20-lyase IC_{50} values (Figure 6.1B). This information seems to suggest that the selective inhibition of the 17,20-lyase reaction demonstrated by orteronel may be related to the processivity of CYP17A1. However, processivity studies have not yet been reported on human CYP17A1, and the relationship between CYP17A1 and selective 17,20-lyase inhibition by orteronel remains unclear.

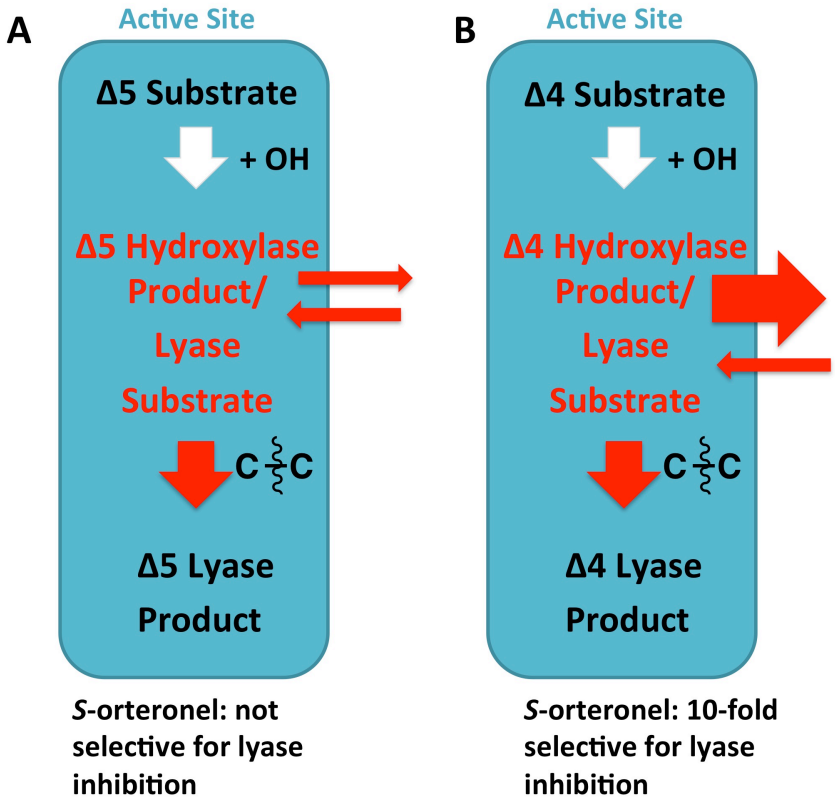

Figure 6.1: Processivity in zebra fish CYP17A1 affects apparent selectivity of *S*-orteronel for 17,20-lyase inhibition over 17α-hydroxylase inhibition. A) Δ5 steroids are less likely to leave the active site after hydroxylation and prior to the 17,20-lyase reaction (more processive) compared to B) Δ4 steroids which are more likely to dissociate from the active site following hydroxylation and prior to 17,20-lyase reaction.

The following study consists of direct comparisons between 17,20-lyase inhibition and 17α-hydroxylase inhibition using purified CYP17A1 and partner proteins in controlled ratios and using concentrations of substrates equivalent to previously determined Michaelis-Menten constants. This allowed us to determine whether reports of selective 17,20-lyase inhibition versus 17α-hydroxylase inhibition are justified, and moreover, whether or not CYP17A1 inhibitors that coordinate the heme iron can even inhibit one reaction over another selectively. The X-ray crystal structures of CYP17A1 were determined with non-steroidal inhibitors *S*-orteronel, *R*-orteronel and VT-464 to determine the potential structural bases for any observed 17,20-lyase selectivity.

METHODS

Protein Expression and Purification

CYP17A1 and human NADPH-cytochrome P450 reductase were expressed and purified as described in Chapter 2. Rat cytochrome b_5 was produced by Dr. Natasha DeVore.

Assays

Spectral ligand binding assays were performed as described in Chapter 2. IC_{50} values for progesterone 17α-hydroxylase, pregnenolone 17α-hydroxylase, and 17α-hydroxypregnenolone 17,20-lyase reactions were determined by performing reactions and sample preparations as described in Chapter 2 for each individual assay, with the following modifications. First, the substrate concentration was constant between samples and equal to the previously determined K_m for the monitored reaction (10 μM, 1 μM, and 1.2 μM for progesterone 17α-hydroxylation, pregnenolone 17α-hydroxylation and 17α-hydroxypregnenolone 17,20-lyase, respectively). Inhibitor concentrations were in the range of 0-30 μM.

Graphpad Prism 5 (Graphpad Software, San Diego, CA) was used to determine the IC_{50} value. The percent enzymatic activity (in pmol product/min/pmol CYP17A1) for each sample containing inhibitor was normalized to enzymatic activity in the absence of inhibitor and plotted as a function of log [inhibitor]. Data were fit to the equation for log [inhibitor] vs. normalized response, Y = 100/ (1+10^((LogIC_{50}-X)*HillSlope))).

Crystallization, Data Collection, and Structure Determination

CYP17A1 was co-crystallized with either racemic orteronel or VT-464 via hanging drop vapor diffusion. CYP17A1 (29 mg/mL) in 50 mM Tris-HCl, pH 7.4, 20% glycerol, 100 mM glycine, 500 mM NaCl, 0.5% (v/v) Emulgen-913, and 100 μM racemic orteronel or 500 μM VT-

464 was mixed in a 1:1 ratio with precipitant to form 2 µL drops. The 2 µL drop used to generate VT-464 crystals was seeded with microcrystals generated in a 1 µL drop via sitting drop vapor diffusion in a 1:1 ratio with precipitant. Drops were equilibrated against 750 µL precipitant at 20°C. The precipitant solution used to crystallize CYP17A1 with orteronel was 175 mM Tris HCl, pH 8.0, 30% (w/v) PEG-3350, 200 mM Li_2SO_4, and 12% glycerol. The precipitant solution used to crystallize CYP17A1 with VT-464 was 100 mM sodium cacodylate trihydrate, pH 6.5, 200 mM ammonium sulfate, and 30% (w/v) PEG-8000. Crystals were cryoprotected using a 7:3 mixture of mother liquor to 80% glycerol and were flash cooled in liquid nitrogen.

Data were collected on beamline 12-2 or 7-1 at the Stanford Synchrotron Radiation Lightsource, and processed using XDS[13]. Parameters for data collection and refinement statistics are described in Table 6.2. Structures were solved by molecular replacement in Phaser[14] using a previous structure of CYP17A1 with heme cofactor (PDB ID: 3SWZ[15]) as a search model and data to the corresponding resolution cutoff (2.2 Å for CYP17A1 with orteronel and 3.15 Å for CYP17A1 with VT-464). Model-building and iterative refinement were performed using COOT[16] and PHENIX[17], respectively. Ligand models were generated using eLBOW in PHENIX[17]. Simulated-annealing composite omit maps were calculated in PHENIX[17]. Figures were generated using PyMOL[18].

Table 6.2: Crystallographic data collection and refinement statistics for CYP17A1 with nonsteroidal inhibitors orteronel and VT-464.

	CYP17A1/orteronel	**CYP17A1/VT-464**
Data Collection		
Beamline	SSRL 7-1	SSRL 12-2
Space Group	$P2_12_12_1$	$P2_12_12_1$
Cell Dimensions		
a,b,c (Å)	90.17, 153.20, 168.12	90.95, 153.50, 169.04
Molecules/a.u.	4	4
Resolution (Å)*	39.28-2.20 (2.32-2.20)	39.44-3.10 (3.27-3.10)
Total reflections*	871,993 (125,334)	142,288 (20,014)
Unique reflections*	118,993 (16,928)	43,069 (6,096)
Redundancy*	7.4 (7.4)	3.3 (3.3)
R_{pim*}	0.053 (0.608)	0.087 (0.579)
$\langle I/\sigma(I)\rangle$*	14.0 (1.6)	8.4 (1.6)
Completeness (%)*	99.8 (99.0)	98.5 (96.5)
Refinement		
Resolution (Å)	39.29-2.20	39.44-3.10
No. reflections	117,964	42,930
R/R_{free} (%)	19.76/24.94	18.27/24.88
Ramachandran (%)		
Favored	95.26	94.28
Allowed	4.09	5.40
Outliers	0.65	0.32
No. atoms/B factors ($Å^2$)		
Protein	14901 / 44.1	15013 / 67.9
Ligand	92 / 43.8	112 / 45.0
Heme	172 / 32.0	172 / 53.4
Water	648 / 45.3	0 / NA§
RMSD bond (Å)	0.009	0.011
RMSD angle (°)	1.157	1.356
Coordinate error (maximum-likelihood based) (Å)	0.29	0.44

*Statistics for highest resolution shell are shown in parentheses.
§Not Applicable

RESULTS

Binding of Non-steroidal Inhibitors to CYP17A1

CYP17A1 was titrated with the non-steroidal inhibitors *S*-orteronel, *R*-orteronel, VT-464, and VT-463 and the observed spectral shift was used to determine the dissociation constant (K_d)

for the enzyme-inhibitor complex. All inhibitors exhibited a type II shift over the course of titration typified by an increase in absorbance at 424 nm and a decrease in absorbance at 393-410 nm (Figure 6.2). Such changes indicate direct coordination of the heteroaromatic ring in each structure to the heme iron of the P450. Of the four non-steroidal inhibitors tested, VT-463 demonstrated the lowest affinity for the enzyme by far, with an estimated K_d of 290 ± 10 nM (Figure 6.3A). VT-464 and both enantiomers of orteronel exhibited significantly higher affinity. For these three highest affinity nonsteroidal inhibitors, fits to the tight-binding equation yielded K_d values of 31 ± 7 nM for VT-464; (Figure 6.3B), 40 ± 7 nM for *S*-orteronel (Figure 6.2C), and 56 ± 8 nM for *R*-orteronel (Figure 6.3D). However, the changes in absorbance as a function of inhibitor concentration deviate substantially from a hyperbolic curve for the tight-binding equation (Figure 6.3 B-D), as all available ligand is tightly engaged in a complex with the enzyme and there is little free inhibitor in solution. This behavior has previously been observed for extremely tight binding ligands for CYP17A1 and is especially pronounced for the steroidal inhibitors abiraterone (Figure 6.3E) and galeterone (Figure 6.23). In each case, though correlation coefficients range from 0.94 to 0.99 for both steroidal and tight-binding non-steroidal inhibitors, the residuals are not random and the data is better described as a linear increase followed by a plateau as CYP17A1 is saturated. In such cases, one would typically further reduce the concentration of enzyme, but herein the concentration of enzyme (100 nM) is already as low as experimentally feasible to maintain a good signal-to-noise ratio. The net outcome is that for these tight-binding inhibitors the determined K_d values are, at best, upper limits and do not fully reflect the high affinity of these ligands for CYP17A1.

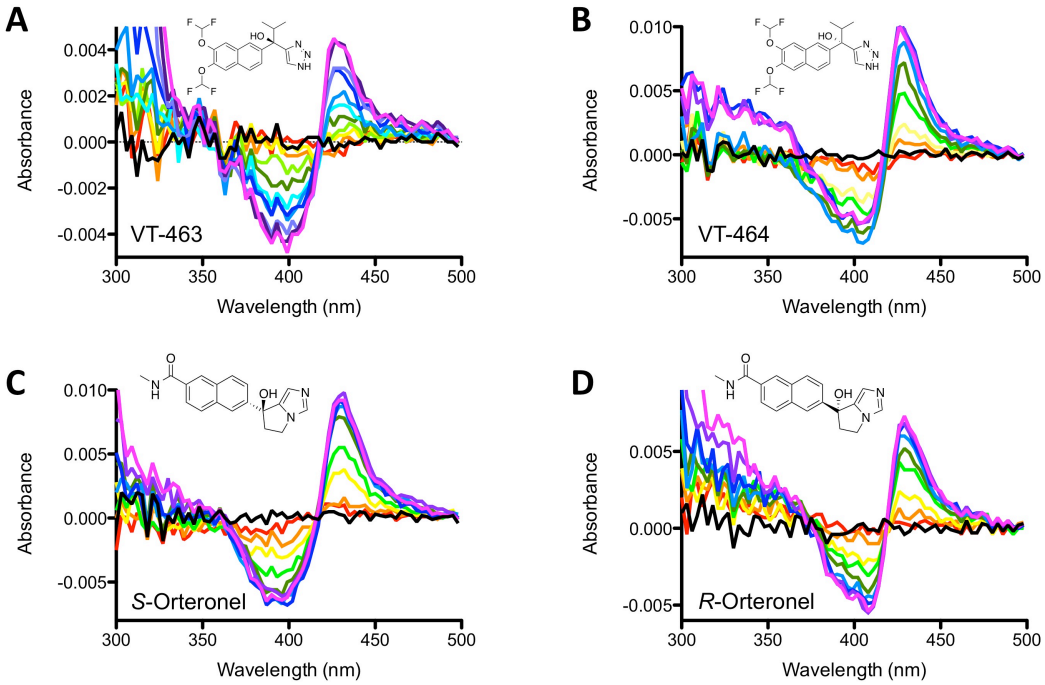

Figure 6.2: Type II spectral shifts were observed upon titration of CYP17A1 with non-steroidal inhibitors A) VT-463, B) VT-464, C) S-orteronel, and D) *R*-orteronel. Increasing concentrations of inhibitors are shown from low concentrations (red/orange) to intermediate concentrations (yellow/green) to high concentrations (blue/violet). The difference in absorbance between the resulting peak and trough (ΔAbsorbance) were used to monitor binding of ligand to enzyme (Figure 6.3).

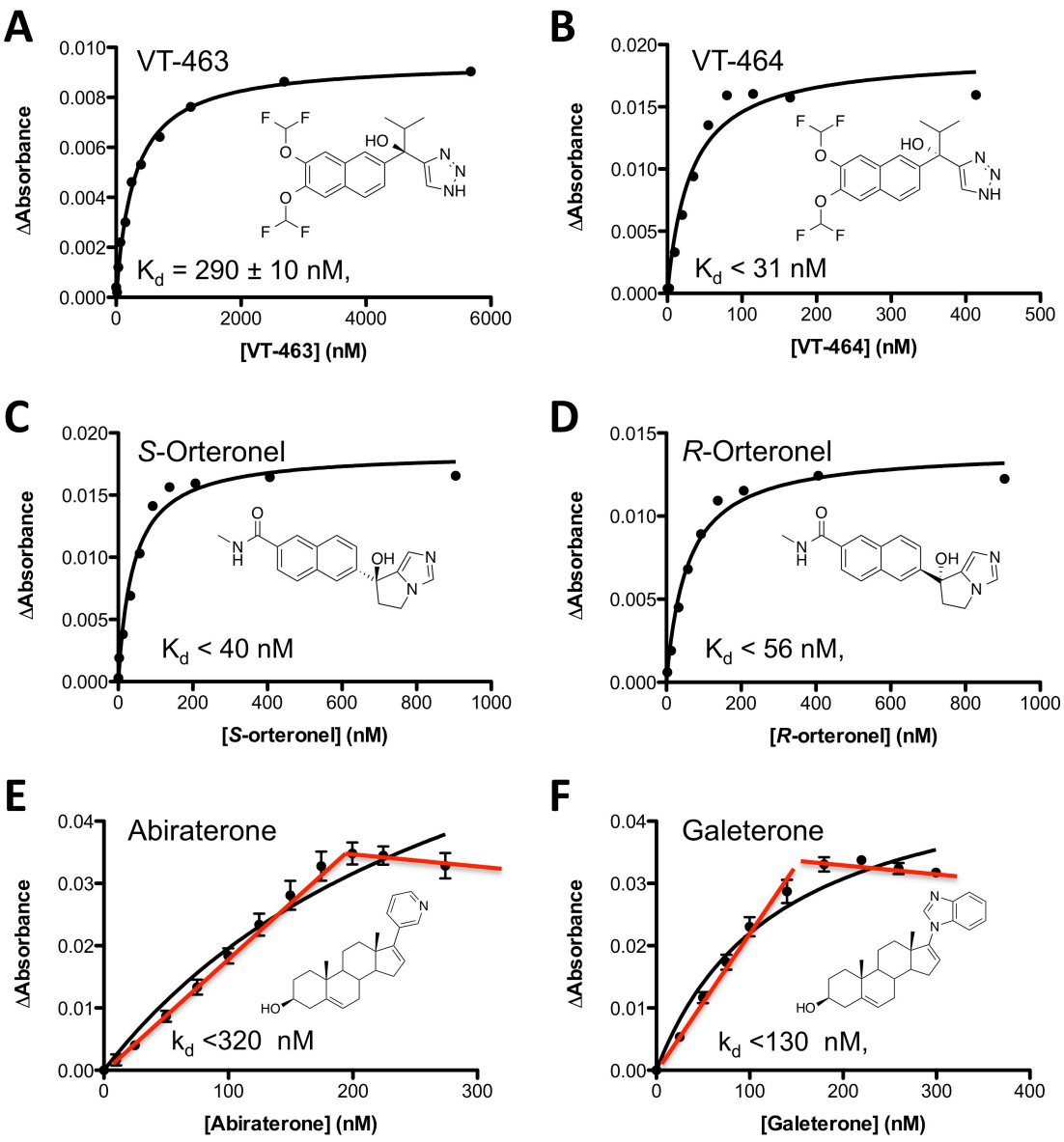

Figure 6.3: Binding of non-steroidal CYP17A1 inhibitors A) VT-463, B) VT-464, C) *S*-orteronel, and D) *R*-orteronel monitored as change in absorbance with increasing concentrations of inhibitor. Binding of steroidal CYP17A1 inhibitors E) abiraterone and F) galeterone (data generated by Dr. Natasha DeVore) are shown for comparison.

Based on such observations however, steroidal and non-steroidal inhibitors can be roughly rank-ordered according to their affinity for the CYP17A1 active site. Steroidal inhibitors abiraterone and galeterone show higher affinity than any of the non-steroidal inhibitors evaluated. VT-464 demonstrates the highest affinity non-steroidal inhibitor, followed by *S*-

orteronel and *R*-orteronel. Of all inhibitors evaluated, VT-463 clearly demonstrated the lowest affinity for CYP17A1.

Inhibition of Targeted 17,20-Lyase Reaction

Steroidal inhibitors (abiraterone and galeterone) as well as non-steroidal inhibitors that had entered clinical trials (*S*-orteronel and VT-464) and their corresponding enantiomers (*R*-orteronel and VT-463) were evaluated for desired inhibition of the 17,20-lyase reaction using the primary physiological substrate 17α-hydroxypregnenolone. IC_{50} determination was conducted at a substrate concentration corresponding to the previously determined K_m of this reaction (1.2 μM; see Chapter 4) and in the presence of cytochrome b_5. Product formation was plotted as a function of log [inhibitor] concentration to determine IC_{50} values for each inhibitor (Figure 6.4).

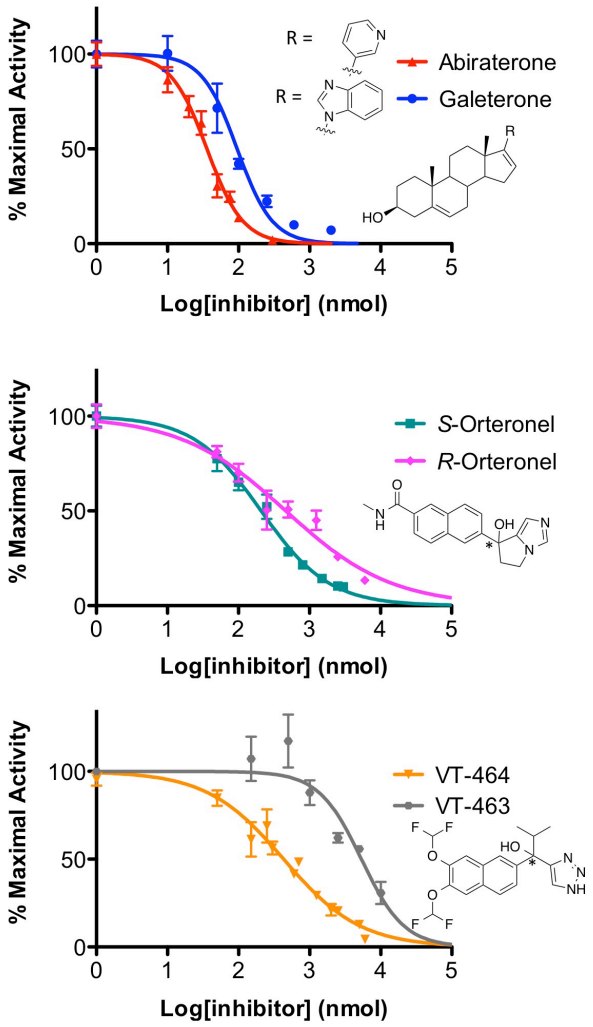

Inhibitor	Lyase IC_{50} (nM)
Abiraterone	36 ± 2
Galeterone	100 ± 10
S-Orteronel	210 ± 20
R-Orteronel	460 ± 90
VT-464	430 ± 40
VT-463	5000 ± 1000

Figure 6.4: Inhibition of CYP17A1 17,20-lyase activity by steroidal inhibitors (top panel), orteronel (*S*- and *R*- enantiomers, middle panel) and VT-464 analogs (*S*- and *R*- enantiomers, bottom panel).

The FDA-approved first-in-class CYP17A1 inhibitor abiraterone demonstrated the highest potency with an IC_{50} value of 36 ± 2 nM. The other steroidal inhibitor, galeterone, was ~3-fold less potent than abiraterone (IC_{50} = 100 ± 10 nM), but still showed higher potency than any of the non-steroidal inhibitors. Of the non-steroidal inhibitors, *S*-orteronel exhibited only 6-fold lower potency than abiraterone for inhibition of the 17,20-lyase reaction (IC_{50} = 210 ± 20

nM), while *R*-orteronel (IC_{50} = 460 ± 90 nM) exhibited nearly 13-fold lower potency compared to abiraterone. Finally, VT-464 and VT-463 were 12-fold and nearly 140-fold less potent than abiraterone (IC_{50} values of 430 ± 40 and 5000 ± 1000 nM), respectively.

Inhibition of Off-Target Progesterone Hydroxylation Reaction

Each inhibitor was also evaluated for inhibition of progesterone hydroxylation. Consistent with the 17,20-lyase inhibition assay, these reactions were also performed using purified human CYP17A1 and P450 oxidoreductase and a substrate concentration equal to the previously determined K_m of this reaction (10 μM; Chapter 4). Since the hydroxylase reaction does not appear to require cytochrome b_5 physiologically, this protein was not included in the *in vitro* enzyme system to prevent subsequent conversion of the hydroxylase product to androstenedione via the subsequent 17,20-lyase reaction.

The rank order potency for inhibition of this off-target reaction was identical to that of 17,20-lyase inhibition (Figure 6.5). Abiraterone displayed the greatest potency (IC_{50} = 76 ± 5 nM), followed by the other steroidal inhibitor, galeterone (IC_{50} = 130 ± 10 nM). All four non-steroidal inhibitors demonstrated less potency than abiraterone and galeterone. Of the non-steroidal inhibitors evaluated, *S*-orteronel was the most potent inhibitor of the progesterone hydroxylase reaction (IC_{50} = 950 ± 70 nM), but was still 13-fold less potent than abiraterone. The other non-steroidal inhibitor, VT-464, was the second most potent non-steroidal inhibitor of this reaction (IC_{50} = 1170 ± 90 nM), followed by *R*-orteronel (IC_{50} = 4000 ± 300 nM). Consistent with inhibition of the 17,20-lyase reaction and binding data, VT-463 exhibited the lowest potency (IC_{50} = 11.3 ± 0.9 μM).

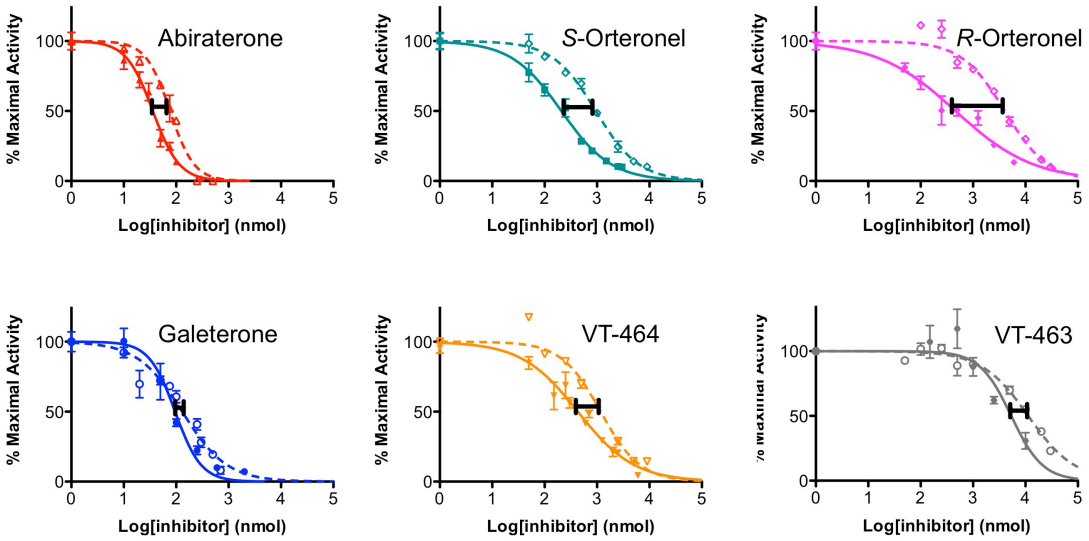

Inhibitor	Abiraterone	Galeterone	*S*-Orteronel	*R*-Orteronel	VT-464	VT-463
Progesterone Hydroxylase IC_{50} (nM)	76 ± 5	130 ± 10	950 ± 70	4000 ± 300	1170 ± 90	11300 ± 900
Lyase IC_{50} (nM)	36 ± 2	100 ± 10	210 ± 20	460 ± 90	430 ± 40	5000 ± 1000
Progesterone $\frac{\text{Hydroxylase } IC_{50}}{\text{Lyase } IC_{50}}$	2.1 ± 0.2	1.3 ± 0.2	4.5 ± 0.5	8 ± 2	2.7 ± 0.3	2.3 ± 0.5

Figure 6.5: Inhibition of progesterone hydroxylation by CYP17A1 inhibitors (shown as open symbols) and resulting nonlinear fits used to estimate the progesterone hydroxylase IC_{50} (shown as dotted lines). These data are compared with 17,20-lyase inhibition data (closed symbols, solid lines) to illustrate selectivity for the targeted 17,20-lyase reaction.

Comparison of IC_{50} values for 17,20-lyase inhibition and progesterone hydroxylation (Figure 6.5) can be used to evaluate inhibitor selectivity for the targeted reaction (17,20-lyase) over the non-targeted reaction (progesterone hydroxylase). The most selective inhibitors exhibit high IC_{50} values for the off-target hydroxylase reaction and low IC_{50} values for the targeted 17,20-lyase reaction. Selectivity factors in this section and following sections is determined using the following ratio: 17-hydroxylase IC_{50} / 17,20-lyase IC_{50}. A selectivity factor of 1 therefore indicates no selectivity for 17,20-lyase reaction, while higher selectivity factors indicate more selectivity toward inhibition of the 17,20 lyase reaction.

All inhibitors evaluated were more effective in suppressing the 17,20-lyase reaction than the 17-hydroxylase reaction, and therefore all have selectivity factors greater than 1. The steroidal inhibitors abiraterone and galeterone demonstrate 2.1-fold and 1.3-fold selectivity for 17,20-lyase inhibition over progesterone hydroxylase inhibition, respectively. The *S*-enantiomer of non-steroidal orteronel showed 4.5-fold selectivity, while *R*-orteronel exhibited greater (8-fold) selectivity for inhibition of the targeted 17,20-lyase reaction over progesterone hydroxylation. In contrast, the non-steroidal inhibitor VT-464 demonstrated only 2.7-fold selectivity for inhibition of the 17,20-lyase reaction over inhibition of progesterone hydroxylation, very similar to the 2.3-fold selectivity observed for its *R*-enantiomer, VT-463.

Inhibition of Off-Target Pregnenolone Hydroxylation Reaction

Since both progesterone and pregnenolone are physiologically relevant substrates for the 17α-hydroxylase reaction, inhibitors were also evaluated for inhibition of 17α-hydroxylation of pregnenolone as a substrate (Figure 6.6). As with progesterone hydroxylase and 17,20-lyase inhibition, these studies were also conducted at a concentration of substrate corresponding to the previously determined K_m of this reaction (1 μM; Chapter 4).

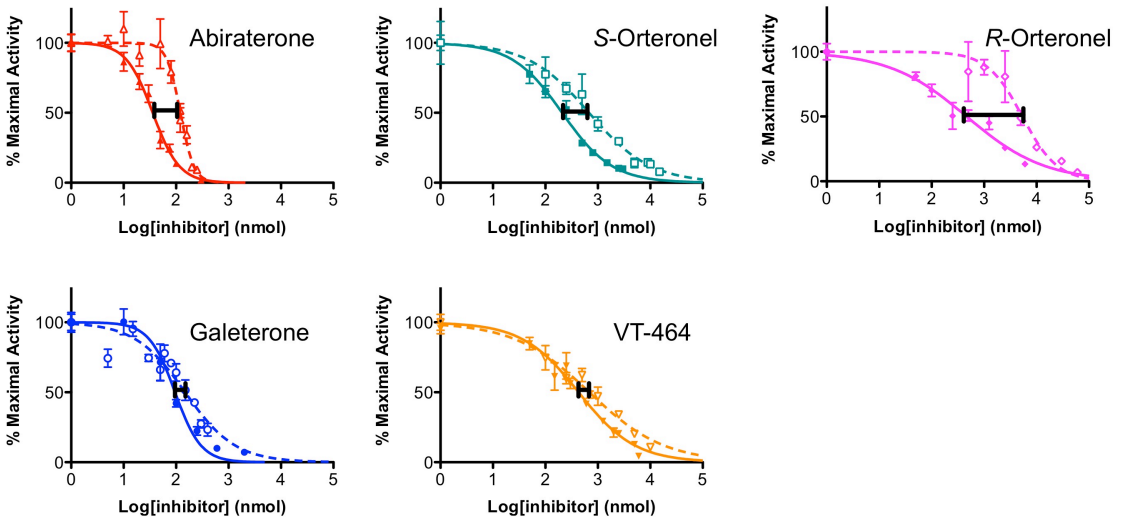

Inhibitor	Abiraterone	Galeterone	*S*-Orteronel	*R*-Orteronel	VT-464
Pregnenolone Hydroxylase IC_{50} (nM)	121 ± 7	150 ± 20	700 ± 100	5000 ± 1000	700 ± 100
Lyase IC_{50} (nM)	36 ± 2	100 ± 10	210 ± 20	460 ± 90	430 ± 40
Pregnenolone Hydroxylase IC_{50} / Lyase IC_{50}	3.3 ± 0.3	1.5 ± 0.3	3.3 ± 0.6	11 ± 3	2.1 ± 0.4

Figure 6.6: Inhibition of pregnenolone hydroxylation by CYP17A1 inhibitors (shown as open symbols) and resulting nonlinear fits used to estimate the pregnenolone hydroxylase IC_{50} (shown as dotted lines). These data are compared with 17,20-lyase inhibition data (closed symbols, solid lines) to determine selectivity for the targeted 17,20-lyase reaction.

Similar to inhibition of the other reactions performed by CYP17A1, abiraterone was the most potent inhibitor of pregnenolone hydroxylation (IC_{50} = 121 ± 7 nM), followed by the other steroidal inhibitor, galeterone (IC_{50} = 150 ± 20 nM). Non-steroidal inhibitors *S*-orteronel and VT-464 were the most potent non-steroidal inhibitors of pregnenolone hydroxylation, both exhibiting an IC_{50} value of 700 ± 100 nM. *R*-orteronel was significantly less potent than its *S*-enantiomer, demonstrating an IC_{50} value of 6000 ± 1000. Due to its low affinity for CYP17A1 and general lack of both potency and selectivity toward inhibition of the 17,20-lyase reaction, inhibition of pregnenolone hydroxylation by VT-463 was not evaluated.

Selectivity for 17,20-lyase inhibition was evaluated against pregnenolone hydroxylation in the same way it was evaluated against progesterone hydroxylation, as the pregnenolone hydroxylase IC_{50} value / 17,20-lyase IC_{50} value (Figure 6.6). In general, selectivity for 17,20-lyase inhibition versus pregnenolone hydroxylase inhibition was similar to selectivity of 17,20-lyase inhibition versus progesterone hydroxylase inhibition. Steroidal inhibitors abiraterone and galeterone demonstrated 3.3-fold and 1.5-fold selectivity for inhibition of the 17,20-lyase reaction compared to inhibition of pregnenolone hydroxylation. *S*-orteronel exhibited 3-fold selectivity for the 17,20-lyase reaction compared to pregnenolone hydroxylation. Selectivity for the *R*- enantiomer of orteronel for inhibition of the 17,20-lyase reaction compared to pregnenolone hydroxylation was again estimated to be higher than that of *S*-orteronel (11-fold selectivity). VT-464 exhibited only 2-fold selectivity for 17,20-lyase inhibition compared to pregnenolone hydroxylation, consistent with its poor selectivity for inhibition of the 17,20-lyase reaction against progesterone hydroxylation.

In most cases, each inhibitor's selectivity for 17,20-lyase inhibition versus pregnenolone hydroxylase inhibition was similar to selectivity of 17,20-lyase inhibition versus progesterone hydroxylase inhibition (Table 6.3). This is the case for galeterone (1.3 and 1.5-fold selectivity) and VT-464 (2.1 and 2.7-fold selectivity). Slight differences in the selectivity were observed for abiraterone, *S*-orteronel, *R*-orteronel. For example, *S*-orteronel 17,20-lyase selectivity appears slightly higher against progesterone hydroxylation (progesterone hydroxylase IC_{50} / 17,20-lyase IC_{50} = 4.5) than against pregnenolone hydroxylation (pregnenolone hydroxylase IC_{50} / 17,20-lyase IC_{50} = 3.3). Given the higher IC_{50} values for progesterone and pregnenolone hydroxylation overall and higher error associated with the values, differences between progesterone and

pregnenolone hydroxylase IC_{50} values and therefore differences in 17,20-lyase selectivity versus these reactions likely are not significant.

Table 6.3: Summary of IC_{50} values for 17α-hydroxypregnenolone 17,20-lyase inhibition (targeted reaction), progesterone and pregnenolone hydroxylation (off-target reactions), and resulting selectivity ratios.

Inhibitor	Lyase IC_{50} (nM)	Progesterone Hydroxylase IC_{50} (nM)	Progesterone Hydroxylase IC_{50}/ Lyase IC_{50}	Pregnenolone Hydroxylase IC_{50} (nM)	Pregnenolone Hydroxylase IC_{50} / Lyase IC_{50}
Abiraterone	36 ± 2	76 ± 5	2.1 ± 0.2	121 ± 7	3.3 ± 0.3
Galeterone	100 ± 10	130 ± 10	1.3 ± 0.2	150 ± 20	1.5 ± 0.3
S-Orteronel	210 ± 20	950 ± 70	4.5 ± 0.5	700 ± 100	3.3 ± 0.6
R-Orteronel	460 ± 90	4000 ± 300	8 ± 2	5000 ± 1000	11 ± 3
VT-464	430 ± 40	1170 ± 90	2.7 ± 0.3	700 ± 100	2.1 ± 0.4
VT-463	5000 ± 1000	11300 ± 900	2.3 ± 0.5	N/D	N/D

Crystal Structure of CYP17A1 with Orteronel

Steroidal inhibitors of CYP17A1 show very little selectivity (1.3 to 3.3-fold) for 17,20-lyase inhibition over 17α-hydroxylase inhibition. This is consistent with the X-ray crystal structure of CYP17A1 abiraterone and galeterone in which the nitrogen of the inhibitor pyridine ring coordinates to the heme iron, an interaction that should non-selectively prevent all turnover by the enzyme. Of the inhibitors evaluated as part of this study, only two inhibitors demonstrated greater selectivity for 17,20-lyase inhibition compared to abiraterone. *S*- and *R*-orteronel exhibit 3 to 5-fold and 8 to 11-fold selectivity for inhibition of the targeted 17,20-lyase reaction over off-target hydroxylation reactions. However, the mechanism by which these inhibitors do so is not understood. There is no published structural information on any CYP17A1 complexes with non-steroidal inhibitors to guide our understanding in this area.

To elucidate a structural basis for selective inhibition of the 17,20-lyase reactions over hydroxylase reactions, purified CYP17A1 was co-crystallized with commercial material

purchased as *S*-orteronel (Selleckchem). The resulting structure of CYP17A1 was determined at 2.2 Å resolution in the space group ($P2_12_12_1$). This is the same space group as previous CYP17A1 structures with both inhibitors and substrates[11,15]. The overall structure was consistent with the aforementioned structures, with four molecules comprising the asymmetric unit. Also in agreement with previous structures of CYP17A1, there is high symmetry between molecules A and B (RMSD over all Cα = 0.28 Å), and between molecules C and D of (RMSD over all Cα = 0.42 Å), but greater deviation is observed when comparing molecules A/B against C/D (average RMSD over all Cα = 1.20 ± 0.02 Å). This is the result of some conformational changes to the protein backbone, localized in the N-terminus and the region between F-G helices, as described for previous structures of CYP17A1[11].

Although density was observed for ligand in the active sites of all four molecules, the density observed in the active site of molecules A and B was significantly different compared to that observed in molecules C and D. In all cases, electron density clearly indicates that the ligand is coordinated to the heme iron (Figure 6.7), consistent with the Type II spectral shifts observed upon ligand binding (Figure 6.2). Ligand density in molecules C and D was very identifiably *S*-orteronel (Figure 6.7A), however, this ligand was a poor fit for the density observed in the active sites of molecules A and B. The inconsistent ligand density observed in the active site of molecules A and B led to an in-house characterization of the commercially-purchased *S*-orteronel, which actually contained both enantiomers of orteronel, along with an unidentified impurity. *R*-orteronel provides a reasonable fit for the ligand density in molecules A and B (Figure 6.7B) and is fairly consistent with the $2F_o$-F_c map. However, the F_o-F_c maps are not completely satisfied by inclusion of this ligand in a single orientation. Some negative F_o-F_c density is observed around the fused imidazole group interacting with the heme iron and some

positive density on one face of the naphthalene ring opposite the I helix, as well as between the heme iron and coordinating heterocycle.

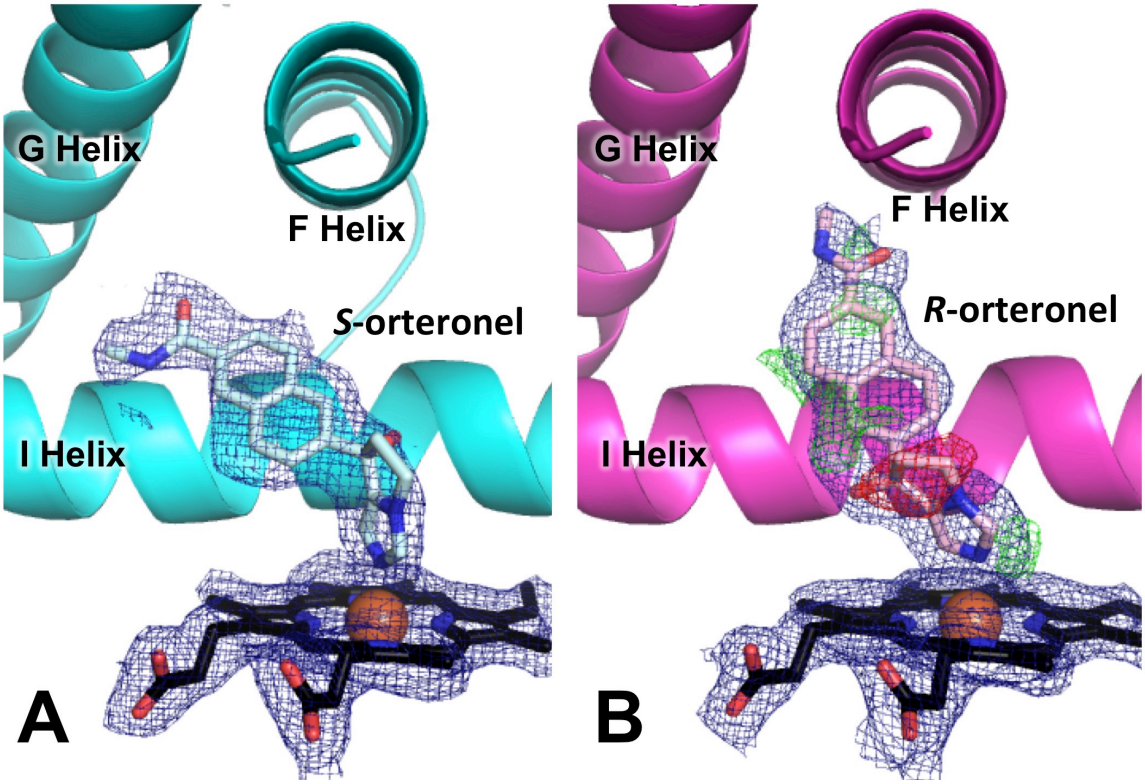

Figure 6.7: The contrasting ligand density in molecules C/D (panel A) compared to molecules A/B (panel B) in the 2.2 Å structure of CYP17A1 with orteronel suggests binding of different enantiomers of orteronel in different molecules of the structure (*S*-orteronel in panel A, *R*-orteronel in panel B). Simulated annealing composite omit map (contoured to 1.0 σ) is shown as blue mesh. *R*- orteronel, modeled into molecules A/B of the structure (panel B), does not fully satisfy electron density as demonstrated by Fo-Fc map for molecule A (negative density shown in red mesh and positive density shown in green mesh, contoured to 3.0 σ), but is the best solution.

R-Orteronel modeled into the ligand density of molecules A/B is oriented similar to steroidal substrates and inhibitors, at a 60° angle from the plane of the heme, with one face of the naphthalene ring positioned flat against the I helix and the oxygen of the amide substituent oriented toward a residue on the F helix, asparagine 202 (N202). This residue has been shown to hydrogen bond with the C3 substituent of steroidal inhibitors and substrates, and appears to

participate in a weak hydrogen bond (distances of 3.4 and 3.0 Å for molecules A and B, respectively) with *R*-orteronel (Figure 6.8A).

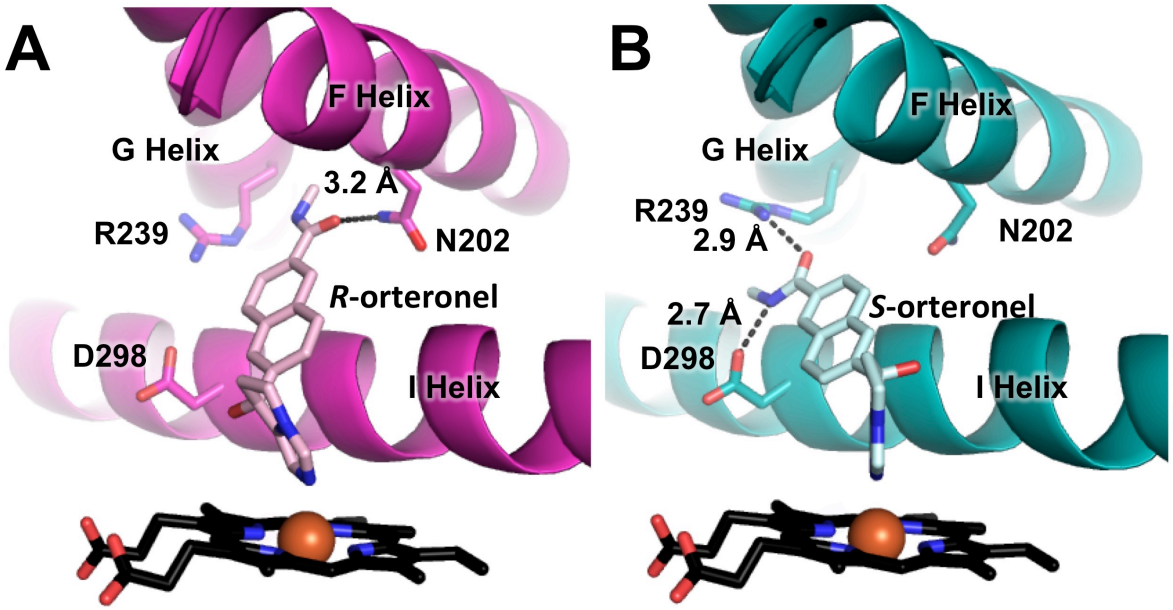

Figure 6.8: Interaction of A) *R*-orteronel and B) *S*-orteronel with CYP17A1 active site residues. All distances shown are averages for molecules A and B (in panel A) or C and D (in panel B).

The orientation of *S*-orteronel in the active site of molecules C/D shares some characteristics with *R*-orteronel as well as steroidal inhibitors and substrates. The ligand also forms an approximate 60° angle from the plane of the heme, with one face of the naphthalene core positioned flat against the I helix. However, in contrast to *R*-orteronel and steroidal inhibitors, *S*-orteronel is oriented toward the G helix (Figure 6.8B). The amide substituent hydrogen bonds with arginine 239 (R239; H-bonding distance of 2.7 and 3.0 Å for molecules C and D, respectively) and aspartic acid 298 (D298; H-bonding distance of 2.7 and 2.8 Å for molecules C and D respectively) on the I helix.

Crystal Structure of CYP17A1 with VT-464

Of the two non-steroidal CYP17A1 inhibitors to enter clinical trials, only *S*-orteronel demonstrated better selectivity than abiraterone for 17,20-lyase inhibition over 17α-hydroxylase

inhibition in the current study. VT-464, reportedly 10-fold selective for 17,20-lyase inhibition[4], only demonstrated 2-3-fold selectivity using purified CYP17A1 and partner proteins. Nonetheless, structural information for this inhibitor in complex with CYP17A1 is useful for comparison to the CYP17A1/orteronel complex, as such comparisons can be useful in establishing the structural basis for orteronel's selectivity.

The crystal structure of CYP17A1 bound to VT-464 was determined at 3.1 Å in the space group $P2_12_12_1$. The asymmetric unit was comprised of four copies of CYP17A1, which were similar to previous structures of CYP17A1 with substrates and inhibitors, including that of CYP17A1 with orteronel. As previously described for the CYP17A1/orteronel structure, molecules A and B demonstrated very similar overall structure, as did molecules C and D. Less similarity was observed between molecules A/B and C/D as a consequence of the same conformational changes to the N-terminus and F/G loop observed in the CYP17A1/orteronel structure.

Density corresponding to the ligand is present in all four copies of CYP17A1 (Figure 6.9A), and was consistent between copies. The density clearly indicates that the ligand is coordinated to the heme iron, consistent with the type II shift observed upon ligand binding (Figure 6.2). As with orteronel, the naphthalene ring is positioned flat against the I helix. However, unlike the structures with all other CYP17A1 inhibitors, VT-464 does not appear to form hydrogen bonds with any residues on the F or G helices. Instead, the hydroxyl group of carbon 1 participates in a hydrogen bond with the backbone carbonyl of V482 (average distance over four molecules = 2.9 ± 0.1 Å), while one of the nitrogens of the triazole coordinated to the heme iron is positioned within weak hydrogen bonding distance of the T306 side chain (average distance over four molecules = 3.1 ± 0.2 Å) (Figure 6.9B).

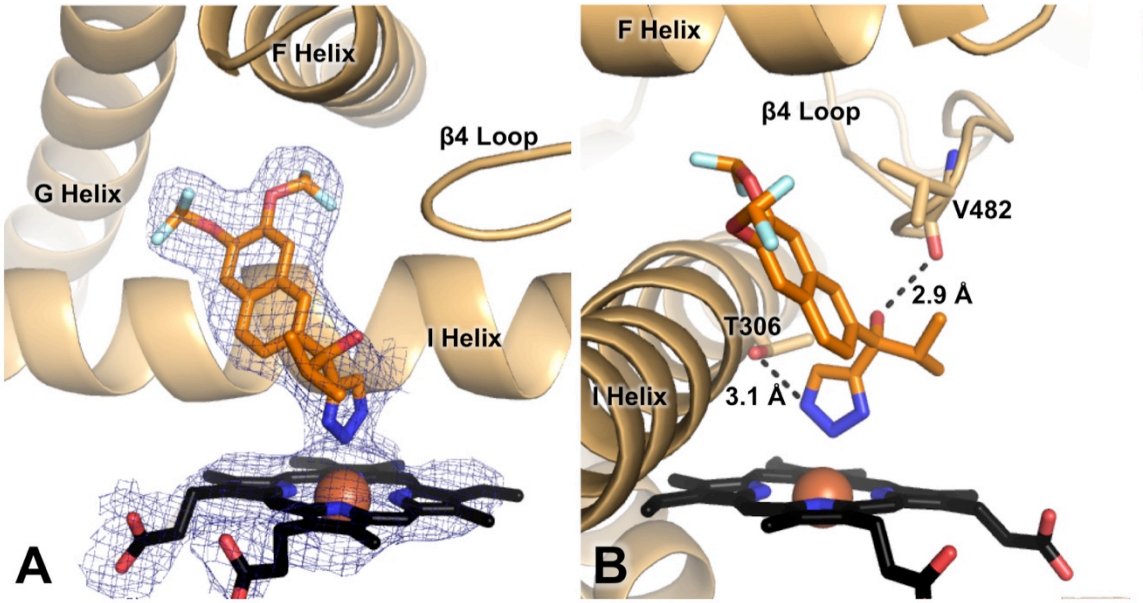

Figure 6.9: The 3.1 Å structure of CYP17A1 with VT-464. A) Ligand density corresponding to VT-464 (orange sticks) in structure of CYP17A1 with VT-464. Composite omit map with simulated annealing is shown as blue mesh contoured to 1.00 σ. B) Interactions between CYP17A1 active site and VT-464. Distances shown are averages from all four molecules.

DISCUSSION

All cytochrome P450 17A1 inhibitors that have undergone clinical trials or FDA approval have been individually evaluated for inhibition of the target enzyme, CYP17A1 in one context or another. These *in vitro* studies determine the each compound's half-maximal inhibitory concentration (IC_{50}) for CYP17A1, but this value can vary depending on substrate concentration and other experimental conditions as demonstrated by the wide range of IC_{50} values reported for abiraterone (Table 6.1). Catalysis by cytochrome P450 enzymes is especially complex and depends on multiple partner proteins. Since turnover is modulated by the quantities of these partner proteins relative to the cytochrome P450 and one another, the use of various catalytic systems (whole cells expressing P450 and catalytic partners, microsomes, or individual purified proteins) to evaluate cytochrome P450 turnover and inhibition contributes greatly to differences in experimental conditions and therefore apparent IC_{50} values. Moreover, CYP17A1 has two

physiologically relevant substrates for the 17α-hydroxylase reaction, and the concentration of substrate used in most studies is not often justified by kinetic characterization of the reaction

To summarize, cytochrome P450 inhibition studies are often not performed using a standardized set of conditions. Although such studies can identify and determine rank order potency of inhibitors evaluated internally, comparisons of IC_{50} values between studies are not always useful. Such comparisons are becoming more essential in the development of second generation steroidal and non-steroidal inhibitors which are increasingly being evaluated for selective inhibition of the 17,20-lyase reaction over the 17α-hydroxylase reaction.

This study uses tightly controlled conditions including known quantities of highly purified enzyme and partner proteins with substrate concentrations based on the individual kinetic parameters of the reaction under study. This allows the determination of IC_{50} values that can be used to make meaningful comparisons across inhibitor types. These comparisons can be used to establish rank order potency for inhibitors of the enzyme, which significantly impacts clinical efficacy. More importantly, it allows us to compare potency of inhibition between target and off-target reactions and determine whether selective inhibition of the 17,20-lyase reaction is indeed possible for compounds that inhibit CYP17A1 through direct coordination to the heme iron.

In previous studies using microsomes and purified CYP17A1 with partner proteins, the steroidal inhibitor abiraterone (often the only inhibitor used as a control) is a more potent inhibitor of both the 17α-hydroxylation and the 17,20-lyase reaction than non-steroidal inhibitors. The other steroidal inhibitor, galeterone, has only been evaluated for 17,20-lyase inhibition alongside abiraterone using whole cell systems, and was reportedly nearly 3-fold more potent than abiraterone.

Among the inhibitors tested for the desired inhibition of the 17,20-lyase reaction herein, the steroidal inhibitors abiraterone and galeterone were the most potent. This is consistent with binding data, which suggests that abiraterone and galeterone have the highest affinity for the CYP17A1 active site. Abiraterone exhibited the highest potency overall (36 ± 3 nM). Its estimated IC_{50} in this system with purified protein is broadly consistent with previous studies in microsomes and purified protein systems, which report IC_{50} values between 3 and 27 nM[1,3,4]. Galeterone exhibited nearly 3-fold lower potency than abiraterone in the current studies. Since abiraterone and galeterone are both based on the steroidal scaffold, differences in potency likely indicate that the benzimidazole substituent of galeterone coordinates the heme iron less effectively than the pyridine ring of abiraterone. Previous reports of galeterone as a more potent inhibitor than abiraterone in a whole cell system may instead reflect other factors such as differences in cellular penetration between the inhibitors evaluated[2].

The most potent non-steroidal inhibitor was *S*-orteronel (IC_{50} = 210 ± 20), which was 5.8-fold less potent than abiraterone in inhibiting of the 17,20-lyase reaction. VT-464 exhibited an even lower potency (IC_{50} = 430 ± 40 nM; 12-fold lower than abiraterone) for inhibition of 17,20 lyase activity. Binding data suggests that VT-464 has higher affinity for the CYP17A1 active site than *S*-orteronel. This apparent incongruity between affinity for the CYP17A1 active site and inhibition of the 17,20-lyase reaction may suggest that inhibition of the 17,20-lyase reaction by *S*-orteronel is not mediated entirely through heme coordination, but estimated affinities for CYP17A1 by VT-464 and *S*-orteronel (31 ± 7 and 40 ± 7, respectively) are too low to be determined with a high degree of certainty as discussed previously. The ranking of inhibitor potency based on IC_{50} values is therefore more meaningful.

The *R*- enantiomers of both non-steroidal inhibitors demonstrated lower potency for 17,20-lyase inhibition than the *S*- enantiomers used in clinical trials. *R*-orteronel was 2.2-fold less potent an inhibitor of the 17,20-lyase reaction compared to *S*-orteronel, while VT-463 was nearly 12-fold less potent than its *S*-enantiomer, VT-464. Binding data suggests that VT-463 has a much lower affinity for the CYP17A1 than VT-464, but while *R*-orteronel may have lower affinity for the CYP17A1 active site than *S*-orteronel, the margin between these two enantiomers is much smaller. Overall, there appears to be an advantage to *S*-stereochemistry at the chiral center in potency for 17,20-lyase inhibition.

Rank order potency determined by the current study is consistent the clinical success of CYP17A1 inhibitors. Abiraterone has been successful in clinical trials, successfully improving overall survival in Phase III clinical trials[19]. Decreased potency for 17,20-lyase inhibition by *S*-orteronel when compared to abiraterone is consistent with its failure to achieve this end point in Phase II clinical trials[20]. Based on the failure of *S*-orteronel to improve overall survival in Phase II clinical trials, it is improbable that an even less potent inhibitor of 17,20-lyase activity such as VT-464 will demonstrate improved efficacy in a clinical setting. This, however, assumes that overall survival by the steroidal inhibitors is solely mediated by CYP17A1 inhibition, which is almost certainly not the case, as steroidal inhibitors have been reported to both antagonize[2,21] and cause degradation of the androgen receptor[22], and VT-464 has also been reported to act as an anti-androgen[23]. Nonetheless, inhibition of 17,20-lyase activity of CYP17A1 is an important contributor to success of these compounds in a clinical setting.

Inhibitors of CYP17A1 not only interfere with the 17,20-lyase reaction responsible for generating androgens, but also the 17α-hydroxylation reactions mediated by CYP17A1 and necessary for glucocorticoid biosynthesis. Side effects observed in patients receiving abiraterone

as treatment, including hypertension and peripheral edema[19,24], are believed to be the result of 17α-hydroxylase inhibition and require coadministration with a synthetic glucocorticoid, typically prednisone[24]. The selectivity of abiraterone for the 17,20-lyase reaction over the 17α-hydroxylase reaction has been estimated to range anywhere from 0.1-fold to 1.4-fold depending on the hydroxylase substrate identity and concentration as well as the system under study[1,3,4]. Using purified CYP17A1 and partner proteins, we observed 2- to 3.3-fold selectivity for 17,20-lyase inhibition over progesterone and pregnenolone 17α-hydroxylation, respectively. The other steroidal inhibitor evaluated, galeterone, demonstrated ~1.5-fold selectivity for desired inhibition of the 17,20-lyase reaction over hydroxylation of either progesterone or pregnenolone. The side effect profile of galeterone based on data from Phase I/II clinical trials has not been reported in the literature. Since galeterone also exhibits poor selectivity for 17,20-lyase inhibition over hydroxylase inhibition similar to abiraterone, it is likely to cause similar side effects related to to secondary mineralocorticoid excess.

The *S*-enantiomers of the non-steroidal inhibitors (*S*-orteronel and VT-464) have been reported in the literature to be 5- and 10-fold more selective for 17,20-lyase inhibition compared to 17α-hydroxylase inhibition[3,4]. Consequently they have been developed as CYP17A1 inhibitors with potentially improved side effect profiles. *S*-orteronel has been reported to be slightly more than 5-fold selective for inhibition of the 17,20-lyase reaction compared to pregnenolone hydroxylation[3]. In the current study, *S*-orteronel demonstrated 3.3- to 4.5-fold selectivity for the 17,20-lyase inhibition over pregneneolone hydroxylase inhibition or progesterone hydroxylase inhibition. It is unknown if this slight increase in selectivity for 17,20-lyase inhibition would significantly improve the side effects resulting from secondary

mineralocorticoid excess *in vivo*, because *S*-orteronel was still co-administered with prednisone in clinical trials[20].

VT-464 has been reported to be an even more selective inhibitor of the 17,20-lyase reaction, purportedly demonstrating 10-fold selectivity for lyase inhibition over pregnenolone 17α-hydroxylase inhibition in studies using CYP17A1 in yeast microsomes[4]. When evaluated using purified CYP17A1 and partner proteins in this study, VT-464 demonstrated only 2- to 3-fold selectivity, similar to abiraterone. Clinical trial data for VT-464 has yet to be reported in the literature, however, the similarity of its selectivity profile to abiraterone suggests that this non-steroidal inhibitor will produce similar side effects to abiraterone.

Both non-steroidal inhibitors in clinical trials (orteronel and VT-464) include stereocenters with *S*- configuration. These enantiomers were pursued since they demonstrated better potency for 17,20-lyase inhibition than their *R*-enantiomers[4,8]. There have been no reports in the literature on whether or not the *R*-enantiomers exhibit more, less, or equal selectivity for 17,20-lyase inhibition compared to 17α-hydroxylase inhibition. To evaluate the effect of the stereocenter on inhibitor 17,20-lyase selectivity, *R*-orteronel and VT-463 (the *R*-enantiomer of VT-464) were evaluated for inhibition of the relevant reactions. VT-463 demonstrated significantly lower potency than VT-464, with no significant difference in selectivity for the 17,20-lyase reaction compared to progesterone hydroxylation (2.7-fold and 2.3-fold selectivity for VT-464 and VT-463, respectively). Although *S*-orteronel demonstrated higher potency, *R*-orteronel actually exhibited better selectivity for 17,20-lyase inhibition compared to inhibition of either hydroxylase reaction. *R*-orteronel inhibited the 17,20-lyase reaction 8-fold better than progesterone hydroxylation and 11-fold better than pregnenolone hydroxylation. This indicates that the configuration of orteronel's stereocenter has an impact on selectivity for 17,20-lyase

inhibition compared to hydroxylase inhibition and suggests that selectivity can be modulated even with inhibitors that coordinate the heme iron.

Although the decreased potency exhibited by *R*-orteronel in suppressing 17,20-lyase activity would likely make it a poor candidate for clinical development, it may provide insight into a possible mechanism for selective 17,20-lyase inhibition. The 2.2 Å crystal structure of CYP17A1 co-crystallized with a racemic mixture of *S*- and *R*- orteronel reveals ligand density corresponding to *S*-orteronel in two of four CYP17A1 molecules comprising the asymmetric unit. In these two molecules, the ligand is both coordinated to the heme iron and forms hydrogen bonds with R239 on the G Helix. Although there was apparent ligand density coordinated to the heme iron in the other two molecules of CYP17A1 comprising the asymmetric unit, this density did not appear to form interactions with any of the G-helix residues and appeared to be engaged in a hydrogen bond with N202 of the F helix. *S*-orteronel was not a reasonable fit to this density, which did resemble *R*-orteronel. A particularly interesting observation is that molecules of CYP17A1 with *S*-orteronel occupying the active site exhibit significant changes in the F/G loop region of the enzyme when compared to those housing ligand density consistent with the *R*-orteronel (Figure 6.10). The affected F/G region of the enzyme is known to be highly flexible and believed to interact with the membrane. Although this conformational difference in the F/G helical region is observed in most structures of CYP17A1 with inhibitors and substrates, usually the ligand adopts the same orientation in the active site of CYP17A1, regardless of the F/G loop conformation. The observation that both *R*- and *S*- orteronel are not observed in the active site of every molecule of CYP17A1 at partial occupancy suggests that *S*-orteronel is selectively bound to CYP17A1 displaying one conformation of the F/G loop while *R*-orteronel selectively populates the active site of CYP17A1 displaying the alternate conformation of this loop. In other

cytochrome P450 enzymes, movement of the F/G loop with respect to the B′ helix is indicated in substrate access to the active site[25], which may suggest that the stereochemistry of orteronel (and the selectivity for 17,20-lyase inhibition associated with different stereochemistry) affects ligand entry and exit. This is consistent with recent work by Pallan *et al.* which demonstrated that the processivity of the two sequential reactions performed by teleost CYP17A1 affects whether or not orteronel is selective for 17,20-lyase inhibition over hydroxylase inhibition[12]. For substrates that were more likely to leave the CYP17A1 active site after the 17-hydroxylase reaction and prior to the 17,20-lyase reaction, *S*-orteronel demonstrated ~10-fold selectivity for 17,20-lyase inhibition. In contrast, using substrates that were less likely to dissociate from the active site between 17-hydroxylase and 17,20-lyase reactions, only 2-fold selectivity for 17,20-lyase inhibition was observed. Processivity of human CYP17A1 with different substrates has not been reported, which prevents direct comparisons with the human enzyme at present, but these studies of teleost CYP17A1 inhibition by orteronel coupled with the structure of human CYP17A1 with orteronel are consistent with a mechanism for 17,20-lyase selectivity of orteronel that involves modulation of intermediate release or reentry from or to the active site of CYP17A1.

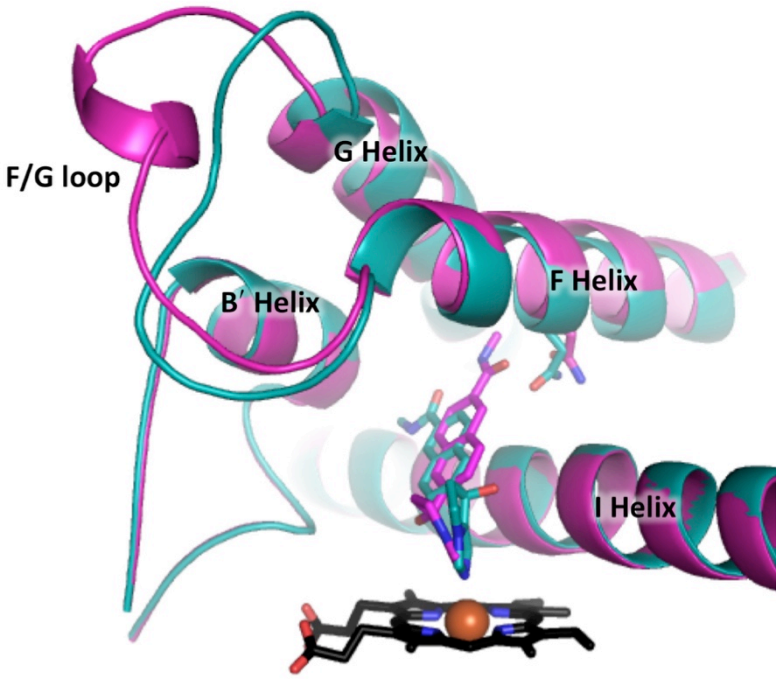

Figure 6.10: The ligand occupying the CYP17A1 active site (*R*-orteronel shown in magenta and *S*-orteronel in teal) depends on the conformation of the CYP17A1 F/G loop, a region implicated in ligand entry and exit for other mammalian cytochrome P450 enzymes.

Unlike the structure of CYP17A1 with orteronel, the structure of CYP17A1 with the much less selective VT-464 demonstrated consistent ligand density in all four molecules of the protein comprising the asymmetric unit. The CYP17A1/VT-464 complex crystallizes exhibiting both F/G-loop conformations, similar to CYP17A1 structures with abiraterone and galeterone. This observation, coupled with the lack of selectivity for 17,20-lyase inhibition exhibited by VT-464 as part of this study, further supports the role of the F/G loop, and likely ligand access to the CYP17A1 active, in the apparent 17,20-lyase selectivity of orteronel. The structure of CYP17A1 with VT-464 is, however, the first structure of CYP17A1 with an inhibitor that does not appear to interact with either the F or G helix. Optimization of this inhibitor to form hydrogen bonds with relevant residues in the F or G helix may improve the potency of VT-464.

In conclusion, parallel examination of a panel of clinically-relevant steroidal and non-steroidal CYP17A1 inhibitors established rank order potency for inhibition of the 17,20-lyase reaction necessary for androgen biosynthesis. More importantly, tight control over experimental conditions allows us to determine whether reported selectivity for 17,20-lyase inhibition against inhibition of the 17α-hydroxylase reaction, believed to cause corticosteroid-related side effects, is possible using compounds that coordinate the heme iron. The steroidal inhibitors were more potent inhibitors than the non-steroidal inhibitors evaluated. The 10-fold selectivity for 17,20-lyase inhibition over 17α-hydroxylase inhibition reported for non-steroidal inhibitor VT-464[4] was not observed, with no improvement in selectivity detected for its less potent enantiomer, VT-463. In contrast *S*-orteronel demonstrated ~3-5-fold selectivity for 17,20-lyase inhibition over 17α-hydroxylase inhibition similar to that reported previously[4]. The less potent enantiomer, *R*-orteronel, exhibited even greater selectivity (8- to 11-fold) for 17,20-lyase inhibition. To better elucidate a structural basis for the observed selectivity of the orteronel enantiomers, CYP17A1 was crystallized in the presence of orteronel, which was later found to be a racemic mixture of *R*- and *S*- enantiomers. The resulting 2.2 Å structure demonstrates different conformations of the F/G region depending on which enantiomer (*S*- or *R*-) occupies the active site. This observation, coupled with studies on CYP17A1 processivity and its effects on the apparent selectivity of *R*-orteronel, seem to suggest that the selectivity of *R*-orteronel is may be in part mediated by promoting exit of intermediate product, and/or preventing lyase substrate reentry. A better understanding of how CYP17A1 inhibitors such as *R*-orteronel achieve selectivity for the target 17,20-lyase reaction compared to off-target reactions performed in the same active site could help inform the development of more selective and potent inhibitors of this enzyme for the treatment of prostate cancer.

ACKNOWLEDGEMENTS

Synthesis of VT-464 and VT-463 and chiral separation of *R*-orteronel and *S*-orteronel were performed by Dr. Steven Rogers.

REFERENCES

(1) Potter, G. A.; Barrie, S. E.; Jarman, M.; Rowlands, M. G. *J. Med. Chem.* **1995**, *38*, 2463.
(2) Handratta, V. D.; Vasaitis, T. S.; Njar, V. C.; Gediya, L. K.; Kataria, R.; Chopra, P.; Newman, D., Jr.; Farquhar, R.; Guo, Z.; Qiu, Y.; Brodie, A. M. *J. Med. Chem.* **2005**, *48*, 2972.
(3) Yamaoka, M.; Hara, T.; Hitaka, T.; Kaku, T.; Takeuchi, T.; Takahashi, J.; Asahi, S.; Miki, H.; Tasaka, A.; Kusaka, M. *J. Steroid Biochem. Mol. Biol.* **2012**, *129*, 115.
(4) Rafferty, S. W.; Eisner, J. R.; Moore, W. R.; Schotzinger, R. J.; Hoekstra, W. J. *Bioorg. Med. Chem. Lett.* **2014**, *24*, 2444.
(5) Al-Masoudi, N. A.; Ali, D. S.; Saeed, B.; Hartmann, R. W.; Engel, M.; Rashid, S.; Saeed, A. *Arch. Pharm. (Weinheim, Ger.)* **2014**, *347*, 896.
(6) Jagusch, C.; Negri, M.; Hille, U. E.; Hu, Q.; Bartels, M.; Jahn-Hoffmann, K.; Pinto-Bazurco Mendieta, M. A.; Rodenwaldt, B.; Muller-Vieira, U.; Schmidt, D.; Lauterbach, T.; Recanatini, M.; Cavalli, A.; Hartmann, R. W. *Bioorg. Med. Chem.* **2008**, *16*, 1992.
(7) Bruno, R. D.; Vasaitis, T. S.; Gediya, L. K.; Purushottamachar, P.; Godbole, A. M.; Ates-Alagoz, Z.; Brodie, A. M.; Njar, V. C. *Steroids* **2011**, *76*, 1268.
(8) Kaku, T.; Hitaka, T.; Ojida, A.; Matsunaga, N.; Adachi, M.; Tanaka, T.; Hara, T.; Yamaoka, M.; Kusaka, M.; Okuda, T.; Asahi, S.; Furuya, S.; Tasaka, A. *Bioorg. Med. Chem.* **2011**, *19*, 6383.
(9) Copeland, R. A. In *Evaluation of Enzyme Inhibitors in Drug Discovery: A Guide for Medicinal Chemists and Pharmacologists*; 2nd ed.; John Wiley & Sons: Hoboken, NJ, 2013.
(10) Yoshimoto, F. K.; Zhou, Y.; Peng, H. M.; Stidd, D.; Yoshimoto, J. A.; Sharma, K. K.; Matthew, S.; Auchus, R. J. *Biochemistry* **2012**, *51*, 7064.
(11) Petrunak, E. M.; DeVore, N. M.; Porubsky, P. R.; Scott, E. E. *J. Biol. Chem.* **2014**, *289*, 32952.
(12) Pallan, P. S.; Nagy, L. D.; Lei, L.; Gonzalez, E.; Kramlinger, V. M.; Azumaya, C. M.; Wawrzak, Z.; Waterman, M. R.; Guengerich, F. P.; Egli, M. *J. Biol. Chem.* **2015**, *290*, 3248.
(13) Kabsch, W. *Acta Crystallogr., Sect. D: Biol. Crystallogr.* **2010**, *66*, 125.
(14) McCoy, A. J.; Grosse-Kunstleve, R. W.; Adams, P. D.; Winn, M. D.; Storoni, L. C.; Read, R. J. *J. Appl. Crystallogr.* **2007**, *40*, 658.
(15) DeVore, N. M.; Scott, E. E. *Nature* **2012**, *482*, 116.
(16) Emsley, P.; Lohkamp, B.; Scott, W. G.; Cowtan, K. *Acta Crystallogr., Sect. D: Biol. Crystallogr.* **2010**, *66*, 486.

(17) Adams, P. D.; Afonine, P. V.; Bunkoczi, G.; Chen, V. B.; Davis, I. W.; Echols, N.; Headd, J. J.; Hung, L. W.; Kapral, G. J.; Grosse-Kunstleve, R. W.; McCoy, A. J.; Moriarty, N. W.; Oeffner, R.; Read, R. J.; Richardson, D. C.; Richardson, J. S.; Terwilliger, T. C.; Zwart, P. H. *Acta Crystallogr., Sect. D: Biol. Crystallogr.* **2010**, *66*, 213.
(18) Schrodinger, LLC 2010.
(19) Fizazi, K.; Scher, H. I.; Molina, A.; Logothetis, C. J.; Chi, K. N.; Jones, R. J.; Staffurth, J. N.; North, S.; Vogelzang, N. J.; Saad, F.; Mainwaring, P.; Harland, S.; Goodman, O. B., Jr.; Sternberg, C. N.; Li, J. H.; Kheoh, T.; Haqq, C. M.; de Bono, J. S.; Investigators, C.-A.-. *Lancet Oncol.* **2012**, *13*, 983.
(20) Saad, F.; Fizazi, K.; Jinga, V.; Efstathiou, E.; Fong, P. C.; Hart, L. L.; Jones, R.; McDermott, R.; Wirth, M.; Suzuki, K.; MacLean, D. B.; Wang, L.; Akaza, H.; Nelson, J.; Scher, H. I.; Dreicer, R.; Webb, I. J.; de Wit, R.; investigators, E.-P. *Lancet Oncol.* **2015**, *16*, 338.
(21) Richards, J.; Lim, A. C.; Hay, C. W.; Taylor, A. E.; Wingate, A.; Nowakowska, K.; Pezaro, C.; Carreira, S.; Goodall, J.; Arlt, W.; McEwan, I. J.; de Bono, J. S.; Attard, G. *Cancer Res.* **2012**, *72*, 2176.
(22) Yu, Z.; Cai, C.; Gao, S.; Simon, N. I.; Shen, H. C.; Balk, S. P. *Clin. Cancer Res.* **2014**, *20*, 4075.
(23) Toren, P.; Pham, S.; Kim, S.; Adomat, H.; Zoubeidi, A.; Moore, W. R.; Gleave, M. E. In *Genitourinary Cancers Symposium*; American Society of Clinical Oncology: Vancouver, BC, Canada, 2014.
(24) Attard, G.; Reid, A. H.; Auchus, R. J.; Hughes, B. A.; Cassidy, A. M.; Thompson, E.; Oommen, N. B.; Folkerd, E.; Dowsett, M.; Arlt, W.; de Bono, J. S. *J. Clin. Endocrinol. Metab.* **2012**, *97*, 507.
(25) Poulos, T. L.; Johnson, E. F. In *Cytochrome P450: Structure, Mechanism, and Biochemistry*; 3rd ed.; Ortiz de Montellano, P., Ed.; Kluwer Academic / Plenum Publishers: New York, 2005.

Chapter 7.

Structure of Human Steroidogenic Cytochrome P450 21A2 (CYP21A2)

INTRODUCTION

Cytochrome P450 21A2 (CYP21A2) is one of six P450 enzymes involved in human steroid biosynthesis. CYP21A2 generates corticosteroids by hydroxylating the Δ4 steroids progesterone and 17α-hydroxyprogesterone on carbon 21 to form 11-deoxycorticosterone and 11-deoxycortisol, respectively. Metabolites of CYP21A2 are intermediates for molecules that regulate sodium balance, directly affecting water retention and therefore homeostatic functions such as blood pressure. Even further downstream, other metabolites regulate stress response, particularly inflammation. Thus, impairment of CYP21A2 function can greatly disrupt homeostasis.

The consequences of hindered CYP21A2 activity have been observed in human patients with congenital adrenal hyperplasia. The most common cause of this disorder (>90% of all cases) is mutation of CYP21A2[1]. The degree to which CYP21A2 function is compromised directly affects the severity of the resulting phenotypes. When CYP21A2 is impaired >98%, symptoms include severe hypokalemia (low levels of circulating potassium ions), low blood pressure, and cardiovascular disorders due to deficient production of corticosteroids[1,2]. Substrates for CYP21A2 also accumulate and are alternatively metabolized by CYP17A1, resulting in an excess of androgens and some gender-dependent phenotypes including ambiguous genitalia in women and extreme virilization in men[1]. Overproduction of androgens can also occur in individuals with as much as 60% retention of CYP21A2 activity. However, the resulting phenotypes, such as infertility and polycystic ovarian syndrome in women, are generally less severe than those associated with the more complete reduction in CYP21A2

activity.[1,3] The effects of CYP21A2 dysfunction on androgen biosynthesis further demonstrate the interconnection between different branches of human steroidogenic pathways.

In addition to sharing the substrates progesterone and 17α-hydroxyprogesterone, CYP21A2 and CYP17A1 have 39% sequence identity. To some extent, these enzymes even exhibit further overlapping metabolic profiles. CYP17A1 has been shown to convert progesterone to very small amounts 11-deoxycorticosterone. Although this is only ~1% of total product formation in the wild type CYP17A1 enzyme[4], it can be increased to 5% by the A105L mutant[4]. CYP21A2 has also demonstrated the capacity to produce 16α-hydroxyprogesterone, which is a minor metabolite of CYP17A1 progesterone hydroxylation[4,5]. It is therefore not surprising that inhibitors of CYP17A1, especially those based on the steroidal scaffold, have also been shown to interact with CYP21A2[6].

Inhibitors of CYP17A1 have recently been developed to prevent the production of tumor-promoting androgens in patients with prostate cancer. FDA-approved abiraterone is based on the structure of pregnenolone, a steroidal substrate of CYP17A1. Abiraterone is very effective in preventing catalysis by CYP17A1. However, treatment with abiraterone and related inhibitors often also result in clinical side effects due to glucocorticoid deficiency and an excess of mineralocorticoids. This corticosteroid imbalance is believed to partially result from inhibition of progestagen hydroxylation by CYP17A1. However, the ubiquitous steroidal core on which abiraterone is based makes these compounds likely to interact with many other physiological targets, but especially the other cytochrome P450 enzymes involved in steroid biosynthesis and metabolism.

Abiraterone has been shown to both bind and inhibit human CYP21A2. Titration of CYP21A2 with abiraterone results in a Type II spectral shift, consistent with coordination of the

inhibitor's nitrogen-containing heterocycle to the heme iron (Victoria Jasion, unpublished data, Figure 7.1A). This is the same interaction mode observed for abiraterone with human CYP17A1. Although an accurate K_d has yet to be determined, it is currently estimated to be <1 μM (Victoria Jasion, unpublished data). Additionally, abiraterone demonstrates dose-dependent inhibition of progesterone 21-hydroxylation by CYP21A2 with an IC_{50} value (determined in a system with purified enzymes) of 300 ± 30 nM (Figure 7.1B)[6]. This is 8-fold higher than the IC_{50} for inhibition of CYP17A1-mediated 17,20-lyase activity by CYP17A1 (CYP17A1 17,20-lyase IC_{50} = 36 ± 2) and ~2-4-fold higher than the IC_{50} for CYP17A1-mediated 17α-hydroxylase reactions (CYP17A1 17α-hydroxylase IC_{50} = 121 ± 7 and 76 ± 5 for pregnenolone and progesterone as substrates, respectively).

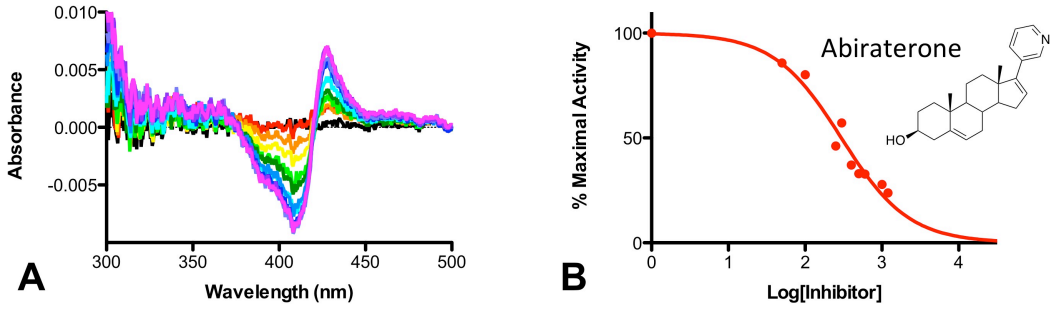

Figure 7.1: Abiraterone interacts with CYP21A2. A) Binding of abiraterone to CYP21A2 results in a type II spectral shift as evidenced by an increase in absorbance at 424 nm and a decrease in absorbance at 409 nm. Increasing inhibitor concentrations are shown from red/orange to blue/magenta. Data provided courtesy of Victoria Jasion (unpublished). B) Abiraterone demonstrates dose-dependent inhibition of progesterone 21-hydroxylation by human CYP21A2 with an IC_{50} of 300 ± 30 nM[6].

The physiological impact of off-target CYP21A2 inhibition by abiraterone is largely unknown since inhibitors that selectively interact with CYP17A1 compared to CYP21A2 have not been tested *in vivo*. However, the potential effects of CY21A2 deficiency are known based on mutations in human patients as discussed above (Figure 7.2A). Therefore, it is logical to suggest that mineralocorticoid production would also be reduced for abiraterone and other

compounds that inhibit both CYP17A1 and CYP21A2 (Figure 7.2B) compared to CYP17A1 inhibitors that do not inhibit CYP21A2 (Figure 72.C). However in patients it is observed that dual inhibitors depress glucocorticoid production, which ultimately leads to a secondary mineralocorticoid excess via the adrenocorticotropin hormone feedback loop. Additionally, undesired CYP21A2 inhibition could contribute to a build-up of CYP17A1 substrate capable of overwhelming CYP17A1 inhibition and facilitating resistance to traditional CYP17A1 inhibitors over time (Figure 7.2.B). Therefore, development of CYP17A1 inhibitors that do not interfere with CYP21A2 activity will help illuminate contributions of CYP21A2 inhibition to therapeutic outcomes.

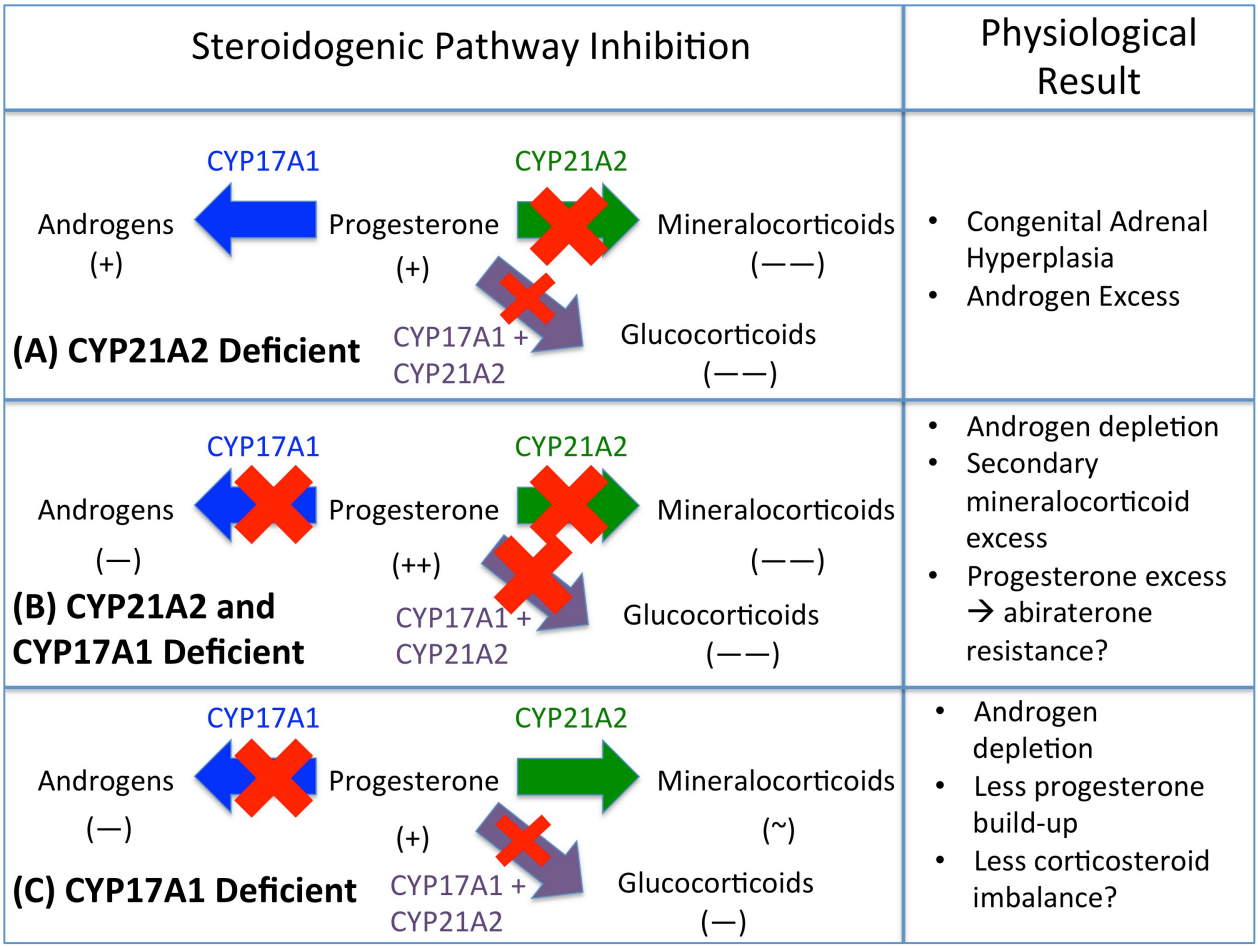

Figure 7.2: Effects of steroidogenic cytochrome P450 inhibition on steroid hormone levels. A) CYP21A2 inhibition results in a decrease of mineralocorticoids and glucocorticoids with a concomitant increase in androgens. B) Inhibition of both CYP17A1 and CYP21A2 would certainly result in a decrease in glucocorticoids and likely a decrease in mineralocorticoids, but an increase in CYP17A1 substrate could overwhelm CYP17A1 inhibition, resulting in an increase in androgen production over time. C) Selective inhibition of CYP17A1 results in a decrease in androgens and glucocorticoids and an increase in mineralocorticoids.

Structural information regarding the CYP21A2 countertarget can be extremely beneficial in directing design of more selective CYP17A1 inhibitors. At the time this project was initiated, the most relevant structural information about CYP21A2 was an X-ray crystal structure of bovine CYP21A2 in complex with substrate 17α-hydroxyprogesterone[7]. Bovine and human CYP21A2 share 80% sequence identity and both perform 21-hydroxylation on both progesterone and 17α-hydroxyprogesterone, but the human enzyme is more catalytically efficient[8]. Thus, the goal of the following study was to determine the X-ray crystal structure of human CYP21A2 in

complex with CYP17A1 inhibitor abiraterone approved for treatment of prostate cancer. However, shortly after I solved a structure of human CYP21A2, a structure of human CYP21A2 in complex with substrate progesterone was published[8]. Unfortunately, in our CYP21A2 X-ray crystal structure the ligand density for abiraterone in the active site is relatively weak, likely the result of poor occupancy, and this ultimately prohibited modeling of the ligand. The remainder of the CYP21A2 structure I determined is very similar to that of the substrate-bound enzyme[8]. Both human CYP21A2 structures display significant differences compared to bovine CYP21A2, including translation of the I helix with respect to the heme cofactor. Such structural information may help guide the design of CYP17A1 inhibitors with lower affinity for CYP21A2, and help inform the biochemical consequences of CYP21A2 inhibition in prostate cancer treatment.

METHODS

Expression of CYP21A2

The gene encoding CYP21A2 bearing a truncation of the N-terminus (residues 2-28 and a leading sequence of "AKKTSSKGK", and a C-terminal 4x histidine tag was cloned into the pCWori+ vector by Linda Blake (pCW/CYP21A2dH)[9].

pCW/CYP21A2dH (1 µL, 211 ng/mL) was transformed into 100 µL of DH5α/pGro7 competent cells. The cells were incubated with vector at 4°C for 30 minutes, heated to 42°C for 30 seconds, and returned to ice for two minutes. Cells were incubated in 1 mL super optimal broth for 45 minutes at 37°C with 220 rpm shaking. Following outgrowth, 600 µL of the cells were spread onto a lysogeny broth agar plate with 100 µg/mL carbenicillin and 30 µg/mL chloramphenicol.

All media in the following expression was supplemented with 100 μg/mL carbenicillin and 30 μg/mL chloramphenicol to select for the pCWori+ and pGro7 vectors, respectively. A starter culture of 5 mL lysogeny broth was inoculated with single colony from the aforementioned plate and incubated at 37°C with 220 rpm shaking for 8 hours. An overnight culture of 200 mL lysogeny broth was inoculated with 200 μL starter culture and incubated for ~16 hours at 37°C with 220 rpm shaking. Terrific broth (1L / 2.8 fernbach flask) was inoculated with 20 mL overnight culture and incubated at 37°C with 220 rpm shaking. At a 1.10 optical density at 600 nm, CYP21A2 expression was induced by addition of β-D-1-thiogalactopyranoside to a concentration of 0.5 mM and 1 g/L arabinose was also added to induce chaperone expression. The heme precursor δ-aminolevulinic acid was added at a concentration of 1 mM. Flasks were incubated at 25°C with 120 rpm shaking for 48 hours. Cells were pelleted by repeated centrifugation at ~6000 x g and resuspended in buffer containing 20 mM KPi, pH 6.8, and 20% glycerol. Resuspended cells were stored at -80 °C until purification.

Purification of CYP21A2

All stages of the purification were conducted at 4 °C. Resuspended cells were thawed and stirred in the presence of lysozyme (0.3 mg/mL) for 30 minutes. The mixture was treated with an equal volume of deionized water and stirred for an additional 10 minutes prior to centrifugation at 9900 x *g* for 15 minutes. The resulting pellet was resuspended in buffer containing 500 mM KPi, pH 6.8, 300 mM NaCl, and 20% glycerol, and homogenized using a tissue grinder. Resuspended cells were lysed by sonication (6 x 30 seconds with 1 minute intervals on ice), and cellular debris removed by centrifugation at 9900 x *g* for 15 minutes.

Membrane proteins were extracted from the supernatant by stirring for 60 minutes in the presence of 1% (v/v) detergent Emulgen-913 (Desert Biologicals), followed by centrifugation at 100,000 x *g* for 60 minutes.

Supernatant was loaded onto a column of ~30 mL Ni-NTA resin (Qiagen) that was pre-equilibrated with nickel buffer (100 mM KPi, pH 6.8, 20% glycerol, 300 mM NaCl, and 0.2% Emulgen-913). The resin-bound protein was washed with 4 column volumes (CV) of nickel buffer, followed by 5 CV of nickel buffer supplemented with 12 mM histidine. Protein was eluted using 4 CV of nickel buffer supplemented with 80 mM histidine. Fractions were pooled based on absorbance at 417 nm, the λ_{max} for the heme Soret peak.

Pooled fractions were diluted 3-fold in buffer containing 5 mM KPi, pH 6.8, 20% glycerol, 1 mM EDTA, and 0.2% Emulgen-913. Diluted protein was loaded onto a 5 mL carboxymethyl sepharose fast-flow column (GE Healthcare) and washed with 24 CV of buffer containing 5 mM KPi, pH 6.8, 20% glycerol, and 1 mM EDTA. Protein was eluted using 5 CV of buffer containing 50 mM KPi, pH 6.8, 20% glycerol, 350 mM NaCl, and 1 mM EDTA. Fractions were pooled based on absorbance at 417 nm and concentrated to ~1 mL.

Concentrated protein was injected onto a 120 mL Superdex 200 gel filtration column (GE Healthcare) pre-equilibrated with CM buffer containing 50 mM KPi, pH 6.8, 20% glycerol, 350 mM NaCl, and 1 mM EDTA. Fractions corresponding to the major peak with absorbance at 417 nm were collected and pooled.

Protein concentration was determined by measuring the absolute absorbance as described in Chapter 2.

Crystallization, Data Collection, and Structure Determination

CYP21A2 (36 mg/mL) in 50 mM KPi, pH 6.8, 20% glycerol, 350 mM NaCl, 1 mM EDTA, 75 μM abiraterone, and 3 mM n-dodecyl-N,N-dimethylglycine was mixed in a 1:0.8 ratio with precipitant to form a 1.8 μL drop. The precipitant solution consisted of 150 mM MES, pH 6.5, 12% PEG-20,000, 6% glycerol. 1,6-Hexanediol (50%, 0.2 μL) was added to the drop. The protein/precipitant drop was equilibrated against 750 μL precipitant solution at 20°C. The small resulting crystals were seeded into 2 μL drops consisting of a 1:0.8:0.2 mixture of protein, precipitant solution (as described above) and 50% 1,6-hexanediol, which were also equilibrated against 750 μL precipitant at 20°C. Crystals were cryoprotected in a 7:3 mixture of mother liquor to 80% glycerol and flash cooled in liquid nitrogen.

Data were collected on beamline 12-2 of the Stanford Synchrotron Radiation Lightsource and processed using XDS[10]. Data collection and refinement statistics are shown in Table 7.1. Initial phases were determined by molecular replacement in Phaser[11]. The bovine CYP21A2 structure with heme cofactor (PDB ID: 3QZ1) was first used as a search model, yielding a solution with a log likelihood of 1,570. After the coordinates for the structure of human CYP21A2/progesterone complex with heme cofactor (PDB ID: 48YW) were deposited into the PDB, phases were again determined using the coordinates of human CYP21A2 as a search model, yielding a log likelihood of 3,372. Model building and iterative refinement were performed using COOT[12] and PHENIX[13], respectively. Active site voids were analyzed using VOIDOO[14] (probe radius = 1.4 Å, grid spacing = 0.33). Overlays between structures of human CYP21A2, bovine CYP21A2, and CYP17A1 were generated using the secondary structure matching algorithm in COOT[12], and optimized using a least-squares fit to overlay heme cofactors. Figures were generated in PyMOL[15].

Table 7.1: Statistics for x-ray data collection and refinement of CYP21A2 crystallized with abiraterone.

Data Collection	
Space group	$P12_11$
Cell dimensions	
a, b, c (Å)	118.95, 54.99, 166.29
α, β, γ (°)	90.00, 106.82, 90.00
Molecules/a.u.	4
Resolution (Å)*	28.91 – 2.74 (2.89 – 2.74)
Total reflections*	334,649 (42,852)
Unique reflections*	53,642 (7,417)
Redundancy*	6.2 (5.8)
R_{pim}*	0.047 (0.528)
$<I/\sigma(I)>$*	9.5 (1.5)
Completeness*	97.8 (93.5)
Refinement	
Resolution (Å)	38.91-2.74
No. reflections	53,444
R/R_{free} (%)	22.98 / 30.06
Ramachandran (%)	
Favored	92.35
Allowed	6.56
Outliers	1.08
Wilson B Factor ($Å^2$)	69.05
No. Atoms/B Factors ($Å^2$)	
Protein	14302 / 77.8
Heme	172 / 46.9
Water	47 / 54.9
RMSD bonds (Å)	0.008
RMSD angles (°)	1.228
Coordinate error (maximum-likelihood based) (Å)	0.47

RESULTS

Overall Structure of CYP21A2

Data collected on a crystal of CYP21A2 grown in the presence of 75 μM abiraterone was processed to 2.74 Å in the $P12_11$ space group. The phases were first estimated by molecular replacement using molecule A of the bovine CYP21A2 structure (Top LLG = 1570). However, shortly thereafter, release of the human CYP21A2 structure in complex with progesterone

allowed molecular replacement with this structure as an improved search model (Top LLG = 3372). The asymmetric unit is comprised of four molecules of enzyme, all of which exhibited the traditional cytochrome P450 fold (Figure 7.3) including 12 major helices (A-L), 4 smaller helices conserved among all four molecules (B′, F′, G′, K′), two smaller helices observed in at least one of the four molecules (A′ and K′′) and 9 beta strands participating in three separate sheet systems (two near the N-terminus and one near the C-terminus). Some surface loop regions, including those between helices J and K, and between K′ and K′′, were not modeled due to poor electron density. These same regions were not modeled in the structure of human CYP21A2 with progesterone, suggesting that these regions are dynamic parts of the enzyme. Additionally, the loop between helices H and I could be modeled in only one of four molecules, again, suggesting higher flexibility in this region.

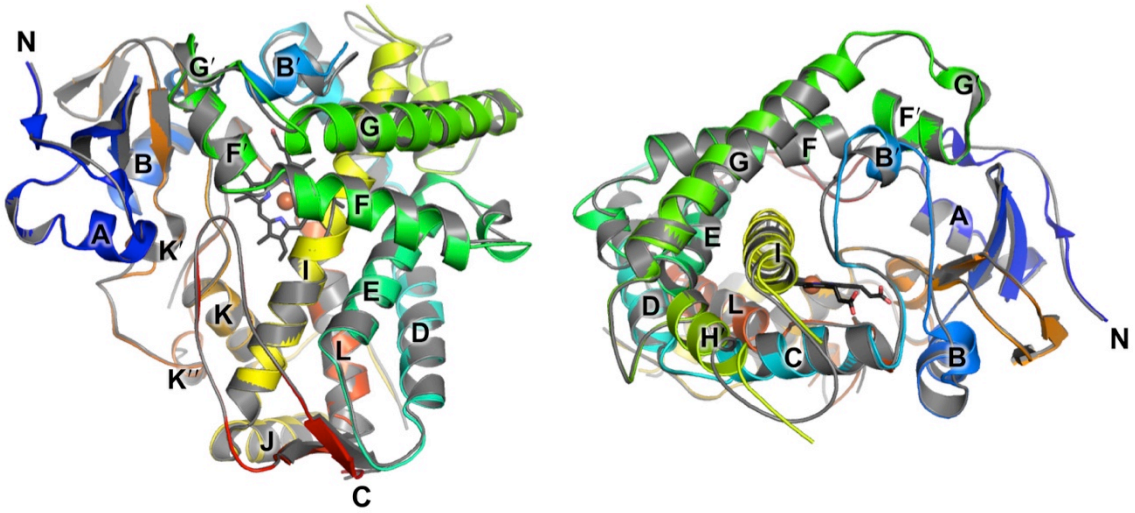

Figure 7.3: CYP21A2 2.74 Å global structure shown from the distal face (left) and perpendicular to the I helix (right). Molecule C is shown in Jones' rainbow (ranging from the blue N-terminus to the red C-terminus). Molecule D is shown overlaid in gray to demonstrate small variations in the protein backbone between copies in the asymmetric unit.

Three of the four copies of the enzyme comprising the asymmetric unit were very similar (average RMSD among all Cα = 0.65 ± 0.04 Å). However one copy of the enzyme, molecule D

in our structure, deviates somewhat from the other three (average RMSD among all Cα = 1.05 ± 0.07 Å compared to molecules A, B, and C). The most significant changes in backbone structure between molecule D and the other three copies appear N-terminal to the poorly-ordered H/I loop (average local RMSD over Cαs from residues 250-270 = 3.5 ± 0.3 Å). Molecule C, while very similar to other copies of the protein, displays some differences in the B′, G′, and G helices as well as their surrounding loops.

Active Site

Although reasonable density permits modeling of both backbone and side chains of active site amino acids and the heme cofactor, there is not sufficient electron density to support the modeling of abiraterone. F_o-F_c difference maps demonstrate a fragment of positive electron density protruding from the distal face of the heme in all four copies of the enzyme, suggesting that there is a ligand coordinated to the heme iron (Figure 7.4). This density is likely the result of a strong interaction between the nitrogen heterocycle of abiraterone and the heme iron, albeit at partial occupancy. There may not be sufficient interactions between the remainder of the steroid and the active site to stabilize the remainder of the ligand in a single orientation. The C3 substituent of progesterone in the structure of human CYP21A2 with progesterone forms a hydrogen bond with R234, equivalent to R239 in CYP17A1, on the G helix. The C3 substituent of abiraterone in its structure with CYP17A1, forms a hydrogen bond with N202 on the F helix. The corresponding residue in human CYP21A2 is an isoleucine, which would not be able to participate in a similar hydrogen interaction. Therefore, it is possible that pyridine ring coordination to the heme iron might not be ideal for formation of a C3 hydrogen bond between abiraterone and R234. A lack of hydrogen bonding between the C3 substituent of the steroid

may prevent stabilization of the steroid core in a single orientation within the active site and therefore poor density associated with this part of the ligand. Alternatively, the CYP21A2 (660 μM) used to generate the crystal on which data was collected had been exchanged into buffer containing a lower concentration of abiraterone, 75 μM, which is near the solubility limit of this ligand in aqueous solution. Although abiraterone appears to have reasonable affinity for the enzyme (<1 μM), this ligand concentration would have been insufficient to occupy all available CYP21A2 active sites, resulting in partial occupancy. Although crystallization of abiraterone at higher ligand concentrations might result in higher ligand occupancy, this would require addition of ligand past its solubility limit in aqueous buffer. At partial occupancy, as observed in the structure described herein, a lack of substantial interactions to order the steroid core in a single orientation would be consistent with the absence of electron density for this part of the ligand molecule.

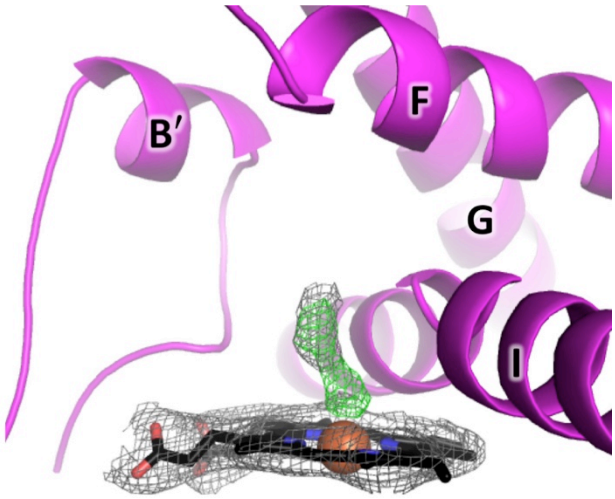

Figure 7.4: The active site of human CYP21A2 in the 2.74 Å structure demonstrates clear density for the heme prosthetic group and some adjacent density. Difference maps (F_o-F_c maps contoured to 3σ and shown as green mesh) show positive density over the heme suggesting a coordinating ligand, as expected for abiraterone. However, F_o-F_c maps and $2F_o$-F_c maps (shown in gray mesh and contoured to 1σ) are not sufficient to support modeling of a steroidal four-membered ring.

Despite similar backbone structure between copies of the protein, the active site volume varies widely between them. The active site volumes of molecules A and B are isolated from the protein surface and are 430 and 415 $Å^3$ (Figure 7.5), very similar in size to that of progesterone-bound human CYP21A2 (Average active site volume = 520 ± 10 $Å^3$). However, the remaining two copies of CYP21A2 in the partially-occupied complex with abiraterone have significantly larger active site cavities (1014 and 686 $Å^3$ for molecules C and D, respectively), both of which demonstrate channels connecting the active site with the protein surface. This extension of the active site cavity is observed in all four molecules of the bovine structure of CYP21A2 structure, yielding an average active site volume of 1250 ± 60 Å.

These substantial differences in both the size of the active site itself and access are largely the result of repositioning the B′ helix (Figure 7.5.C). Changes in the backbone of this helix are also accompanied by differences in side chain torsions (particularly tyrosine 98) which also expand the active site in this region. However, the structural elements responsible for exposure of the active site to the enzyme's substrate access channel (observed in molecules C and D) are more subtle, apparently mediated by small changes in backbone as well as side chain torsions for residues Y98 (B′ helix), W202 (F helix), V470 (loop region between C-terminal β strands), V360, and L364 (K/K′ loop) (Figure 7.5C). An additional difference between the structure of bovine CYP21A2 and both structures of human CYP21A2 is the position of the I helix relative to the heme cofactor. The I helix is significantly closer to the heme cofactor in both human CYP21A2 structures solved to date, whereas a kink in the helix of the bovine CYP21A2 structure provides more space above the heme. It has yet to be determined whether or not the difference in I helix between human and bovine CYP21A2 structures is the consequence of the ligand bound to the bovine CYP21A2 structure, 17α-hydroxyprogesterone, which has a

hydroxyl group projected toward the I helix, or if it is a fundamental difference between the two enzymes.

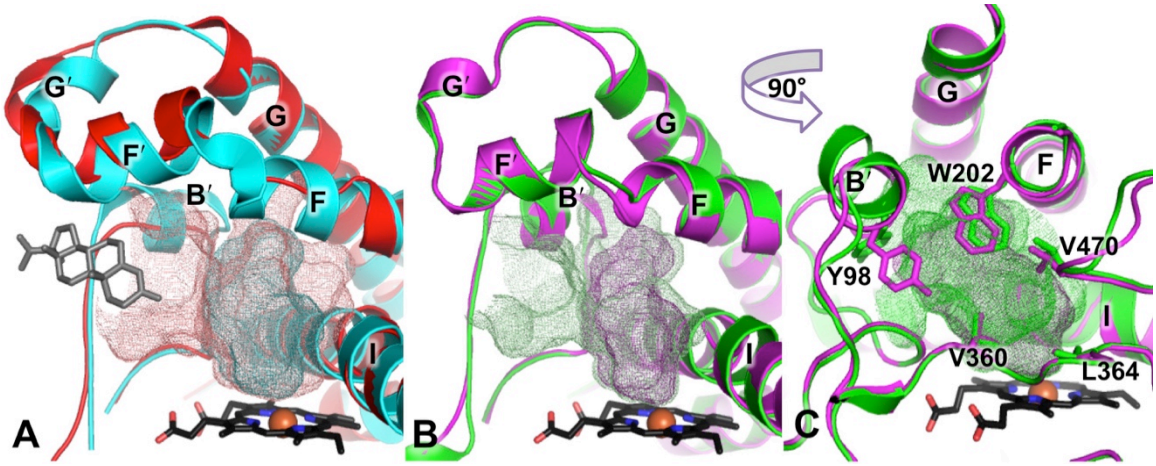

Figure 7.5: Variation in active site size between bovine CYP21A2 and different copies of human CYP21A2. A) The active site cavities of bovine CYP21A2 (red ribbons, cavity shown in red mesh) is substantially larger than that of the closed conformation for the human enzyme (cyan ribbons, molecule A cavity shown in cyan mesh), largely as a result of differences in the B′ and I helix and variations in the F-G region of the enzyme. The bovine CYP21A2 active site over the heme is accessible via a channel from the surface that was occupied by a second copy of the 17α-hydroxyprogesterone substrate (shown as gray sticks). B) The human CYP21A2 structure determined herein with partial abiraterone occupancy demonstrates substantial variation in active site volume between molecules B (magenta, cavity shown in magenta mesh) more similar to the structure of bovine CYP21A2 and C (green, cavity shown in green mesh) more similar to the structure of human CYP21A2 with progesterone. C) Comparisons of molecules B (magenta, cavity shown in magenta mesh) and C (green, cavity shown in green mesh) human CYP21A2 from the mouth of the channel opening shows that this is the result of small changes in backbone and side chain torsions of surrounding residues.

A second copy of the ligand, 17α-hydroxyprogesterone, was observed in the structure of bovine CYP21A2 in a cavity ~10 Å from the active site ligand[7]. This cavity forms a surface-exposed channel that is likely involved in ligand entry and exit (Figure 7.5A). Density corresponding to a second ligand in the human CYP21A2 structure with progesterone was also observed, albeit at a lower occupancy, and the peripheral ligand was therefore not modeled. This suggests that steroidal ligands are less stabilized in this peripheral binding site of human CYP21A2 than the active site. In the CYP21A2 structure described herein, there is little

evidence for a ligand in this peripheral site. However, the active site was not fully occupied, so the absence of density in this second, likely lower affinity binding site is not surprising.

DISCUSSION

CYP21A2 is one of six cytochrome P450 enzymes involved in steroid biosynthesis, including CYP17A1 involved in androgen production. Agents designed to inhibit CYP17A1-mediated androgen production have also been shown to interfere with CYP21A2 metabolism. Abiraterone, which was specifically designed to inhibit CYP17A1 and therefore interrupt androgen biosynthesis in patients with hormone-dependent prostate cancer also binds and inhibits human CYP21A2[6]. A more thorough understanding of how coincident CYP21A2 inhibition affects biochemistry, physiology, and clinical outcomes for those undergoing abiraterone treatment would require the development of inhibitors more selective for CYP17A1 over CYP21A2. The crystal structure of countertarget enzyme CYP21A2 with abiraterone was expected to provide useful structural information for the design of more selective inhibitors of CYP17A1.

Toward this end, CYP21A2 was crystallized in the presence of abiraterone, and the X-ray crystal structure of one such crystal was determined at a resolution of 2.74 Å. Unfortunately, complete ligand density was not observed in any of the four copies of protein. This is likely the result of partial ligand occupancy within the CYP21A2 active site due to inadequate concentrations of ligand present during crystallization. However, density was apparent coordinated to the heme iron, which is likely the pyridine ring of abiraterone, and would be consistent with spectral changes observed upon titration of CYP21A2 with abiraterone. Although incomplete ligand density frustrated efforts to model abiraterone into the active site,

the structure of human CYP21A2 described herein can be compared to a recently-published structure of human CYP21A2 bound to one of its substrates, progesterone.

The structures of human CYP21A2 with progesterone and partially-occupied abiraterone are more similar to one another (average RMSD over all Cα = 0.90 ± 0.07 Å) than either structure is to the bovine CYP21A2 structure. Relative to the bovine CYP21A2 structure, the human CYP21A2 substrate-bound and inhibitor-bound structures demonstrate have average Cα RMSD of 1.90 ± 0.04 and 2.03 ± 0.03 Å, respectively. Some of the larger deviations observed between the substrate bound human and bovine CYP21A2 structures, include changes in the I helix that draw it closer to the heme cofactor, as well as the orientation of the F′/G′ region. However, these features were conserved between substrate-bound and partially-inhibitor bound structures of human CYP21A2. Some regions of the protein demonstrated variability between the substrate-bound structure and the structure with inhibitor bound at partial occupancy, and even between copies of protein in the latter structure. Those elements of the enzyme include the B′ helix and the loop between helices H and I, demonstrating the flexibility of these components within the human enzyme. One of these changes, the conformation of the B′ helix seems to affect the active site topography, and could reflect a critical role of this structural feature in substrate access to the active site.

Although there was little ligand density to direct modeling of abiraterone into the CYP21A2 active site based on crystallographic data, spectral shift assays strongly suggest the nitrogen of the pyridine ring coordinates to the heme iron. Moreover, it is very likely that the steroidal core of the ligand assumes an orientation similar to substrate progesterone in the active site, with the 3β-hydroxyl group oriented toward the G-helix[8]. If abiraterone is modeled in this orientation and overlaid with the CYP17A1/abiraterone structure (Figure 7.6), differences in

active site configuration and distinct ligand interactions are revealed that could be exploited to design inhibitors more selective for CYP17A1 versus CYP21A2[16]. One substantial difference is that the CYP17A1 active site extends over the top of the I helix beyond the C3 hydroxyl group of abiraterone, but this is not observed in the CYP21A2 active site (Figure 7.6A). Functionalization of C3 with bulky substituents may therefore selectively hinder inhibitor binding to CYP21A2 compared to CYP17A1. Alterations in the A ring of steroidal inhibitors may facilitate this approach (Chapter 4). There is also some unoccupied space in the CYP17A1 active site in the plane of the steroid near carbons 1 and 11 that is not available as part of the CYP21A2 active site. Functionalization and modification of the steroid at these positions may also assist in achieving selectivity by introducing steric interference with the CYP21A2 active site.

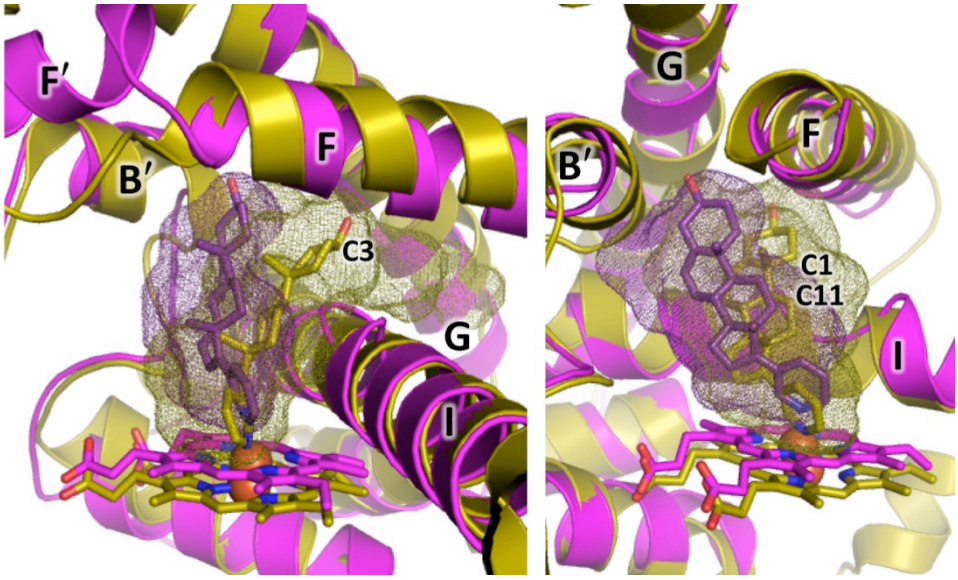

Figure 7.6: Overlay of CYP17A1 (gold ribbons and mesh active site) and CYP21A2 (magenta ribbons and active site mesh) by least squares fit demonstrates differences in the two active sites. Comparison suggests the presence of some accessible space in the CYP17A1 active site that is not available in the CYP21A2 active site, particularly near steroidal carbons C3 (A), C1, and C11 (B).

Comparison of the CYP17A1 and CYP21A2 active sites also suggests a basis for selectivity observed for some CYP17A1 inhibitors against CYP21A2. One such analog of

abiraterone with an oxime substituent at carbon 6 was reported (C. Fehl, unpublished data) to demonstrate nearly 70-fold selectivity for CYP17A1 progesterone 17α-hydroxylation (IC_{50} = 150 ± 10 nM) over CYP21A2 progesterone 21-hydroxylation (IC_{50} = 10,300 ± 600)[6]. An X-ray crystal structure of this inhibitor bound to CYP17A1 determined by Charlie Fehl revealed that the C6 oxime hydrogen bonds with the A105 backbone and D298 side chain of CYP17A1 (Figure 7.7A)[6]. When this same steroidal inhibitor was modeled into the CYP21A2 active site with the steroidal core positioned similar to progesterone in the human CYP21A2 structure with substrate is positioned ~4.8 Å and ~4.7 Å from the corresponding residues (D288 and V101) (Figure 7.7B). The absence of available hydrogen bond contacts in CYP21A2 compared to CYP17A1 could account for the disparate inhibitory potency for CYP21A2-mediated progesterone 21-hydroxylation compared to CYP17A1-mediated progesterone 17α-hydroxylation.

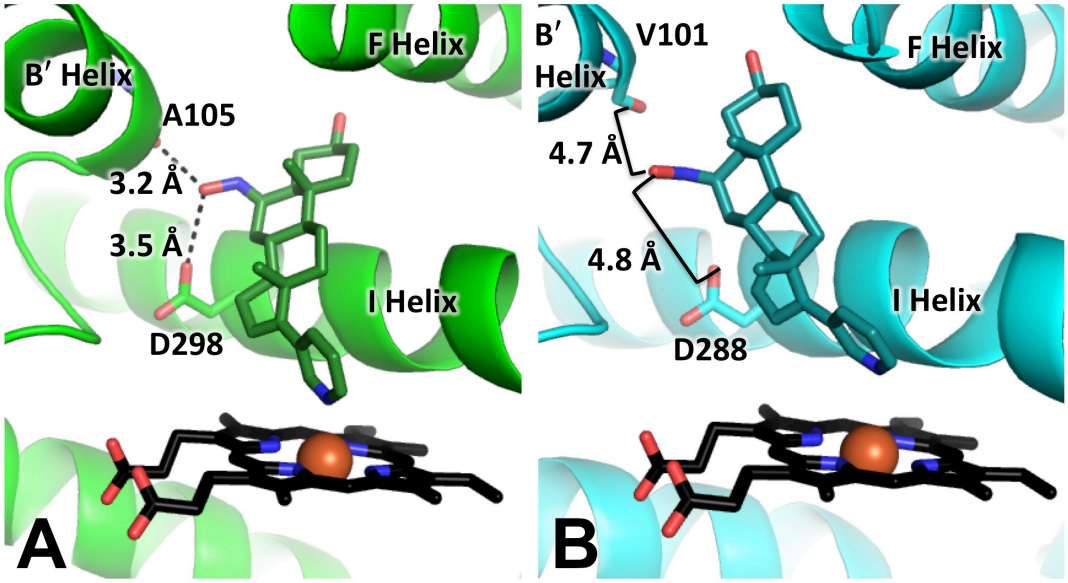

Figure 7.7: Interactions of a C6-substituted analog of abiraterone[6] 70-fold selective for inhibition of CYP17A1 over CYP21A2. A) In the X-ray crystal structure of CYP17A1 with this abiraterone analog, the C6 oxime hydrogen bonds with the backbone carbonyl of A105 and the side chain of D298. B) In the proposed orientation within the human CYP21A2 active site, this C6-substituted abiraterone analog is not positioned to hydrogen bond to corresponding residues V101 and D288.

In conclusion, human CYP21A2 was successfully crystallized in the presence of abiraterone and the X-ray crystal structure of the enzyme was solved at a resolution of 2.74 Å. Unfortunately, there was not sufficient electron density in the CYP21A2 active site to model abiraterone, suggesting only partial occupancy due to insufficient ligand concentrations during crystallization. This structure is very similar to a recently published structure of CYP21A2 bound to substrate progesterone. There are some small changes in the helices on the distal face of the enzyme between molecules of the human CYP21A2 structure described herein, including B′, F′, and G′, which can have substantial effects on the active site topography. Conformational dynamics in these regions may modulate access to the active site from the surface of the enzyme. The active site of CYP21A2 in some copies of the asymmetric unit is accessible to the substrate access channel, a space reported to be ligand-occupied in the bovine and human structures of CYP21A2.

Despite our inability to model abiraterone into the human CYP21A2 structure based solely on crystallographic data, we can hypothesize the orientation of the steroidal ligand within the active site is supported by spectral binding data consistent with heteroatom/heme coordination, as well as the structure of human CYP21A2 bound to its steroidal substrate, progesterone. Comparison of abiraterone modeled into the CYP21A2 active site and the experimental complex with CYP17A1 suggest that functionalization of steroidal inhibitors on C3 of the steroid or near C1 or C11 might interfere with binding to human CYP21A2 and may demonstrate more selectivity for CYP17A1. If C6-substituted analogs of abiraterone adopt a similar orientation within the CYP21A2 active site, the hydrogen-bonds observed between these inhibitors and CYP17A1 would not be formed with corresponding residues in CYP21A2. At a minimum, development of CYP17A1 inhibitors with greater selectivity over the countertarget

CYP21A2 is crucial to understanding the biochemical and physiological impacts of CYP21A2 inhibition by abiraterone. However such studies also have the potential to inform the design of more selective and effective CYP17A1 inhibitors for the treatment of prostate cancer.

REFERENCES

(1) Turcu, A. F.; Auchus, R. J. *Endocrinol. Metab. Clin. North. Am.* **2015**, *44*, 275.
(2) Auchus, R. J.; Miller, W. L. In *Cytochrome P450: Structure, Mechanism, and Biochemistry*; 4th ed.; Ortiz de Montellano, P., Ed.; Springer: New York, 2015; Vol. II, p 851.
(3) Haider, S.; Islam, B.; D'Atri, V.; Sgobba, M.; Poojari, C.; Sun, L.; Yuen, T.; Zaidi, M.; New, M. I. *Proc. Natl. Acad. Sci. U. S. A.* **2013**, *110*, 2605.
(4) Yoshimoto, F. K.; Zhou, Y.; Peng, H. M.; Stidd, D.; Yoshimoto, J. A.; Sharma, K. K.; Matthew, S.; Auchus, R. J. *Biochemistry* **2012**, *51*, 7064.
(5) Swart, P.; Swart, A. C.; Waterman, M. R.; Estabrook, R. W.; Mason, J. I. *J. Clin. Endocrinol. Metab.* **1993**, *77*, 98.
(6) Fehl, C., University of Kansas, 2014.
(7) Zhao, B.; Lei, L.; Kagawa, N.; Sundaramoorthy, M.; Banerjee, S.; Nagy, L. D.; Guengerich, F. P.; Waterman, M. R. *J. Biol. Chem.* **2012**, *287*, 10613.
(8) Pallan, P. S.; Wang, C.; Lei, L.; Yoshimoto, F. K.; Auchus, R. J.; Waterman, M. R.; Guengerich, F. P.; Egli, M. *J. Biol. Chem.* **2015**, *290*, 13128.
(9) Blake, L. C., University of Kansas, 2012.
(10) Kabsch, W. *Acta Crystallogr., Sect. D: Biol. Crystallogr.* **2010**, *66*, 125.
(11) McCoy, A. J.; Grosse-Kunstleve, R. W.; Adams, P. D.; Winn, M. D.; Storoni, L. C.; Read, R. J. *J. Appl. Crystallogr.* **2007**, *40*, 658.
(12) Emsley, P.; Lohkamp, B.; Scott, W. G.; Cowtan, K. *Acta Crystallogr., Sect. D: Biol. Crystallogr.* **2010**, *66*, 486.
(13) Adams, P. D.; Afonine, P. V.; Bunkoczi, G.; Chen, V. B.; Davis, I. W.; Echols, N.; Headd, J. J.; Hung, L. W.; Kapral, G. J.; Grosse-Kunstleve, R. W.; McCoy, A. J.; Moriarty, N. W.; Oeffner, R.; Read, R. J.; Richardson, D. C.; Richardson, J. S.; Terwilliger, T. C.; Zwart, P. H. *Acta Crystallogr., Sect. D: Biol. Crystallogr.* **2010**, *66*, 213.
(14) Kleywegt, G. J.; Jones, T. A. *Acta Crystallogr., Sect. D: Biol. Crystallogr.* **1994**, *50*, 178.
(15) Schrodinger, LLC 2010.
(16) DeVore, N. M.; Scott, E. E. *Nature* **2012**, *482*, 116.

Chapter 8.

Conclusions

The overall goal of the research described herein is to gain a better understanding of steroidogenic cytochrome P450 function by 1) using systems of purified proteins to establish whether inhibitors and loss of function mutations can selectively disrupt a single reaction performed in the same active site and 2) comparing interactions between these enzymes and corresponding substrates and inhibitors to address questions of substrate specificity and regioselectivity and inhibitor potency and selectivity. The functional analysis performed in this work is intended to inform the design of more potent and selective therapeutics targeting cytochrome P450 17A1. Catalysis by cytochrome P450 enzymes is complex, and is further complicated by the fact that CYP17A1 carries out two different reactions in the same active site. The results described as part of this work advance our modest understanding of this enzyme's function, and suggest further steps in developing a more complete understanding of CYP17A1, which should allow the subsequent design of better therapeutics for the treatment of prostate cancer.

First, structural studies of CYP17A1 with inhibitors suggest a possible mechanism for selective inhibition of the targeted 17,20-lyase reaction versus off-target inhibition of the 17α-hydroxylation. The structure of CYP17A1 with *S*- and *R*-orteronel demonstrates a single enantiomer occupying the active site of the enzyme depending on the conformation of the F/G loop. Conformation A, which was observed to bind the more lyase-selective *R*-orteronel, may be more likely to allow for intermediate product release than conformation B, which was observed to bind the less lyase-selective *S*-orteronel (Figure 8.1). If released from the enzyme, the intermediate 17α-hydroxylase product should be less likely to undergo the 17,20-lyase reaction.

Rebinding to CYP17A1 would require a second productive interaction between CYP17A1 and intermediate product. Additionally, dissociation would allow an inhibitor or a 17α-hydroxylase substrate to compete for occupancy of the CYP17A1 active site. The X-ray crystal structure of CYP17A1 with inhibitor (2), determined at 2.0 Å, substantiated the presence of a peripheral binding site near the flexible F/G loop when it assumes conformation B, but not conformation A. Inhibitor effects on CYP17A1 processivity may therefore be the result of occupation of this peripheral site by an inhibitor in contrast to active site binding. Binding of less selective inhibitors such as *S*-orteronel and abiraterone to the peripheral binding site in conformation B may prevent intermediate product release. Inversion of the stereocenter of *S*-orteronel to *R*-orteronel appears to be inconsistent with occupation of this peripheral site, and could facilitate increased dissociation of intermediate product, ultimately yielding increased selectivity for the 17,20-lyase reaction.

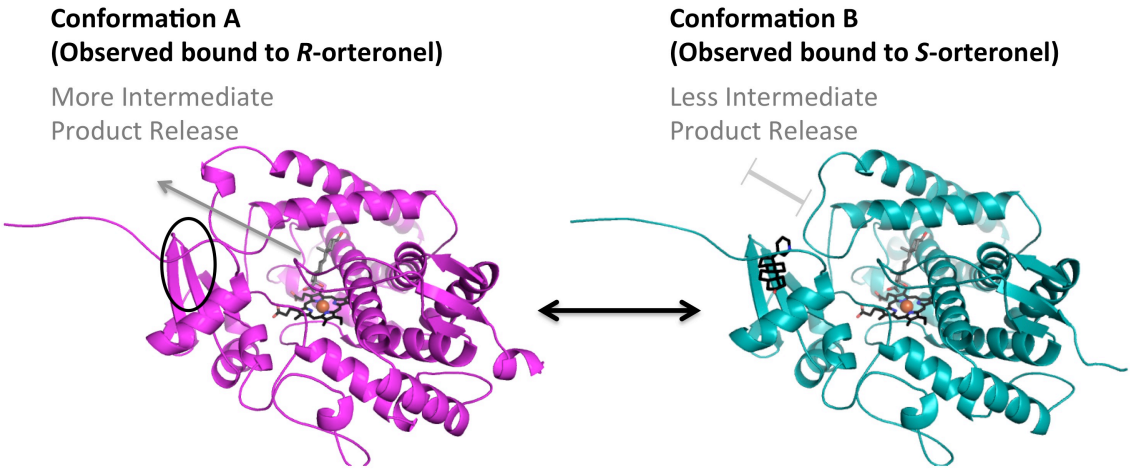

Figure 8.1: Proposed mechanism for 17,20-lyase selectivity of *R*-orteronel. Conformation A (left) is stabilized by *R*-orteronel and does not feature a peripheral ligand binding site. Conformation B (right) is stabilized by *S*-orteronel and observed to bind ligands in the peripheral site. Ligand binding to the secondary site in conformation B may prevent release of intermediate product, facilitating 17,20-lyase turnover. In contrast, conformation A may allow dissociation of intermediate product and allow *R*-orteronel to compete with the intermediate product for the active site.

Future studies should include determination of the X-ray crystal structure of CYP17A1 with purified *R*-orteronel. If *R*-orteronel does not interact with CYP17A1 in conformation B, this may destabilize the B conformation and may prevent normal crystal packing under conditions currently used to crystallize CYP17A1. Alternatively, if CYP17A1 can adopt conformation B without binding *R*-orteronel we would likely observe little to no electron density in the two molecules of the asymmetric unit that adopt conformation B. If the first scenario is true, then crystallization of CYP17A1 with *R*-orteronel might therefore require more thorough investigations into different crystallization conditions for this complex. Structure determination of CYP17A1 with inhibitors that occupy the peripheral binding site at higher resolution (below 2.0 Å) would help further define the site and verify the identity of the ligand present. This could be achieved by using femtosecond crystallography[1]. This technique uses lower levels of radiation, which should prevent reduction of the heme iron from the Fe^{3+} state to the Fe^{2+} state, improving homogeneity of the heme oxidation state, and potentially producing higher resolution data.

The proposed mechanism for 17,20-lyase selectivity could also be supported by kinetic studies that determine the mode of inhibition by *R*-orteronel and non-selective inhibitors. If the proposed mechanism is correct, *R*-orteronel would demonstrate only competitive inhibition for both 17α-hydroxylase and 17,20-lyase reactions. If the reduced selectivity of the other evaluated inhibitors results from occupying the peripheral binding site, inhibition of the hydroxylase and 17,20-lyase reaction would exhibit a much more complicated kinetic profile, likely more consistent with non-competitive inhibition. In summary, characterization of this peripheral binding site may be crucial to the development of 17,20-lyase selective therapeutics, however this will require a much more thorough characterization of the aforementioned site.

Since cytochrome b_5 is reported to selectively augment the 17,20-lyase reaction[2], it is tempting to suggest that therapeutics that block CYP17A1 and cytochrome b_5 interactions might be a reasonable strategy for achieving selective inhibiton of the 17,20-lyase reaction. The lack of selective 17,20-lyase deficiency demonstrated *in vitro* by CYP17A1 with mutations to the cytochrome b_5 binding site suggest that interruption of cytochrome b_5 binding without compromising interaction with NADPH-cytochrome P450 reductase may be a challenging pursuit.

The final consideration for the development of more successful prostate cancer therapeutics is whether or not CYP17A1 should be pursued as a single therapeutic target. The consequences of interactions between intended CYP17A1 inhibitors and some biological targets, such as CYP21A2, are largely unknown. While interaction with some of these targets could result in detrimental side effects or more rapid progression of resistance to treatment, the A-ring modified inhibitor (1) was recently reported to exhibit its anticancer activity by acting as an inhibitor or an antagonist at multiple targets[3]. If inhibitors affect the right set of enzymes and receptors, a multi-target approach could improve therapy by delaying the onset of resistance[4]. Therefore, next generation inhibitors of CYP17A1 may be designed to interact with more than one enzyme or receptor. Compounds designed to interact with a variety of steroid-metabolizing enzymes and nuclear receptors will very likely inhibit other steroidogenic cytochrome P450 enzymes such as CYP21A2 and CYP11B1. A more thorough understanding of such enzymes, including physiological consequences of their inhibition, will be necessary to determine whether their inhibition negatively impacts treatment and if so, what level of priority should be put on designing inhibitors that avoid inhibition of these targets. Studies that examine the physiological effects of dual CYP17A1/CYP21A2 inhibition against selective CYP17A1 vs. CYP21A2

inhibition in animal models would be crucial to address such questions. Analogs of inhibitor (3) with bulky substituents projecting from carbon 3 may access an extension of the CYP17A1 active site cavity unavailable to CYP21A2, and such inhibitors could demonstrate selective inhibition of CYP17A1 over CYP21A2 as described in Chapter 7.

In conclusion, the studies described herein improve our knowledge of CYP17A1. The complex catalysis performed by this enzyme makes its inhibition both a strategy for the treatment of prostate cancer and the source of adverse corticosteroid-mediated effects. The crucial steps made in understanding selective inhibition of the 17,20-lyase inhibition as part of this work and the determination of the X-ray crystal structure for potential countertarget CYP21A2 represent progress toward the development of more effective therapeutics for the treatment of prostate cancer.

REFERENCES

(1) Boutet, S.; Lomb, L.; Williams, G. J.; Barends, T. R.; Aquila, A.; Doak, R. B.; Weierstall, U.; DePonte, D. P.; Steinbrener, J.; Shoeman, R. L.; Messerschmidt, M.; Barty, A.; White, T. A.; Kassemeyer, S.; Kirian, R. A.; Seibert, M. M.; Montanez, P. A.; Kenney, C.; Herbst, R.; Hart, P.; Pines, J.; Haller, G.; Gruner, S. M.; Philipp, H. T.; Tate, M. W.; Hromalik, M.; Koerner, L. J.; van Bakel, N.; Morse, J.; Ghonsalves, W.; Arnlund, D.; Bogan, M. J.; Caleman, C.; Fromme, R.; Hampton, C. Y.; Hunter, M. S.; Johansson, L. C.; Katona, G.; Kupitz, C.; Liang, M.; Martin, A. V.; Nass, K.; Redecke, L.; Stellato, F.; Timneanu, N.; Wang, D.; Zatsepin, N. A.; Schafer, D.; Defever, J.; Neutze, R.; Fromme, P.; Spence, J. C.; Chapman, H. N.; Schlichting, I. *Science* **2012**, *337*, 362.

(2) Fluck, C. E.; Miller, W. L.; Auchus, R. J. *J. Clin. Endocrinol. Metab.* **2003**, *88*, 3762.

(3) Li, Z.; Bishop, A. C.; Alyamani, M.; Garcia, J. A.; Dreicer, R.; Bunch, D.; Liu, J.; Upadhyay, S. K.; Auchus, R. J.; Sharifi, N. *Nature* **2015**.

(4) Yin, L.; Hu, Q. *Nat. Rev. Urol.* **2014**, *11*, 32.